Roles for regulators of cortical ER structure in maintaining NPC integrity

By

Amanda Kathleen Casey

Dissertation

Submitted to the Faculty of the

Graduate School of Vanderbilt University

in partial fulfillment of the requirements

for the degree of

DOCTOR OF PHILOSOPY

in

Cell and Developmental Biology

May, 2015

Nashville, Tennessee

Approved:

Susan R. Wente, Ph.D.

Kathy L. Gould, Ph.D.

Todd R. Graham, Ph.D.

Melanie D. Ohi, Ph.D.

Andrew J. Link, Ph.D.

To my loving husband, Matt

ACKNOWLEDGEMENTS

I would like to thank my mentor, Dr. Susan R. Wente. I am so happy that I was given the opportunity to become a member of her lab, and I know that my time here at Vanderbilt has made me a better scientist because of her guidance and support. I want to thank the members of Wente lab, past and present, for their insights, support, and friendships. I especially want to thank Dr. Renee Dawson for the additional support she has provided. I'm also grateful to my thesis committee members, Dr. Kathleen Gould, Dr. Todd Graham, Dr. Andrew Link, and Dr. Melanie Ohi for their valuable insights and guidance.

My family has encouraged and supported me throughout my education. I'm grateful for my husband Matthew and his support during this time in graduate school. I'm so happy that we could experience Vanderbilt together, and I look forward to our future adventures together. Finally, I want to acknowledge and thank all of the amazing teachers who have shaped my education, interests, and enthusiasm for the natural world. Without these men and women who fostered my confidence and encouraged my natural curiosity, I never would have achieved so much.

TABLE OF CONTENTS

DEDICATION ii

ACKNOWLEDGEMENTS iii

LIST OF TABLES vi

LIST OF FIGURES vii

LIST OF ABBREVIATIONS ix

CHAPTER

I. INTRODUCTION 1

The nucleus and nuclear envelope 1
NPC structure 3
NPC mediated transport 6
Evolution of NE and NPC from an ancestral endomembrane system 11
ER structure 11
NPC assembly 16
Post-mitotic assembly of NPCs 16
De novo assembly 18
Roles of membrane proteins in NPC assembly and stability 21

II. INTEGRITY AND FUNCTION OF THE SACCHAROMYCES CEREVISIAE SPINDLE POLE BODY DEPENDS ON CONNECTIONS BETWEEN THE MEMBRANE PROTEINS NDC1, RTN1, AND YOP1 27

Introduction 27
Materials and Methods 31
Results 38
Rtn1 and Yop1 are required for normal spindle pole body morphology 38
SPB superplaques in *rtn1Δ yop1Δ* cells are unstable in the NE 43
Cells lacking Rtn1 and Yop1 have defects in the mitotic spindle 45
Rtn1 and Yop1 impact proper spindle function 54
Overexpression of SPB insertion factors specifically rescues *rtn1Δ yop1Δ* spindle defects 57
High osmolarity reduces NPC clustering but not spindle defects of *rtn1Δ yop1Δ* cells 63
Rtn1 and Yop1 interact with Ndc1 64
Discussion 67

III. NUCLEAR PORE COMPLEX INTEGRITY REQUIRES LNP1, A REGULATOR OF CORTICAL 74

Introduction 74
Materials and Methods 77
Results 82
lnp1Δ rtn1Δ cells have defects in NPC organization 82
Lnp1 and Sey1 localize to the NE and physically interact with shared ER and NPC components 86
lnp1Δ and *sey1Δ* mutants genetically interact with mutants in genes of the Nup84 subcomplex 90
The function of Lnp1 and Sey1 at NPCs is coupled with the interaction between Rtn1 and the NPC 92
The zinc finger domain of Lnp1 mediates dimerization is required for ER but not NPC function 97
Discussion 103

IV. DISCUSSION AND FUTURE DIRECTIONS 108

Mapping of physical interactions of Rtn1 and Yop1 with the NPC 108
Competitive Binding of Lnp1 and Ndc1 for Rtn1 110
Effects of Lnp1 association on Rtn1 mobility in membranes 111
Localization of ER shaping proteins in the NE 112
Conservation of ER protein function in ER structure and NPC assembly 114
In vitro recruitment of Nups to curved membranes 117
Identification of regulators of NPC number and assembly 120

APPENDIX 123

A. NPC motility: shifting gears between fungal nuclear and cytoplasmic organization 123

B. Analysis of Sec13 function in the Nup84 subcomplex 130

C. Yeast strains used in this study 141

D. Plasmids used in this study 146

REFERENCES 147

LIST OF TABLES

Table Page

1.1: NE proteins connected to NPC assembly 22

2.1: *rtn1Δ yop1Δ* cells have mild SPB positioning defects upon α-factor arrest 49

3.1: Genetic interactions with *lnp1Δ* and *sey1Δ* 91

C.1: Yeast strains used in this study 141

D.1: Plasmids used in this study 146

LIST OF FIGURES

Figure Page

1.1: Organization of the nuclear envelope in *Saccharomyces cerevisiae* 2

1.2: The general structure of the NPC 5

1.3: Mechanism of nuclear trafficking 8

1.4: Model for the evolution of the NE and NPCs 12

1.5: Membrane shaping proteins of the ER 14

1.6: Model for post-mitotic nuclear envelope assembly 17

1.7: Model for *de novo* pore assembly 20

2.1: SPBs have abnormal morphology and colocalize with NPC clusters in *rtn1Δ yop1Δ* cells 39

2.2 Deletion of *RTN1* and *YOP1* result in abnormalities in the SPB 41

2.3. Rtn1 does not colocalize with SPBs 44

2.4: Deletion of reticulons affects superplaque formation 46

2.5: Mitotic arrest leads to collapsed spindles and reduced microtubule function in *rtn1Δ yop1Δ* cells 50

2.6: *rtn1Δ yop1Δ* cells have defects in cytoplasmic microtubules 53

2.7: *rtn1Δ yop1Δ* cells exhibit functional defects in spindle positioning 55

2.8: Overexpression of SPB insertion factors rescues *rtn1Δ yop1Δ* defect 58

2.9: Overexpression of *NDC1* results in rescue of *rtn1Δ yop1Δ growth* defects 60

2.10: Growth in high osmolarity only reduces NPC clusters in *rtn1Δ yop1Δ cells* 61

2.11**:** Rtn1 and Yop1 interact with Ndc1 and NPC components 65

2.12**:** Models of Rtn1 and Yop1 function at NPCs and SPBs 71

3.1: *lnp1Δ rtn1Δ* cells have defects in NPC organization 84

3.2: TEM of nuclear pores in *lnp1Δ rtn1Δ* cells 85

3.3: Lnp1 and Sey1 localize to the NE and physically interact with shared ER and NPC components 87

3.4: Live cell localization of Lnp1-GFP 89

3.5: *lnp1Δ* and *sey1Δ* mutants genetically interact with mutants in genes of the Nup84 subcomplex 93

3.6: The function of Lnp1 and Sey1 with NPCs is coupled with the interaction between Rtn1 and the NPC 95

3.7: The C terminal zinc finger domain of Lnp1 is required for dimerization *in vitro* 99

3.8: The zinc finger of Lnp1 is not required for NPC function. 101

3.9: Models for Rtn1 and Lnp1 function at the NPC 106

A.1: Model of NPC and nuclear organization 124

B1: sec13 bypass mutants results in defects in ER and NPC morphology 134

B2: nup145-K758P disrupts Sec13 binding 136

B3: Loss of Sec13 and Seh1 from the NPC does not result in NPC defects 138

ABBREVIATIONS

Δ	genetic null or domain deletion
3-AT	3-aminotriazole
ALPS	ArfGAP1 lipid packing sensor
CEN	yeast centromere
CSM	complete synthetic minimal
DNA	deoxyribonucleic acid
EM	electron microscopy
EndoH	endoglycosidase H
ER	endoplasmic reticulum
FG	phenylalanine-glycine
FRAP	fluorescence recovery after photobleaching
GDa	gigadalton
GFP	green fluorescent protein
GTP	guanosine-5'-triphosphate
HPF/FS	high-pressure freezing/freeze substitution
hr	hour
HU	hydroxyurea
INM	inner nuclear membrane
KAN^R	kanamycin resistance
KDa	kilodalton
MBP	maltose-binding protein
MDa	megadalton
min	minute
mRNA	messenger RNA
mRNP	messenger ribonucleoprotein particles
NE	nuclear envelope
NES	nuclear export sequences
NLS	nuclear localization sequences
NPC	nuclear pore complex
Nups	nucleoporins
ONM	outer nuclear membrane
Pom	pore membrane protein
RNA	ribonucleic acid
SIM	structured illumination microscopy
SNARE	soluble N-ethylmaleimide-sensitive factor attachment protein receptors
SPB	spindle pole body
STORM	stochastic optical reconstruction microscopy
TAP	tandem affinity purification
TEM	transmission electron microscopy
YPD	yeast extract peptone dextrose media

CHAPTER I

INTRODUCTION

The nucleus, nuclear envelope, and the NPC

The nucleus is the defining characteristic of all eukaryotic cells. This physical compartmentalization of genetic material provides the basic mechanism for controlling gene expression at many levels (HEESSEN and FORNEROD 2007; MALHAS *et al.* 2007; PLOTNIKOV *et al.* 2011; BURNS and WENTE 2014). The partitioning of the nucleus from the cytoplasm is implemented by the nuclear envelope (NE), a double lipid bilayer that encloses this organelle (Figure 1.1) (MAGGIO *et al.* 1963). Besides acting as a physical barrier, the NE also contains many membrane components with nuclear functions. Due to their unique cellular environments, the outer nuclear membrane (ONM) and inner nuclear membrane (INM) both play critical yet unique functions in the cell and contain different protein complexes that facilitate these roles (LUSK *et al.* 2007; HIRAOKA and DERNBURG 2009; ANTONIN *et al.* 2011). In mammalian cells, composition of the NE is also tissue specific (GOMEZ-CAVAZOS and HETZER 2012; DE LAS HERAS *et al.* 2013). Enrichment of these different INM proteins in the NE is linked to changes in stability of the NE, chromatin organization, and nuclear signaling (BLOBEL 2010; DE LAS HERAS *et al.* 2013).

The ONM is continuous with the endoplasmic reticulum (ER) and has a similar lipid and protein composition to the ER (NEWPORT and FORBES 1987; GERACE and BURKE 1988). The ONM joins the INM at points of fusion in the NE where nuclear

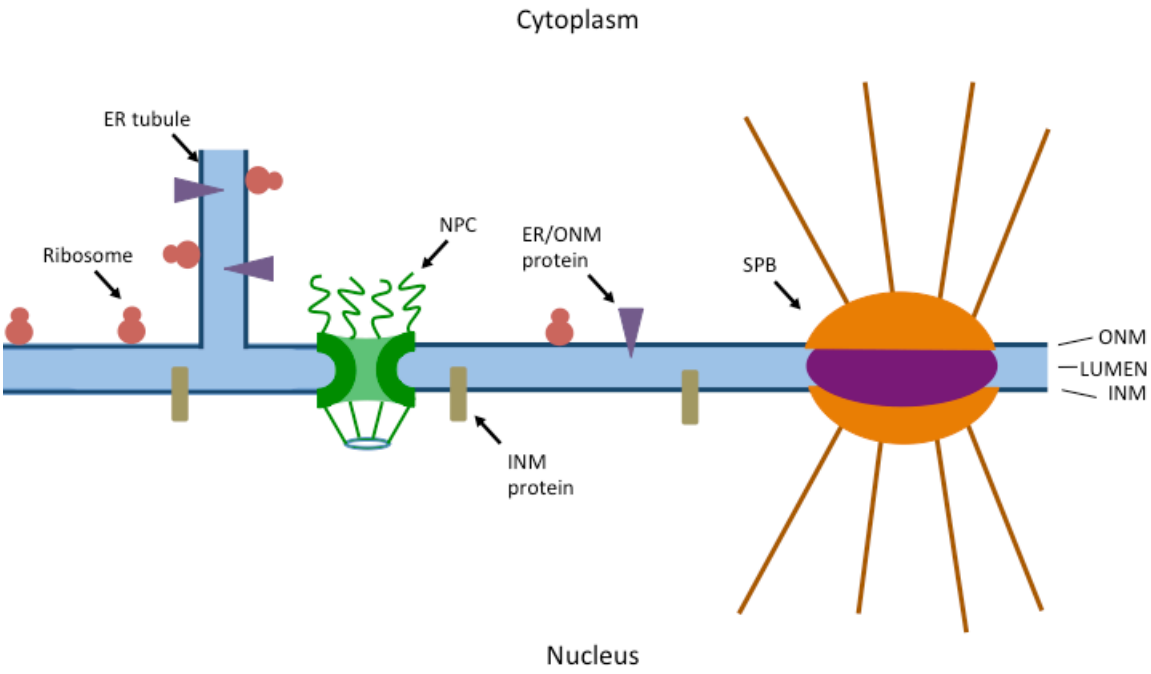

Figure 1.1: Organization of the nuclear envelope in *Saccharomyces cerevisiae*. The NE and ER are part of the same continous membrane system. The outer nuclear membrane (ONM) faces the cytoplasm and has the same protein composition as the rough ER and is studded with ribosomes. The inner nuclear membrane (INM) faces the nucleoplasm and is enriched in many proteins that interact with nuclear components such as chromatin and the nuclear lamina. The INM and ONM are joined at points of fusion that house nuclear pore complexes (NPCs) and at spindle pole bodies (SPBs). The NE lumen is also continuous with the ER.

pore complexes (NPCs) are embedded (HETZER and WENTE 2009). Of note, in *Saccharomyces cerevisiae*, the spindle pole body (SPB) is also embedded in the NE at sites of fusion (ADAMS and KILMARTIN 1999; JASPERSEN and WINEY 2004). The INM surrounds the nucleoplasm and contains as many as 80 different proteins (SCHIRMER and GERACE 2005). Among these are several different protein families with distinct nuclear functions, including chromosomal organization, gene expression, and DNA replication and repair (BURNS and WENTE 2012). In metazoans, the INM also associates with the nuclear lamina, a network of lamin filaments that provides physical connections between the INM and the chromatin (HATCH and HETZER 2014).

The trafficking of proteins into the nucleus and INM is mediated by NPCs (BURNS and WENTE 2012), which are large proteinaceous pores embedded at sites of INM and ONM fusion where these membranes merge into one. INM proteins localize both by diffusion retention and by active transport across the NPC channel (LABA *et al.* 2014). Molecules smaller than 40kDa can move freely through NPCs; however, the transport of larger molecules and complexes through the NPC is tightly regulated (FRIED and KUTAY 2003; BURNS and WENTE 2012).

NPC structure

The structure of the NPC is highly conserved among eukaryotes (NEUMANN *et al.* 2010). NPCs are composed of approximately 30 different protein components, called nucleoporins (Nups). These complexes have a predicted mass of 60 MDa in *S. cerevisiae* and 120 MDa in vertebrates and have a uniform diameter of 100-150nm, depending on the organism (LIM and FAHRENKROG 2006; ANTONIN *et al.* 2008; WENTE

and ROUT 2010). The NPC has three domains: the cytoplasmic face, the nuclear face, and the central core, all with an apparent eightfold rotational symmetry (Figure 1.2) (SUNTHARALINGAM and WENTE 2003; ALBER *et al.* 2007b; ANTONIN *et al.* 2008). The cytoplasmic face contains unstructured filaments that extend into the cytoplasm. On the nuclear face, filaments form a structure that extends into the nucleoplasm known as the nuclear basket. The NPC core consists of a series of concentric rings arranged with symmetry across the plane of the NE. These concentric rings comprise three layers: the central channel, the outer and inner structural rings, and the pore membrane (Figure 1.2). The central channel of the NPC is lined with a family of Nups termed FG Nups (ROUT *et al.* 2000; SUNTHARALINGAM and WENTE 2003; ALBER *et al.* 2007b; FERNANDEZ-MARTINEZ and ROUT 2009). These proteins are named for their protein domains that contain phenylalanine-glycine (FG) rich sequences. FG domains are predicted to be unstructured and extend into the pore's channel. Structural Nups found in the outer and inner rings of the central core make up much of the remaining mass of the NPC and provide scaffolding upon which the many other Nups are secured. The outer ring also provides structural support to the NPC. A majority of the outer ring consists of the Nup84 subcomplex (Nup107/160 in metazoans) (SINIOSSOGLOU *et al.* 2000; ALBER *et al.* 2007b; FERNANDEZ-MARTINEZ *et al.* 2012; SHI *et al.* 2014). The inner ring connects the NPC core to the pore membrane and contains the Nup170 subcomplex (Nup155 in metazoans) (ALBER *et al.* 2007b; FLEMMING *et al.* 2009; AMLACHER *et al.* 2011).

Less is known about the organization of proteins at the pore membrane. It is of note that pore membrane proteins are amongst the least conserved in the NPC

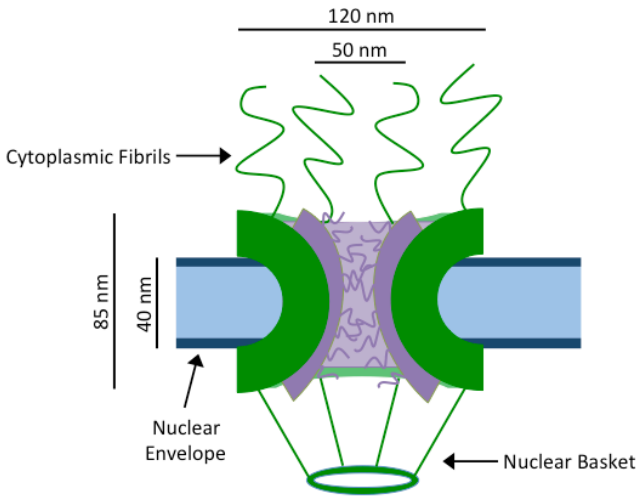

Figure 1.2: The general structure of the NPC.
Schematic of a cross section of an NPC. See text for details. Dimensions labelled are for human NPCs and are derived from measurements taken by cryoEM of human fibroblasts (MAIMON *et al.* 2012).

(NEUMANN *et al.* 2010). Transmembrane pore membrane proteins (Poms) and membrane-associated components of the NPC are predicted to form a ring in the NE and connect soluble Nups to pore membrane surface, anchoring the NPC complex to the NE. Some Poms and membrane associating proteins are predicted to stabilize the high membrane curvature found in nuclear pores at sites of INM and ONM fusion (BECK *et al.* 2007; ANTONIN *et al.* 2008; HETZER and WENTE 2009). Others are thought to act as adapters and associate with soluble structural Nups (NEHRBASS *et al.* 1996; HETZER and WENTE 2009). Finally, the Poms are hypothesized to facilitate transport of transmembrane INM proteins to the NE by establishing and organizing channels in the NPC through which INM proteins may travel (BECK *et al.* 2007; MEINEMA *et al.* 2011; MEINEMA *et al.* 2013).

NPC-mediated transport

The regulation of RNA and protein transport between the nucleus and cytoplasm is a critical step of gene expression. The permeability barrier of the NPC is accomplished via the FG domains of many Nups that extend into the NPC channel (DE SOUZA *et al.* 2004; STRAWN *et al.* 2004; PATEL *et al.* 2007; HULSMANN *et al.* 2012; JOVANOVIC-TALISMAN *et al.* 2014). Whereas FG-Nups provide a permeability barrier to prevent improper nucleocytoplasmic transport, these protein domains also promote the efficient import and export of very large complexes, such as ribosomal subunits, proteasomes, and mRNPs, via direct interactions with transport receptors (ADAMS and WENTE 2013; ENENKEL 2014).

Protein cargoes are targeted for nuclear import and export via short amino acid targeting sequences known as nuclear localization sequences (NLSs) and nuclear export sequences (NESs), respectively (WENTE and ROUT 2010). These localization sequences are recognized by karyopherins (also known as importins and exportins), which mediate the transport of these cargoes through the NPC (ENENKEL *et al.* 1995).

Karyopherins contain binding domains for FG-Nups that facilitate the movement of the karyopherin-cargo complex through the pore (RADU *et al.* 1995; PATEL *et al.* 2007; WENTE and ROUT 2010). There are multiple karyopherins (14 in *S. cerevisiae*, 20 in metazoans) that recognize different transport sequences (FRIED and KUTAY 2003). The transport of karyopherins bound to cargoes is mediated by association with the small GTPase Ran during the nuclear transport cycle (MELCHIOR *et al.* 1993; MOORE and BLOBEL 1993; CORBETT *et al.* 1995). Ran in its GTP bound state is primarily found in the nucleus due to the association of the nucleotide exchange factor RanGEF to DNA (HOPPER *et al.* 1990). Likewise, Ran in its GDP-bound state is concentrated in the cytoplasm as a result of cytoplasmic compartmentalization of RanGAP, which activates the GTPase activity of Ran (BISCHOFF *et al.* 1994; BECKER *et al.* 1995).

This Ran gradient is critical for directional transport of cargoes across the NPC (Figure 1.3A and 1.3B) (MELCHIOR *et al.* 1993; WENTE and ROUT 2010). Once in the nucleus, karyopherin-NLS cargo complexes dissociate via binding of the karyopherin with RanGTP. This promotes export of the karyopherin-RanGTP complex from the nucleus. In the cytoplasm, RanGTP is converted to RanGDP and

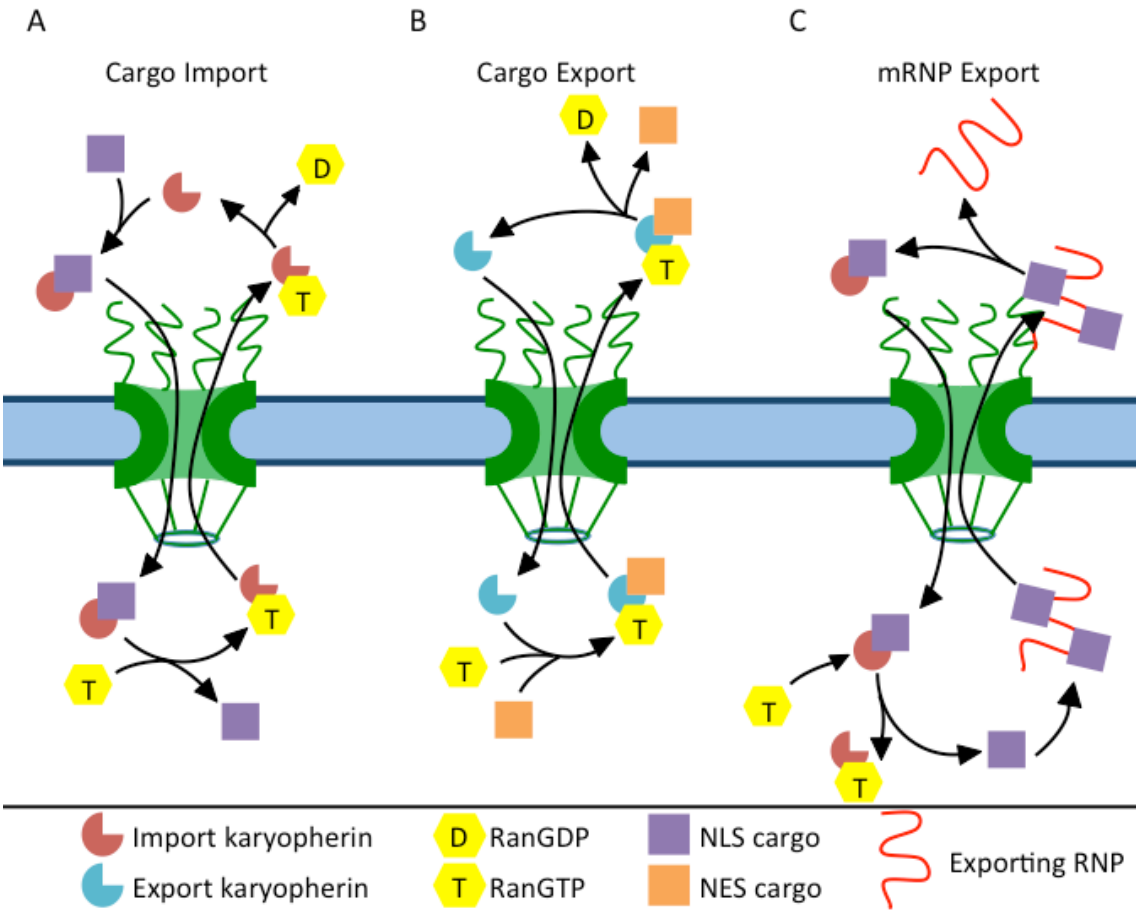

Figure 1.3: Mechanism of nuclear trafficking.
(A) Model of karyopherin mediated nuclear import. (B) Model of karyopherin mediated nuclear export. (C) Transport factors of mRNP export. See text for descriptions and details.

the karyopherin-Ran complex dissociates, freeing the receptor for additional cycles of cargo import (BISCHOFF *et al.* 1994). The export of cargo proteins is regulated in a similar manner. Export complexes are formed as a trimer of the exporting karyopherin, NES-Cargo, and RanGTP. Once in the cytoplasm, RanGAP activates the GTPase activity of Ran, converting RanGTP into RanGDP (BISCHOFF *et al.* 1994; BECKER *et al.* 1995; WENTE and ROUT 2010). This results in the disassociation of the karyopherin complex and the re-import of the karyopherin.

The bulk of mRNPs are exported through a karyopherin independent mechanism (Figure 1.3C). Export of most mRNP complexes is accomplished through association with the transport receptor Mex67-Mtr2 (TAP-p15 in vertebrates) (ERKMANN and KUTAY 2004). This transport receptor associates directly with FG Nups and mediates movement through the NPC via these interactions (TERRY and WENTE 2007). Remodeling of Mex67-Mtr2 from mRNPs regulates directionality of mRNP transport. This occurs at the cytoplasmic face of the NPC by the DEAD box protein Dbp5 (TRAN *et al.* 2007; FOLKMANN *et al.* 2011; HODGE *et al.* 2011; NOBLE *et al.* 2011; FOLKMANN *et al.* 2014). Furthermore, these mRNA transport receptors preferentially bind to different FG Nups in the pore, which could result in further organization of transport through the pore (TERRY and WENTE 2007). The differential regulation of these major pathways of nucleocytoplasmic transport demonstrates the complexity of regulated transport at the NPC.

Disruptions of NE integrity are linked to several diseases. In human laminopathties, genetic disorders caused by mutations in nuclear lamina genes, and in cancer cells, frequent ruptures in the NE are observed, which leads to a

mislocalization of cytoplasmic and nuclear components in the cell (KUSS *et al.* 2013; CAU *et al.* 2014; HATCH and HETZER 2014). Many cancers occur due to improper transport of oncogenes and tumor suppressors that contain NLSs and NESs. The rapid regulation of these factors' localization in response to stress and environmental cues is essential to maintain normal cellular health. In the tumor suppressor BRCA2, point mutations associated with cancer have been identified in the human population in which BRCA2's NES, normally hidden, becomes more exposed. This leads to mislocalization of this BRCA2 mutant to the cytoplasm (JEYASEKHARAN *et al.* 2013). Defects in mRNA export have also been linked to disease. For example, mutations in *GLE1*, the regulator of Dbp5 in mRNP remodeling has been linked to amyotrophic lateral sclerosis and lethal congenital contracture syndrome 1 (FOLKMANN *et al.* 2013; FOLKMANN *et al.* 2014; KANEB *et al.* 2014).

Many viruses disrupt or bypass the mechanisms of nucleocytoplasmic transport in unique ways, including remodeling of the NE. During herpes virus infection, viral proteins induce transport of viral particles from the nucleus to the cytoplasm through budding of the NE, bypassing the NPC completely (HATCH and HETZER 2014). To gain access to the nucleus, parvoviruses also bypass the NPC via rupture of the NE (HATCH and HETZER 2014). Additionally, many viruses target mRNA processing pathways to prevent the efficient export of cellular mRNPs and promote viral mRNA transport (KUSS *et al.* 2013; LE SAGE and MOULAND 2013; YARBROUGH *et al.* 2014). This is achieved through variable strategies including modifications to Nups, targeting Nups for degradation, and sequestration of transport receptors (KUSS *et al.* 2013; YARBROUGH *et al.* 2014).

Evolution of NE and NPC from an ancestral endomembrane system

The morphology of the NE and the interconnection between the NE and the ER suggests a common origin for the NE and ER. Furthermore, evidence indicates that the NE and NPCs coevolved with the endomembrane system as the NE and ER functionally diverged (Figure 1.4) (DEVOS *et al.* 2004; DEGRASSE *et al.* 2009; NEUMANN *et al.* 2010). It is hypothesized that certain NPC components and vesicle coatomers derived from a common ancestral coat protein during this evolutionary process (WILSON and DAWSON 2011). Proteins that comprise the structural rings of the NPC contain structural similarity to COPI and COPII components involved in vesicle trafficking, with both structures consisting of β-propellers and α-solenoids, referred to as ancestral coatomer element 1 domains (ACE1 domains) (DEVOS *et al.* 2004; DEVOS *et al.* 2006; LIM and FAHRENKROG 2006; DEGRASSE *et al.* 2009). Some NPC and vesicle coatomer components have been shown to exhibit shared or overlapping functions at both the NPC and the ER. For instance, the β-propellers Sec13 and Seh1 are key structural components of the *S. cerevisiae* Nup84 subcomplex (Nup107-160 complex in vertebrates) (SINIOSSOGLOU *et al.* 2000; LUTZMANN *et al.* 2002; BROHAWN *et al.* 2008; FIELD *et al.* 2011) and are also required components of vesicle coats (Sec13 in COPII and SEA complexes, Seh1 in SEA complex) (DOKUDOVSKAYA *et al.* 2011).

ER structure

The ER and NE form the largest continuous membrane system in the cell. The structure of the ER is dynamic, and contains regions of flattened sheets as well as a

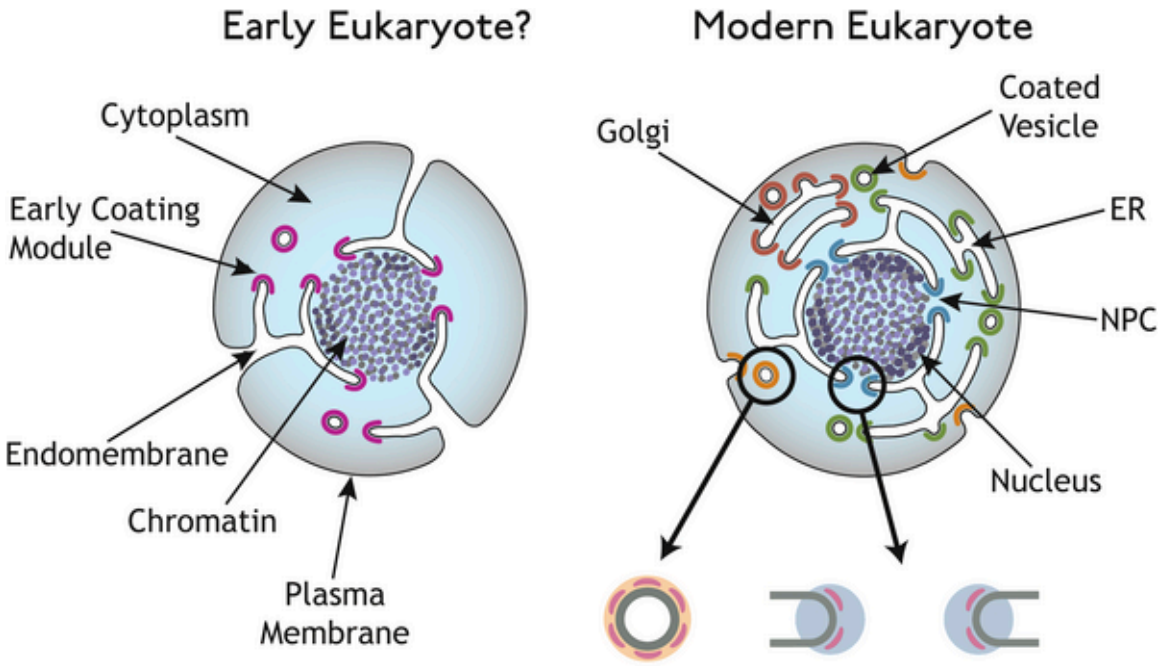

Figure 1.4: Model for the evolution of the NE and NPCs. Reprinted from (DEVOS *et al.* 2004).
The last common eukaryotic ancestor is hypothesized to have one coating complex. The coating complexes of modern eukaryotes have diversified through divergent evolution for multiple tasks including cellular trafficking (shown in green and brown), endocytosis (shown in orange), and NPC formation (shown in blue). Despite functional diversification, these coating complexes retain structural domains (shown in pink) originating in the ancestral coatomer.

network of highly connected membrane tubules (PARK and BLACKSTONE 2010; GOYAL and BLACKSTONE 2013). ER sheets, also referred to as rough ER, are studded with ribosomes and are factories for the biosynthesis of secretory and membrane proteins. The regions of tubular ER, also referred to as smooth ER, are highly reticulated through the formation of three-way tubule branches and are responsible for maintaining the interconnectedness of the whole NE/ER system (CHEN *et al.* 2013). In *S. cerevisiae,* the tubular ER network is positioned just under the plasma membrane and is referred to as the cortical ER. Cytoskeletal dynamics and cortical ER structural proteins maintain these reticulated regions of the ER. Connections to microtubules allow the ER to be regulated with other cellular processes (WATERMAN-STORER and SALMON 1998; FRIEDMAN and VOELTZ 2011; CHEN *et al.* 2013).

The reticulon and DP1/Yop1 families of proteins stabilize the tubular structure of the ER. *In vivo* and *in vitro* studies have demonstrated the shared membrane shaping properties of these proteins. Both reticulons and DP1/Yop1 protein families contain a double hairpin topology that forms a wedge in the outer lipid leaflet of the membrane, promoting positive curvature (Figure 1.5A) (DE CRAENE *et al.* 2006a; FRIEDMAN and VOELTZ 2011; CHEN *et al.* 2013). Furthermore, these proteins self-interact to form large immobile oligomers in membranes. This amplifies positive curvature and induces tubule formation. Indeed, these proteins are both necessary and sufficient for membrane tubule formation. The reticulons and DP1/Yop1 family of proteins also contribute to the maintenance of ER sheets (VOELTZ *et al.* 2006; HU *et al.* 2008; SHIBATA *et al.* 2008; SHIBATA *et al.* 2010). At these locations, oligomers of these proteins associate with the curved edges of these

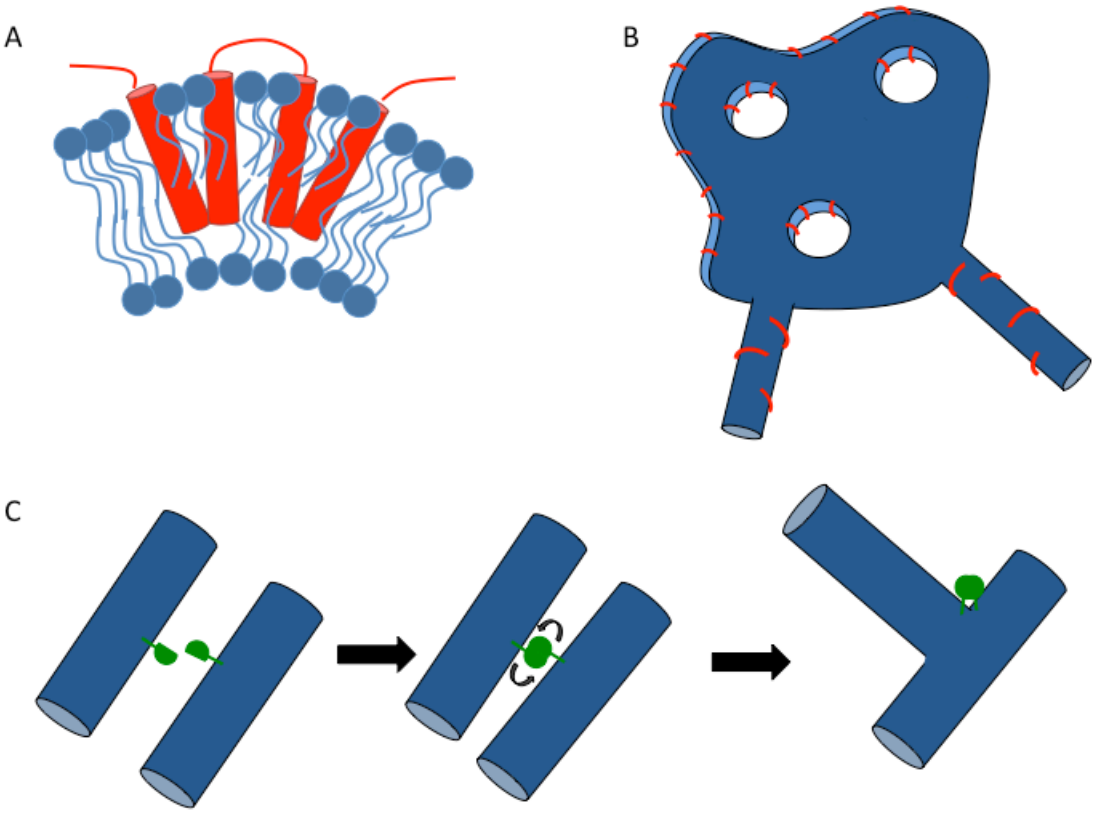

Figure 1.5: Membrane shaping proteins of the ER.
(A) Reticulons and DP1/Yop1, shown in red, stabilize curvature via hairpin-forming transmembrane domains. (B) Reticulons and DP1/Yop1, shown in red, localize to regions of positive curvature in oligomer complexes. These include ER tubules, edges of cisternae, and pores. (C) Model for Sey1 (Atlastin in metazoans), shown in green, mediated fusion of ER tubules. See text for details. Adapted from (FRIEDMAN and VOELTZ 2011)

flattened sheets, stabilizing these regions of curvature and maintaining the lumenal spacing of these formations (Figure 1.5B) (SHIBATA *et al.* 2010; CHEN *et al.* 2013).

The cortical ER is also highly connected, consisting of a network of tubules connected by three-way junctions. These junctions form by the fusion of two tubules (Figure 1.5C) (CHEN *et al.* 2013). This fusion process is mediated by Atlastins (Sey1 in *S. cerevisiae*). Atlastins form a homotypic dimer across opposite membranes in the ER. This dimerization is predicted to induce the GTPase activity of the atlastins and results in a protein conformation change that compels fusion of the two lipid bilayers (Figure 1.5C) (HU *et al.* 2009; ORSO *et al.* 2009; BIAN *et al.* 2011; BYRNES and SONDERMANN 2011).

The network of ER tubules is also mediated by Lnp1, a member of the Lunapark family of proteins (CHEN *et al.* 2012). Lnp1 localizes to three-way junctions in the cortical ER and at ER/NE connections. In *S. cerevisiae,* loss of Lnp1 results in regions of collapsed cortical ER as well as regions of more densely reticulated ER. Recent work from the Ferro-Novick lab found that presence of Lnp1 foci at three-way junctions correlates with increased lifespan and decreased mobility of these structures, indicating that Lnp1 could mediate the dynamics of the ER network through stabilizing three-way junctions (CHEN *et al.* 2014). Whereas both Sey1 and Lnp1 function in conjunction with the reticulons and Yop1/DP1, the relationship between Sey1 and Lnp1 suggests functional antagonism in the assembly and disassembly of the ER network (CHEN *et al.* 2012; CHEN *et al.* 2013).

NPC assembly

Post-mitotic assembly of NPCs

NPCs are assembled in two distinct processes: post-mitotic NPC assembly and interphase assembly, also known as *de novo* assembly. In most eukaryotes, cells undergo an open mitosis. The NE and NPCs disassemble during prophase, disrupting the compartmentalization of the nucleus from the cytoplasm. NPCs are then assembled during NE reformation. To initiate the breakdown of the NE, phosphorylation of several Nups in the pore results in the disassociation of NPC proteins and subcomplexes from the pore (HETZER *et al.* 2005). Several NPC components have additional functions in mitosis at the spindle and kinetochores, linking NPC disassembly with progression through mitosis (ANTONIN *et al.* 2008; GUTTINGER *et al.* 2009; HETZER 2010a). Microtubule attachments to the NE exert physical force on the NE, resulting in the formation of additional holes in the NE (BEAUDOUIN *et al.* 2002; SALINA *et al.* 2002). The nuclear lamina is also deconstructed as lamins depolymerize, detach from the NE, and release into the nucleoplasm (GERACE and BLOBEL 1980). Breakdown of the NE occurs to allow the microtubule-organizing center of the cell to gain access to the chromosomes during mitosis (GUTTINGER *et al.* 2009). The membranes of the NE and its associated proteins are absorbed into the ER (LIU *et al.* 2003).

After the chromosomes are properly segregated, the NE reforms around the daughter nuclei, and post-mitotic NPC assembly is initiated concurrently. The Nup107-160 complex, via a physical interaction with the chromatin binding factor ELYS, seeds sites of NPC assembly (Figure 1.6) (GUTTINGER *et al.* 2009). These

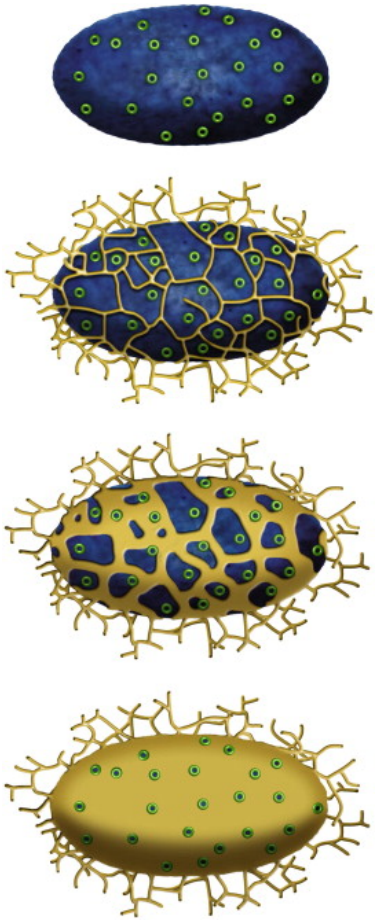

Figure 1.6 Model for post-mitotic nuclear envelope assembly. Reprinted from (ANTONIN *et al.* 2008).
Sites of NPC assembly (green) are seeded on chromatin (blue) and form pre-pore structures. The NE is reformed from networks of ER tubules that flatten to form a NE sheet and anchor NPCs. See text for details.

prepore structures recruit other Nups and associate with the membranes and Poms from the reforming NE to produce a fully assembled pore. There are two models for how NPC assembly is accomplished (ANTONIN *et al.* 2008). One model proposes prepores are inserted into flattened sheets of the NE, requiring fusion of the reforming ONM and INM (see *de novo* assembly below). The second model predicts that prepore complexes are surrounded by membranes of the reforming NE and are integrated into these flattened sheets at this time. Reformation of the NE occurs through the recruitment of NE proteins to the nuclei via cortical ER tubules (ANDERSON and HETZER 2008; ANTONIN *et al.* 2008; FICHTMAN and HAREL 2014). Poms are predicted to localize to the tips of ER tubules and aid in this recruitment via interactions with prepore structures and DNA (GUTTINGER *et al.* 2009). Furthermore, the organization of reticulons in the ER tubules must be altered to allow for the development of flattened NE sheets (ANDERSON and HETZER 2008). INM proteins associate with chromatin, stabilizing flattened membranes around the nucleus (GUTTINGER *et al.* 2009). Finally, these membrane sheets must close to form one continuous sheet around the nucleus. *In vitro* studies have found SNAREs may mediate this fusion event, but whether they are required *in vivo* remains unclear (BAUR *et al.* 2007). Furthermore, NPC assembly between forming sheets could also aid in this process.

De novo assembly of NPCs

The second mode of NPC biogenesis is known as *de novo* assembly. In eukaryotes that undergo an open mitosis, such as many fungi, this form of assembly

occurs during interphase, resulting in the alternate name of interphase assembly. The number of NPCs found in the nuclei of metazoans can vary based on cell activity and thus must be regulated through *de novo* assembly (MAUL *et al.* 1971; MAESHIMA *et al.* 2011). Furthermore, eukaryotes that undergo a closed mitosis, such as *S. cerevisiae,* utilize this mode of NPC biogenesis exclusively. It is not known what event initiates the formation of a new NPC; however, the other steps in *de novo* assembly are more defined. Structural NPC components must be recruited to both the nuclear and cytoplasmic faces of the NE for *de novo* assembly to occur (D'ANGELO *et al.* 2006; ANTONIN *et al.* 2008; FERNANDEZ-MARTINEZ and ROUT 2009). Cytoplasmic and nuclear facing Nups assemble into soluble subcomplexes and localize to the appropriate NE face as well (MAKIO *et al.* 2009).

The next step in *de novo* assembly is the formation of a nascent pore in the NE via the fusion of the INM and ONM (Figure 1.7) (D'ANGELO *et al.* 2006; ANTONIN *et al.* 2008). Multiple studies using cell culture and *Xenopus* extracts indicate that the rate-limiting step in *de novo* assembly is this fusion event (DOUCET *et al.* 2010; DULTZ and ELLENBERG 2010; FICHTMAN *et al.* 2010; TALAMAS and HETZER 2011). Once NE fusion has occurred, the membranes of nascent pores and fully formed NPCs contain regions of high positive and negative curvature that must be stabilized (ANTONIN *et al.* 2008). Structural components such as the Nup84 subcomplex in *S. cerevisiae* (Nup107/160 complex in metazoans) are predicted to stabilize the curved surface of the nuclear pore via membrane bending properties common to many coatomers (BROHAWN *et al.* 2008; LEKSA and SCHWARTZ 2010). The Nup84 subcomplex also contains ArfGAP1 lipid packing sensor (ALPS) motifs that could contribute to the

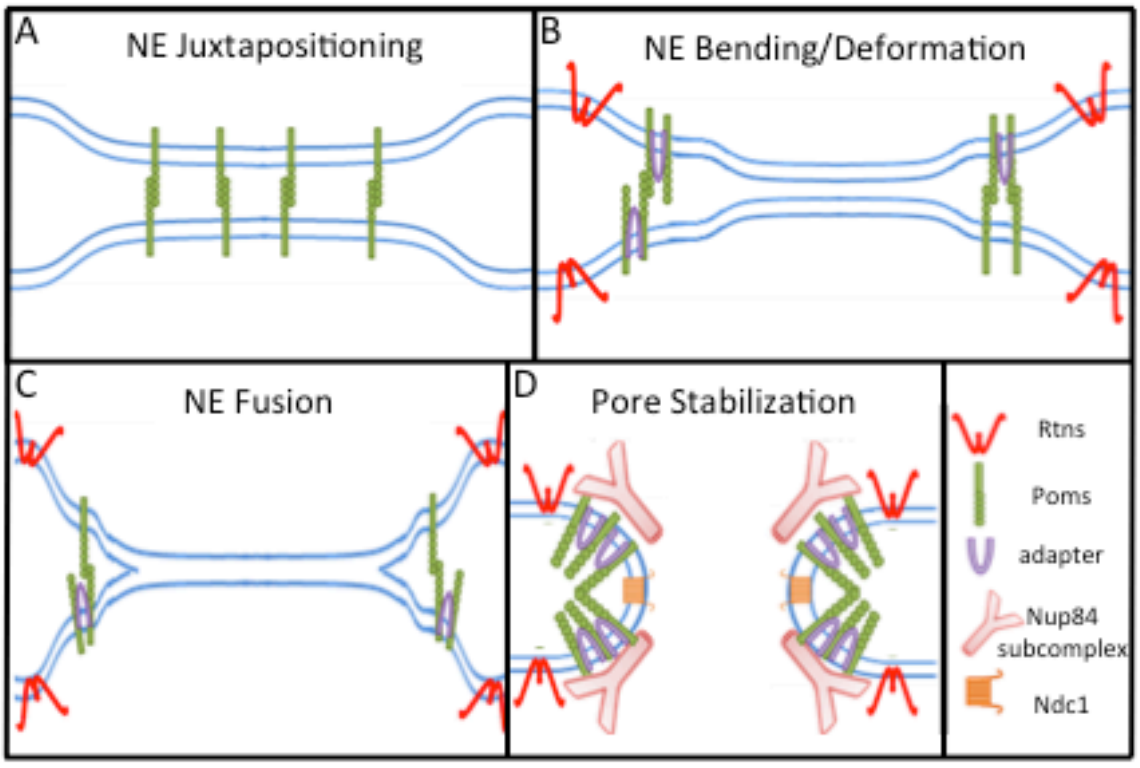

Figure 1.7: Model for *de novo* pore assembly.
NPC assembly into an intact NE is a stepwise process that must initiate with the fusion and stabilization of a nascent pore. (A) Membrane components of the NPC, aka Poms, mediate lumenal interactions across the NE, juxtapositioning the INM and ONM and initiating NE deformation. (B-C) Poms mediate NE fusion events through membrane deformation. The membrane proteins Rtn1 and Yop1, through their ability to stabilize positive curvature, play a role stabilizing these fusion events. (D) Once the NE has fused, the nascent pore is stabilized by the addition of Poms and structural Nups, which provide a scaffold upon which more interior nups assemble.

recruitment of this subcomplex to nascent pores (DRIN *et al.* 2007; DOUCET *et al.* 2010; KIM *et al.* 2014). These structural protein complexes also provide a scaffold upon which other Nups assemble (ALBER *et al.* 2007b; DRIN *et al.* 2007; HSIA *et al.* 2007; BROHAWN and SCHWARTZ 2009).

Roles of membrane proteins in NE fusion, NPC assembly, and stability

The mechanism by which fusion of the NE is mediated during nuclear pore formation is not known; however, Poms and membrane-associated proteins are predicted to play a critical role in this process (Table 1.1). Physical interactions of Pom lumenal and cytoplasmic domains are proposed to induce and stabilize membrane deformation (ANTONIN *et al.* 2008; DOUCET and HETZER 2010; TALAMAS and HETZER 2011; YEWDELL *et al.* 2011). For example, in mammalian cells, the lumenal interactions of Pom121 have been implicated in NE juxtapositioning and membrane deformation in early pore formation (DULTZ and ELLENBERG 2010; TALAMAS and HETZER 2011). In *S. cerevisiae,* Pom152 mediates lumenal interactions and may perform a similar function (TCHEPEREGINE *et al.* 1999; YEWDELL *et al.* 2011). Pom152 also interacts in complex with Ndc1 and Pom34 at the cytoplasmic face of the pore membrane. This complex is predicted to form the bulk of the pore membrane ring of the NPC (ONISCHENKO *et al.* 2009).

The importance of Poms in NPC assembly is supported by the identification of the Poms Ndc1 and gp210 as key components in the NPC of all eukaryotic supergroups (WILSON and DAWSON 2011). Of the known Poms, Ndc1 has been

Table 1.1: NE proteins connected to NPC assembly.

S. cerevisiae homolog	Vertebrate homolog	Confirmed Localization				Topology
		NPC	SPB	ER	INM	
Ndc1	Ndc1	X	X		X	6 transmembrane domains N and C-terminus cytoplasmic
Pom152	-	X			X	Single transmembrane domain N-terminus cytoplasmic C-terminus lumenal
Pom34	-	X			X	2 transmembrane domains N and C-terminus cytoplasmic
Pom33	TMEM33	X		X		6 transmembrane helices N and C-terminus cytoplasmic
Per33	TMEM33	X		X		6 transmembrane helices N and C-terminus cytoplasmic
Nup53	Nup53(Nup35)	X			X	Membrane binding amphipathic helix cytoplasmic
Nup59	Nup53(Nup35)	X			**X**	Membrane binding amphipathic helix cytoplasmic
Heh1	Man1 and Lem2	X			X	Double transmembrane domain N and C-terminus cytoplasmic
Heh2	Man1 and Lem2	X			X	Double transmembrane domain N and C-terminus cytoplasmic
-	Pom121	X			X	Single transmembrane domain N-terminus lumenal C-terminus cytoplasmic C-terminal FG Domains
-	Gp210	X			X	Single transmembrane domain N-terminus lumenal C-terminus cytoplasmic
Rtn1	Reticulon Family	X		X		Double hairpin transmembrane domains N and C-terminus cytoplasmic
Yop1	DP1 Family	X		X		Double hairpin transmembrane domains N and C-terminus cytoplasmic
Lnp1	Lnp1			X		Double transmembrane domain
Sey1	Atlastins			X		Double transmembrane domain N and C-terminus cytoplasmic

characterized as the most conserved and critical for NPC assembly (MANS *et al.* 2004; ANTONIN *et al.* 2008; ONISCHENKO *et al.* 2009). Depletion of Ndc1 leads to severe defects in Nup localization and a block in NPC assembly (MADRID *et al.* 2006). In *S. cerevisiae,* Ndc1 is required for NPC assembly as well as SPB formation (MADRID *et al.* 2006). Ndc1 associates with several distinct subcomplexes at the NPC, including Pom152 and Pom34, Nup170/Nup157, and Nup53/Nup59 (MADRID *et al.* 2006; FLEMMING *et al.* 2009; ONISCHENKO *et al.* 2009). Studying Ndc1 in *S. cerevisiae* has been a challenge in the field for many reasons. Because Ndc1 is a required component of the SPB, *ndc1* mutants lead to defects in mitosis, aneuploidy, and cell death, which can both mask and confound any observable NPC defects. Purification of this six transmembrane domain protein is highly challenging, a further obstacle to biochemical analysis of Ndc1. Furthermore, exogenous expression of *NDC1* results in defects in mitosis (CHIAL *et al.* 1999), which makes mutational dissection of *NDC1* a challenge.

Several lines of evidence support the role of Poms and membrane-associated Nups in stabilizing curvature at nuclear pores (FERNANDEZ-MARTINEZ and ROUT 2009; HETZER and WENTE 2009; DOUCET and HETZER 2010). For example, both metazoan and *S. cerevisiae* Nup53 contain an amphipathic helix that associates with membranes upon homo-dimerization. Furthermore, the association of Nup53 with membranes results in membrane deformation *in vitro* (VOLLMER et al. 2012). Additionally, members of the reticulon and Yop1/DP1 family, Rtn1 and Yop1, aid in these membrane processes (DAWSON *et al.* 2009; DOUCET and HETZER 2010). Loss of Rtn1 and Yop1 in *S. cerevisiae* results in defects in NPC function and NPC instability

in the NE. Both *rtn1* and *yop1* mutants genetically interact with components of the NPC with roles in assembly (DAWSON *et al.* 2009; CHADRIN *et al.* 2010). Furthermore, depletion of Rtn4a in *Xenopus* extracts blocks *de novo* pore formation *in vitro* (DAWSON *et al.* 2009). Colocalization of Rtn1 and Yop1 at NPC clusters indicates that these ER proteins localize to nuclear pores. This supports a direct role for Rtn1 and Yop1 in NPC stability (DAWSON *et al.* 2009).

Because of the established membrane-bending properties of these proteins, I hypothesize that Rtn1 and Yop1 stabilize the curvature of the nuclear pore, which leads to secure anchoring of the NPC. Furthermore, Rtn1 and Yop1 may play a role in the formation of a nascent pore by stabilizing the curvature of deformed membranes during NE fusion. Genetic interactions between *rtn1Δ yop1Δ* and *pom152Δ* indicate that these membrane proteins may have redundant functions at the pore. This is also indicated by the rescue of *rtn1Δ yop1Δ* NPC defects by *POM152* or *NDC1* overexpression (DAWSON *et al.* 2009). Because Pom152 is predicted to work together with the required NPC insertion factor Ndc1, further analysis of the functional interactions between Rtn1, Yop1, and Ndc1 could reveal the mechanisms by which Ndc1 and Pom152 function.

In *S. cerevisiae* NE fusion is also required in the formation and insertion of the SPB, and Ndc1 is also a required in this process. In chapter 2, I examined if Rtn1 and Yop1 are required for the insertion of spindle pole bodies (SPBs) of *Saccharomyces cerevisiae*. Electron microscopy of *rtn1Δ yop1Δ* cells revealed lobular abnormalities in SPB structure**.** Furthermore, large budded *rtn1Δ yop1Δ* cells exhibited a high incidence of short mitotic spindles, which were frequently

misoriented with respect to the mother-daughter axis. This correlated with cytoplasmic microtubule defects. We found that overexpression of the SPB insertion factors *NDC1*, *MPS2*, or *BBP1* rescued the SPB defects observed in *rtn1Δ yop1Δ* cells. However, only overexpression of *NDC1,* which is also required for NPC biogenesis, rescued both the SPB and NPC associated defects. I propose that NPC and SPB biogenesis are altered in cells lacking Rtn1 and Yop1 due to competition between NPCs and SPBs for Ndc1, an essential assembly component of both complexes.

The interconnection and common evolutionary history of the tubular ER and nuclear pores suggests that multiple proteins may be shared between these membrane structures. In addition to Rtn1 and Yop1, the *S. cerevisiae* membrane proteins Pom33 and Per33 also contribute to NPC structure. Pom33 and its homolog Per33 both localize to NPCs and the ER (CHADRIN *et al.* 2010). Both Pom33 and Per33 genetically interact with NPC components as well as having physical interactions with Rtn1 and Pom34 (CHADRIN *et al.* 2010). Furthermore, loss of Pom33 or Per33 in *S. cerevisiae* (or Tts1 its homolog in *S. pombe*) results in defects in NPC distribution (CHADRIN *et al.* 2010; ZHANG and OLIFERENKO 2014). I predict that identification of additional shared components between the ER and NPCs will shed light on the mechanisms that stabilize membrane structures at both of these unique but connected environments.

In chapter 3, I identified NE roles for Lnp1 and Sey1, proteins required for proper cortical ER formation in *S. cerevisiae*. I characterized both genetic and physical interactions that link Lnp1 and Sey1 to the NPC. Both *lnp1Δ* and *sey1Δ* mutants exhibit synthetic genetic interactions with mutants in genes encoding key

NPC structural components. Both Lnp1 and Sey1 physically associate with other ER components that have established NPC roles including Rtn1, Yop1, Pom33, and Per33. Interestingly, *lnp1Δ rtn1Δ* mutants but not *rtn1Δ sey1Δ* mutants exhibit defects in NPC distribution. Furthermore, the essential NPC assembly factor Ndc1 has altered interactions in the absence of Sey1. Lnp1 dimerizes *in vitro* via its C-terminal zinc-finger motif, a property that is required for proper ER structure but not NPC integrity. My findings suggest that Lnp1's role in NPC integrity is separable from functions in the ER and is linked to Ndc1 and Rtn1 interactions.

CHAPTER II

INTEGRITY AND FUNCTION OF THE SACCHAROMYCES CEREVISIAE SPINDLE POLE BODY DEPENDS ON CONNECTIONS BETWEEN THE MEMBRANE PROTEINS NDC1, RTN1, AND YOP1.

INTRODUCTION

The nuclear envelope (NE), which physically separates the nucleoplasm from the cytoplasm, is a characteristic feature of all eukaryotic cells and structurally based upon two distinct yet connected membrane bilayers. These NE membranes harbor specialized functions, with the outer nuclear membrane (ONM) continuous with the endoplasmic reticulum (ER) and the inner nuclear envelope (INM) having a unique protein composition (SCHIRMER *et al.* 2003; LUSK *et al.* 2007; ANTONIN *et al.* 2011). However, specific connections between the ONM and INM are critical for cell function. For example, ONM protein-INM protein interactions that bridge the perinuclear space are required for nuclear positioning (HIRAOKA and DERNBURG 2009; RAZAFSKY and HODZIC 2009). Moreover, the ONM and INM are specifically fused at sites of nuclear pores (DOUCET and HETZER 2010). The NE is further distinguished by the presence of large protein assemblies; for example, the nuclear pore complex (NPC) found in all eukaryotes and the spindle pole body (SPB) in the budding yeast

---

This chapter is adapted from "Integrity and Function of the *Saccharomyces cerevisiae* Spindle Pole Body Depends on Connections Between the Membrane Proteins Ndc1, Rtn1, and Yop1. Amanda K Casey, T. Renee Dawson, Jingjing Chen, Jennifer M. Friederichs, Sue L. Jaspersen, Susan R. Wente. Genetics, 2012 Oct; 192(2):441-55."

Saccharomyces cerevisiae. A full understanding of the dynamics between the NE membranes and its different NE protein assemblies has not yet been achieved.

The NPCs in the NE are responsible for regulating the trafficking of macromolecules between the nucleoplasm and cytoplasm, and between the ONM and INM (LUSK *et al.* 2007; TETENBAUM-NOVATT and ROUT 2010). As >60 MDa proteinaceous complexes, the NPCs are assembled from ~30 different proteins termed nucleoporins (Nups) or pore membrane proteins (Poms) with each Nup or Pom present in multiples of eight-fold stoichiometry (8, 16, or 32 copies) (ALBER *et al.* 2007b). NPCs have structurally distinct modules: the nuclear basket filaments, the cytoplasmic filaments, the outer, central and lumenal rings, and a set of linker complexes (Figure 1.2). In the closed mitosis of *Saccharomyces cerevisiae* and during metazoan interphase, all NPCs assemble *de novo* into an intact NE (D'ANGELO *et al.* 2006; ALBER *et al.* 2007b; ANTONIN *et al.* 2008; BROHAWN *et al.* 2008; BROHAWN *et al.* 2009; CAPELSON *et al.* 2010; TALAMAS and HETZER 2011). This NPC biogenesis mechanism requires a multistep process that is dependent on both ONM and INM events. The first steps of *de novo* NPC assembly require ONM/INM fusion and stabilization of the resulting highly curved pore membrane, a process that is not yet fully understood (D'ANGELO *et al.* 2006; ANTONIN *et al.* 2008; FERNANDEZ-MARTINEZ and ROUT 2009; DOUCET and HETZER 2010; TALAMAS and HETZER 2011). Membrane bending and curvature-stabilizing proteins, as well as potential changes in lipid composition, are likely required (DOUCET and HETZER 2010). Current models propose that the initial pore fusion event is mediated by NPC-associated Poms. In *S. cerevisiae*, this potentially includes Ndc1, Pom152, Pom34, and Pom33. (MADRID *et*

al. 2006; MANSFELD *et al.* 2006; ANTONIN *et al.* 2008; HETZER and WENTE 2009; ONISCHENKO *et al.* 2009; CHADRIN *et al.* 2010; DOUCET and HETZER 2010). In addition, an early step in *de novo* NPC biogenesis requires the Reticulons (Rtn) and Yop1/DP1 (DAWSON *et al.* 2009; CHADRIN *et al.* 2010), proteins in the outer membrane leaflet that act to stabilize/maintain membrane curvature (DE CRAENE *et al.* 2006b; VOELTZ *et al.* 2006; HU *et al.* 2008; WEST *et al.* 2011). Post-fusion of the INM and ONM, the Rtns and Yop1/DP1 are speculated to transiently localize at and stabilize the nascent pore (DAWSON *et al.* 2009; HETZER and WENTE 2009). The subsequent recruitment of peripheral membrane Nups would maintain the curved pore membrane and provide a scaffold on which other Nups then assemble.

The *S. cerevisiae* SPB is the functional equivalent of the centrosome, nucleating both cytoplasmic microtubules involved in nuclear positioning and cytoplasmic transport as well as nuclear microtubules required for chromosome segregation (BYERS and GOETSCH 1975). Much like the NPC, the SPB is a modular structure and is formed by five sub-complexes: the γ-tubulin complex that nucleates microtubules, the linker proteins that connect the γ-tubulin complex to the cytoplasmic and nuclear face of the core SPB, the soluble core SPB/satellite components that form the foundation of the SPB and SPB precursor, the membrane anchors that tether the core SPB in the NE and the half-bridge components that are important for SPB assembly (JASPERSEN and WINEY 2004). Duplication of the ~0.5 GDa SPB begins with formation of a SPB precursor, known as the satellite, at the distal tip of the half-bridge (ADAMS and KILMARTIN 1999). Continued expansion of the satellite by addition of soluble precursors, and expansion of the half-bridge, leads to

the formation of a duplication plaque. The SPB is then inserted into a pore in the NE, allowing for assembly of nuclear components to create duplicated side-by-side SPBs (BYERS and GOETSCH 1974; BYERS and GOETSCH 1975; ADAMS and KILMARTIN 1999; JASPERSEN and WINEY 2004; WINEY and BLOOM 2012). The membrane anchors and half-bridge components both play a role in this SPB insertion step (WINEY *et al.* 1991; WINEY *et al.* 1993; SCHRAMM *et al.* 2000; ARAKI *et al.* 2006; SEZEN *et al.* 2009; WITKIN *et al.* 2010; FRIEDERICHS *et al.* 2011; KUPKE *et al.* 2011; WINEY and BLOOM 2012). Unlike NPC assembly, SPB duplication is spatially and temporally restricted. The new SPB is assembled during late G1 phase, approximately 100 nm from the pre-existing SPB (BYERS and GOETSCH 1975). However, although the exact mechanism of SPB insertion is unknown, its insertion into the NE is thought to require the formation of a pore membrane similar to that found at the NPC.

Interestingly, previous studies have revealed physical and/or functional links between the factors required for NPC and SPB assembly and integrity. One of the SPB membrane anchors is Ndc1, a conserved integral membrane protein that is also an essential NPC Pom and required for NPC assembly (CHIAL *et al.* 1998; MANSFELD *et al.* 2006; STAVRU *et al.* 2006; KIND *et al.* 2009). Some NPC components are required for proper remodeling of SPB core components and regulation of SPB size (NIEPEL *et al.* 2005; GREENLAND *et al.* 2010), whereas the loss of other NPC components rescues SPB mutant assembly phenotypes (CHIAL *et al.* 1998; SEZEN *et al.* 2009; WITKIN *et al.* 2010). The exact mechanism by which all of these NPC components influence SPB assembly is not known. With the relationships between NPC and SPB biogenesis, I examined *S. cerevisiae* cells lacking Rtn1 and Yop1 for altered SPB structure and

function. Indeed, I found perturbations in SPB integrity and NE attachment that were rescued by Ndc1 overproduction. Physical and genetic data indicated that Ndc1 function at NPCs is specifically altered in *rtn1 null (Δ) yop1Δ* cells. I propose that these observations reflect the known dual requirement for Ndc1 in both NPC and SPB assembly and pinpoint a role for Rtn1 and Yop1 in Ndc1 function at the NPC. These results also further implicate the role of Ndc1 in a common NPC and SPB biogenesis step that potentially requires NE membrane remodeling events for pore formation and complex insertion.

MATERIALS AND METHODS

Yeast strains and plasmids

All strains and plasmids used in this study are listed Tables C1 and D2 (Appendix C and D). Strains denoted with SWY are derived from the BY4741 and BY4742 S288C lineage, whereas SLJ strains are derivatives of W303. Unless otherwise noted, yeast genetic techniques were performed by standard procedures described previously (SHERMAN *et al.* 1986), and yeast were transformed by the lithium acetate method (ITO *et al.* 1983). All strains were cultured in either rich (YPD: 1% yeast extract, 2% peptone, and 2% dextrose) or complete synthetic minimal (CSM) media lacking appropriate amino acids and supplemented with 2% dextrose. Kanamycin resistance (conferred by the KAN^R gene) was selected on medium containing 200 μg/ml G418 (US Biological). Yeast were serially diluted and spotted onto YPD to assay fitness and temperature sensitivity as previously described (TRAN *et al.* 2007).

The plasmids pSW3673, pSW3674, pSW3675 and pSW3676 were generated by subcloning genomic DNA fragments containing the coding sequence, promoter and 3'-UTR into the SacI and SacII sites of pRS425. For *MPS2*, a 2.5kb genomic fragment was isolated by PCR amplification with Klentaq-LA (Sigma) using primers 5'-TCGACCGCGGTGGTGGAAGGTTTCCTTGAG-3' and 5'-CGCATCTGAGCTGTAACATGACTCGAGTCGA-3'. A 2.2kb *BBP1* genomic fragment was amplified with 5'-TCGACCGCGGCGTGCGATACGCAAATAGAA-3' and 5'-CGGGAATTACAGCTCGTGTTCTCGAGTCGA-3', 1.6kb, 1.9kb) into SacI and SacII sites of pRS425 (CHRISTIANSON *et al.* 1992). Likewise, *APQ12* and *BRR6* were isolated in 1.6 kb and 1.9 kb PCR fragments, respectively using the primers (5'-TCGACCGCGGCGAATCCGTCAACGAGTTTT-3', 5'-CAATGCTGCTGCTGTTGTTTCTCGAGTCGA-3'), and (5'-TCGACCGCGGTTAAAGAGGCAGGGAGAGCA-3',5'-TCCACAAGTTGGAAGTGCATCTCGAGTCGA-3') .

The plasmid pSW3594 (for amino(N)-terminal tagging with GFP) was generated by subcloning the GFP coding sequence into pSW3447 at HindIII and SalI using the oligos 5'-GCATAAGCTTATGAGTAAAGGAGAAGAACTTTTCACT-3' and 5'-GTACGTCGACgtTTTGTATAGTTCATCCATGCCATG-3'. The *GFP-TUB3* integration cassette was generated by PCR from this plasmid using the oligonucleotides 5'-GATCAGGTATCTCATAAAGTACATTAATCGACTAAGCAAGCGACTTGAGACAATGAGTAAAGGAGAAGAACTTTTCACTGGAGTTGTCCC3' and 5'-CCAGCATGCATTACCTATTTGACAACCTGCTTGACCAACATTAATACTAATGACCTCTCTAGTGGATCTGATATCACCTA-3'. Integration of the *GFP-TUB3-HIS5* cassette and

excision of the *HIS5* marker sequence were accomplished as previously described (TERRY and WENTE 2007).

Cell cycle arrest

Wild type and *rtn1Δ yop1Δ* cells were arrested at different stages in the cell cycle by the addition of hydroxyurea (HU) (Sigma), nocodazole (Sigma) or alpha (α)-factor (ZymoResearch) at a concentration of 200 mM, 2.5 μg/ml or 5 μg/ml, respectively as described (JACOBS *et al.* 1988). Arrest was observed as 95% population synchronization by phase contrast microscopy. For HU arrest, early log phase (O.D. 0.2) cultures of wild type (YOL183) and *rtn1Δ yop1Δ* (SWY3811) cells were arrested in YPD for 3 hr at 30°C. For indirect immunofluorescence, cells were fixed in 3.7% formaldehyde for 1.5 hr at room temperature and processed as described (STRAWN *et al.* 2004) with mouse α-alpha tubulin (clone DM1A, 1:200, Sigma). Bound antibodies were detected by incubation with Alexa Fluor 594-conjugated goat α-mouse IgG (1:300, Molecular Probes). Samples were washed and mounted for imaging in 90% glycerol and 1 mg/ml *p*-phenylenediamine, pH 8.0. All images were taken on a confocal microscope (LSM 510; Carl Zeiss, Inc.) with a 63× Plan-Apochromat 1.4 NA oil immersion lens at a zoom of 4. Fluorescence was acquired using a 543-nm laser and an LP560-nm long pass filter. Images were processed with ImageJ (National Institutes of Health; (ABRAMOFF *et al.* 2004) and Adobe Creative Suite 4 (Adobe).

For nocodazole release experiments, cells were grown to an OD_{600} of 0.15 in YPD with 1% DMSO at 23°C and arrested for 3.5 hr. Cells were washed two times

with cold CSM, suspended in room temperature CSM and plated onto small CSM agarose pads on VALAP sealed slides. To visualize spindles in live cells, endogenously expressed GFP-Tub3 was used. Since Tub3 is a minor component of microtubules, I reasoned that tagging *TUB3* would be less detrimental to microtubule function than tagging *TUB1*. Live cell results using GFP-Tub3 were consistent with IF results stained for Tub1 (data not shown). For time-lapse microscopy, Z stacks of bright field and direct GFP-Tub3 epifluorescence were taken for individual cells every 5 min using a microscope (BX50; Olympus) equipped with a motorized stage (Model 999000, Ludl), a UPlanF1 100X NA 1.30 oil immersion objective and digital charge coupled device camera (Orca-R^2; Hamamatsu). Images were collected and scaled using Nikon Elements and processed with ImageJ or Photoshop 12.0 software.

To monitor spindle dynamics following α-factor arrest, cells were grown to an OD_{600} of 0.15 at 30°C in YPD, pH 3.9 and then arrested for 2 hr at 30°C. Cells were washed twice with equal volumes of YPD, pH 6.5, suspended in fresh YPD equal to the original volume and incubated at 30°C. At 15 min intervals, cell samples were fixed for indirect immunofluorescence as described (STAGE-ZIMMERMANN *et al.* 2000) and mounted on slides. Asynchronous cell populations expressing endogenous GFP-Tub3 were also imaged using a microscope (BX50; Olympus) equipped with a motorized stage (Model 999000, Ludl), a UPlanF1 100X NA 1.30 oil immersion objective and digital charge coupled device camera (Orca-R^2; Hamamatsu). Images were collected and scaled using Nikon Elements and processed with ImageJ or Photoshop 12.0 software. Images of cells were scored by bud index and position of

SPB or spindle within the cell. Large budded cells were counted and scored as having separate GFP positive foci in mother and daughter bud (post mitosis), GFP positive foci in mother and daughter bud connected by GFP positive spindle (anaphase spindle), or GFP positive foci connected by spindle sequestered the mother bud (pre-anaphase spindle). Pre-anaphase spindles were considered misaligned if the closest SPB within the cell was greater than 1 μm from the bud neck, or greater than 60 degrees different than the mother bud axis.

GFP-Tub1/Spc42-mCherry images were acquired with a 100X 1.4 NA oil objective on an inverted Zeiss 200m equipped with a Yokagawa CSU-10 spinning disc. 488 nm excitation and 568 nm excitation were used for GFP and mCherry, respectively, and emission was collected through BP 500-550 nm and BP 590-650 nm filters, respectively, onto a Hamamatsu EMCCD (C9000-13). For each channel, a Z-stack was acquired using 0.6 or 0.7 micron spacing. 13 total slices were acquired and a maximum projection image was created using ImageJ (NIH).

Hydroxyurea Survival

To assay recovery from arrest at early S phase, 200 mM HU was added to wild type (YOL183) and *rtn1Δ yop1Δ* (SWY3811) cells at an O.D. of 0.15 in YPD with 1% DMSO. Cells were incubated for 6 hr at 30°C, washed in ddH_2O, and equivalent cell counts were plated onto YPD agar. Cell survival was calculated after 3 days growth at 30°C by the percentage of colonies formed from HU-arrested cultures versus those treated with DMSO alone.

Immunoprecipitation

Lysates from Ndc1-TAP cells were prepared from mid-log phase cultures using a bead beater (Biospec) as described (BOLGER *et al.* 2008). Solubilized fractions were added to 25µl of packed IgG-coated sepharose beads and incubated for 4 hr at 4°C. Proteins bound to the sepharose beads were washed in wash buffer (0.05% Tween, 150mM NaCl, 50mM Tris-HCl ph6.5), eluted by boiling in SDS sample buffer, resolved by SDS-PAGE and detected with rabbit affinity purified α-GFP IgG (a gift of M. Linder, Washington University School of Medicine, St. Louis, MO. (1:2000) and Horseradish Peroxidase-conjugated donkey α-rabbit antibodies (1:5000, GE Healthcare).

For Yop1-3xFLAG, liquid nitrogen ground lysates were prepared from 200 OD_{600} mid-log phase cells as described (JASPERSEN *et al.* 2006) and 40 µl α-Flag resin (Sigma-Aldrich) was added. After overnight incubation at 4°C, beads were washed five times at 4°C and resuspended with loading buffer. Samples were analyzed by SDS-PAGE followed by immunoblotting. The following primary antibody dilutions were used: 1:1000 α-HA 3F 10 (Roche) and 1:1000 α-FLAG M2 (Sigma-Aldrich). Alkaline phosphatase-conjugated secondary antibodies were used at 1:10,000 (Promega).

Membrane yeast two-hybrid system

Bait and prey constructs were created by amplifying SFII-SFII fragments and directionally inserted into the SFII site of pBT3N or pBT3-STE or pPR3N. Plasmids were co-transformed into SLJ5572 (Dualsystem Biotech NMY51). Transformants

were spotted onto SD-LEU-TRP and SD-LEU-TRP-HIS-ADE plates and grown for 2-3 days at 30°C.

Superplaque assay and **Thin-section Electron Microscopy**

Myc-Spc42 localization and spindle morphology was analyzed by indirect immunofluorescence microscopy as described (JASPERSEN *et al.* 2002). Cells were examined with a Zeiss Axioimager using a 100X Zeiss Plan-Fluar lens (NA = 1.45), and images were captured with a Hamamatsu Orca-ER digital camera and processed using ImageJ (NIH). Superplaque formation was assayed by electron microscopy (EM) as described (CASTILLO *et al.* 2002) Samples were frozen on the Leica EM-Pact (Wetzlar, Germany) at ~ 2050 bar, then transferred under liquid nitrogen into 2% osmium tetroxide/0.1 % uranyl acetate/acetone and transferred to the Leica AFS (Wetzlar, Germany). The freeze substitution protocol was as follows: -90°C for 16 hr, up 4°C/hr for 7 hr, -60°C for 19 hr, up 4°C/hr for 10 hr, -20°C for 20 hr. Samples were removed from the AFS and placed in the refrigerator for 4 hr, then allowed to incubate at room temperature for 1 hr. Samples went through 3 changes of acetone over 1 hr and were removed from the planchettes. They were embedded in acetone/Epon mixtures to final 100% Epon over several days in a stepwise procedure as described (MCDONALD 1999). 60 nm serial thin sections were cut on a Leica UC6 (Wetzlar, Germany), stained with uranyl acetate and Sato's lead and imaged on a FEI Technai Spirit (Hillsboro, OR).

For thin-section transmission electron microscopy (TEM) of SPBs, early log phase cultures of parental (BY4724) and *rtn1Δ yop1Δ* yeast strains (SWY3811)

grown in YPD were processed to preserve and stain dense protein and membrane structures and as previously described (DAWSON *et al.* 2009). Grids were examined on a CM-12 120-keV electron microscope (FEI, Hillsboro, OR). Images were acquired with an Advantage HR or MegaPlus ES 4.0 camera (Advanced Microscopy Techniques, Danvers, MA) and processed with ImageJ and Photoshop 12.0 software.

RESULTS

Rtn1 and Yop1 are required for normal spindle pole body morphology

In *S. cerevisiae* lacking Rtn1 and Yop1, NPCs are clustered in a limited NE region and NPC assembly is altered (DAWSON *et al.* 2009). Based on connections between SPB and NPC assembly (CHIAL *et al.* 1998; ADAMS and KILMARTIN 1999; JASPERSEN and WINEY 2004; SEZEN *et al.* 2009; WITKIN *et al.* 2010), we speculated that the *rtn1Δ yop1Δ* mutant cells might have SPB perturbations. Using thin section electron microscopy (TEM), SPB morphology was assessed in *rtn1Δ yop1Δ* cells. In wild type cells, SPBs were embedded in the NE with the documented laminar structure of central, inner and outer plaques (Figure 2.1A). Nuclear microtubules organized from the inner plaque were also apparent. However, in the micrographs from *rtn1Δ yop1Δ* cells, the SPBs had strikingly altered morphology (Figure 2.1B-E, Figure 2.2). SPBs appeared to have unusually separated laminar structure with atypical plaque densities as well as peripheral lobular densities adjacent to the central plaque (Figure 2.1B-C, Figure 2.2). Of the 15 SPBs identified by this method, 12 exhibited this altered SPB morphology. As illustrated in Figure 2.1E, the aberrant SPB morphologies in the *rtn1Δ yop1Δ* cells were distinct from mutants with defects

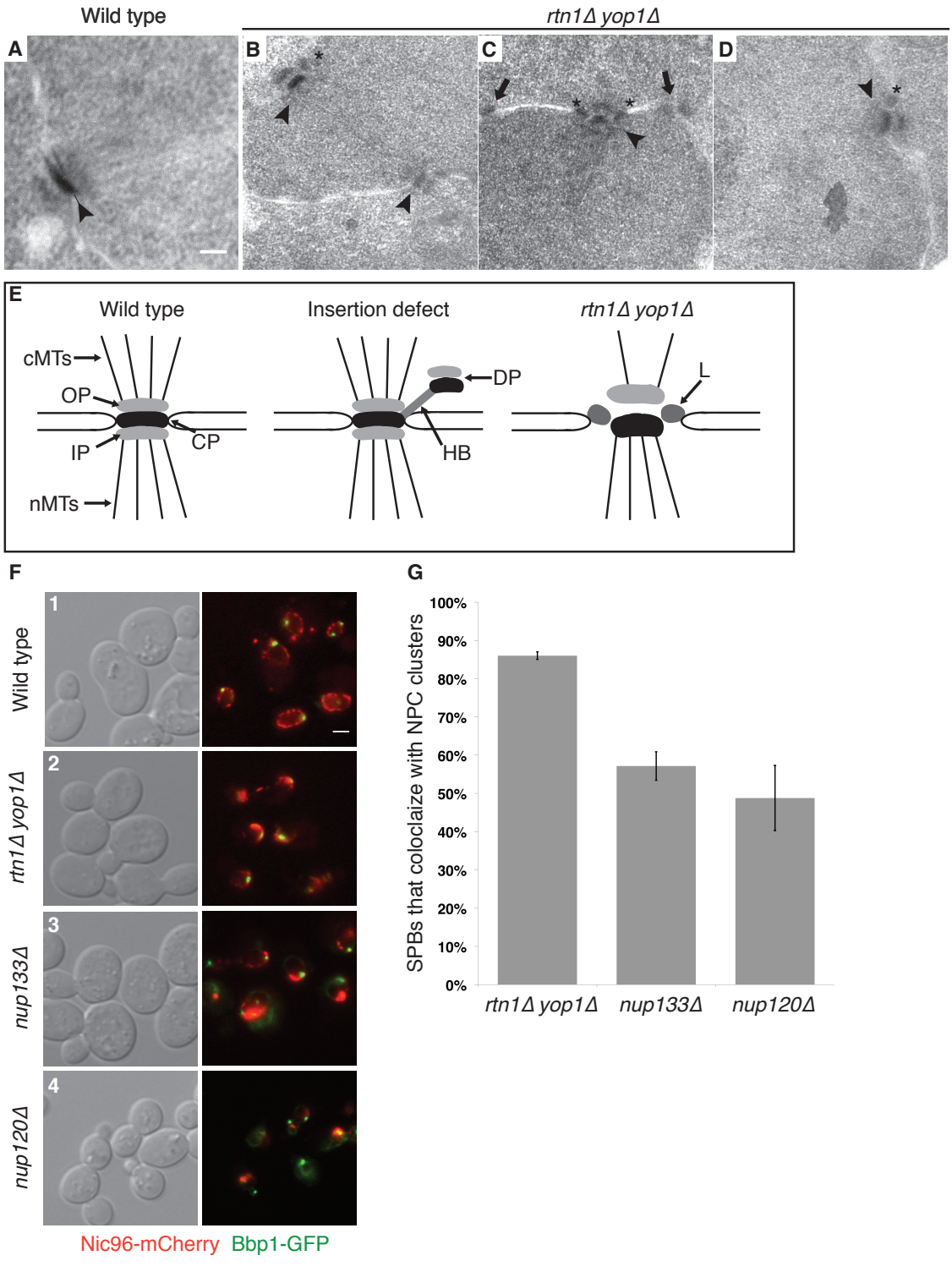
Wild type
rtn1Δ yop1Δ
A
B
C
D
E
Wild type
Insertion defect
rtn1Δ yop1Δ
cMTs
OP
IP
CP
nMTs
DP
HB
L
F
Wild type
rtn1Δ yop1Δ
nup133Δ
nup120Δ
1
2
3
4
Nic96-mCherry
Bbp1-GFP
G
SPBs that coloclaize with NPC clusters
100%
90%
80%
70%
60%
50%
40%
30%
20%
10%
0%
rtn1Δ yop1Δ
nup133Δ
nup120Δ

Figure 2.1: **SPBs have abnormal morphology and colocalize with NPC clusters in *rtn1Δ yop1Δ* cells**.
(A-D) Parental wild type (A) or *rtn1Δ yop1Δ* (B-D) cells were grown to early log phase at 23°C and processed for TEM. Scale bar, 100 nm. Arrowheads point to SPBs, arrows point to NPCs, asterisks indicate abnormal lobular structures on SPBs. (E) Cartoon representations of SPBs from wild type, SPB-insertion mutants, and *rtn1Δ yop1Δ* cells. cMTs: cytoplasmic microtubules; nMTs: nuclear microtubules; OP: outer plaque; IP: inner plaque; CP: central plaque; HB: half-bridge; DP: duplication plaque/uninserted SPB; L: lobular abnormalities (F) Parental wild type, *rtn1Δ yop1Δ, nup133Δ,* and *nup120Δ* cells expressing endogenously tagged Nic96-mCherry and Bbp1-GFP were grown to early log phase at 25°C. Representative DIC and direct fluorescence microscopy images are shown. Scale bar, 2 μm (G) Quantitative analysis of Bbp1-GFP and Nic96-mCherry colocalization. Cells were scored for presence of a Bbp1 foci within the Nic96 cluster (SWY4950: n=882; SWY5033: n=602; SWY4971: n=571). Error bars represent standard error.

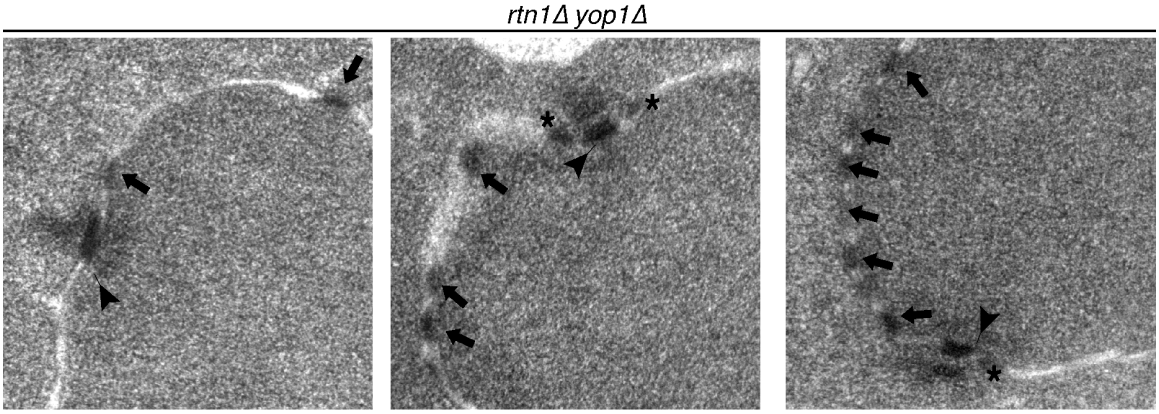

Figure 2.2: **Deletion of *RTN1* and *YOP1* result in abnormalities in the SPB**. *rtn1Δ yop1Δ* (SWY3811) cells were grown to early log phase at 23°C and processed for TEM. Scale bar, 100 nm. Arrowheads point to SPBs, arrows point to NPCs, asterisks indicate abnormal lobular structures on SPBs.

in SPB membrane components wherein the SPB structural perturbations typically include half bridge instability or an inability to insert the newly duplicated SPB into the NE, both of which result in a monopolar mitotic spindle (JASPERSEN and WINEY 2004). Moreover, to date, there are no reports of SPB structural alterations in other NPC clustering mutants (e.g. *nup133Δ* and *nup120Δ*); however, others have documented shorter spindles in *nup120Δ* cells (AITCHISON *et al.* 1995).

The *rtn1Δ yop1Δ* TEM micrographs also revealed a prevalence of NPCs clustering near the aberrant SPB structures (Figure 2.1C). Others have reported NPC localization near SPBs in the NE in both wild type and NPC clustering strains (HEATH *et al.* 1995; WINEY *et al.* 1997; ADAMS and KILMARTIN 1999; SCHRAMM *et al.* 2000). To gain a further understanding of their distributions in the NE, colocalization of SPBs and NPC clusters was assayed in *rtn1Δ yop1Δ* cells. For direct comparison, the same analysis was conducted in *nup133Δ* and n*up120Δ* cells that also have clustered NPCs (HEATH *et al.* 1995; PEMBERTON *et al.* 1995). Strains expressing chromosomally integrated *BBP1-GFP* (encoding a SPB component (SCHRAMM et al. 2000)) and *NIC96-mCherry* (encoding a Nup (GRANDI *et al.* 1993)) were analyzed by direct fluorescence microscopy (Figure 2.1F). As determined by the association of Bbp1-GFP foci with a Nic96-mCherry cluster, the SPBs localized coincident with NPC clusters at a frequency of 57.2% and 48.8%, respectively, for the *nup133Δ* and n*up120Δ* cells. In wild type cells NPCs do not cluster and the Bbp1-GFP foci were found on the Nic96-mCherry-labeled NE rim. Strikingly, in *rtn1Δ yop1Δ* cells, the co-localization of NPC clusters with SPBs increased significantly to 86.0% of cells (Figure 2.1G). Taken together, the *rtn1Δ yop1Δ* mutant resulted in both SPB morphology defects that

were distinct from other known NPC clustering mutants and an increased coincidence of NPC clusters and SPBs. Since SPBs were associated with NPC clusters in 57.2% of *nup133Δ* cells, I speculated that this mutant could be used to determine if Rtn1 is enriched at SPBs. For this, *nup133Δ RTN1-GFP* cells expressing *SPC42-MCHERRY* (encoding a SPB component) were analyzed by direct fluorescence confocal microscopy (Figure 2.3).

In cells where the Spc42-mCherry foci were clearly distinct from the Rtn1-GFP/NPC cluster, no coincident Rtn1-GFP intensity was observed at the Spc42-mCherry foci. Although this did not eliminate the possibility that Rtn1 and Yop1 colocalize with SPBs, it suggests that any association is below the detection limit of this method.

SPB superplaques in rtn1Δ yop1Δ cells are unstable in the NE

When the SPB component Spc42 is overproduced, the excess protein is incorporated into the central plaque of the SPB. This results in a lateral expansion of the SPB to form a structure termed the superplaque (DONALDSON and KILMARTIN 1996). Others have found that many of the same molecular and regulatory events required for SPB duplication are also required for superplaque formation (DONALDSON and KILMARTIN 1996; CASTILLO *et al.* 2002; JASPERSEN and WINEY 2004). To further test SPB structural integrity and connections of the SPB to the NE, we examined the ability of *rtn1Δ yop1Δ* cells to stably maintain superplaque attachment. Using a galactose-inducible *myc-SPC42*, superplaque formation was induced in wild type and *rtn1Δ yop1Δ* cells. By indirect immunofluorescence, as

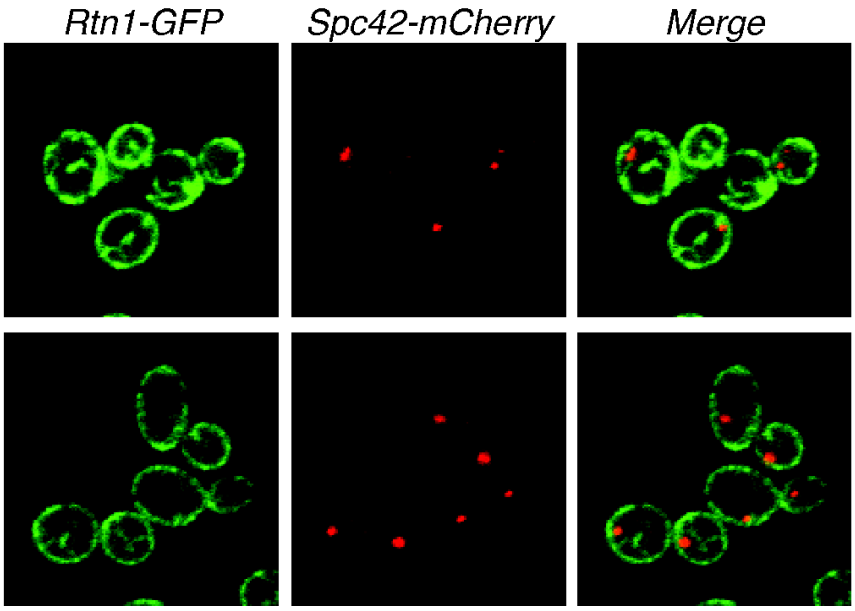

Figure 2.3: **Rtn1 does not colocalize with SPBS.**
Asynchronous cultures of *nup120Δ RTN1-GFP*(SWY4047) expressing pSPC42-MCHERRY were grown to log phase and imaged. Scale bar, 2 μm.

compared to superplaques in wild type cells, the *rtn1Δ yop1Δ* superplaques were more variable in size. In addition, an increased proportion was extended away from the microtubules and DNA (Figure 2.4A). Examination of superplaques by TEM revealed that 29% of the *rtn1Δ yop1Δ* superplaques were completely disconnected from the NE, compared to 10% in wild type cells (Figure 2.4B-G). Interestingly, the overall laminar structure of the superplaques in *rtn1Δ yop1Δ* cells was not significantly altered, with over 50% of these structures showing a straight layered structure similar to the SPB central plaque (Figure 2.4B-G). These data suggested that Rtn1 and Yop1 play a role in stable attachment of SPB structures to the NE.

Cells lacking Rtn1 and Yop1 have defects in the mitotic spindle

The observation that SPB morphology is altered in *rtn1Δ yop1Δ* cells indicated that SPB function might also be impaired. To assay SPB function, we used a variety of cellular arrest factors to examine SPBs and spindles at distinct stages in the cell cycle. SPB remodeling occurs throughout the cell cycle, starting with duplication of a new SPB in late G1 phase and then growth of the SPB core through exchange of subunits in S phase and G2/M. SPB size decreases as cells exit mitosis, presumably through the removal of core subunits (BYERS and GOETSCH 1975; YODER *et al.* 2003). Therefore, SPBs in wild type cells arrested with hydroxyurea (HU) or nocodazole in S phase or G2/M, respectively, undergo a lateral expansion and increase the overall size. In contrast, the SPBs in wild type cells arrested in G1 phase using α-factor are contracted in the size.

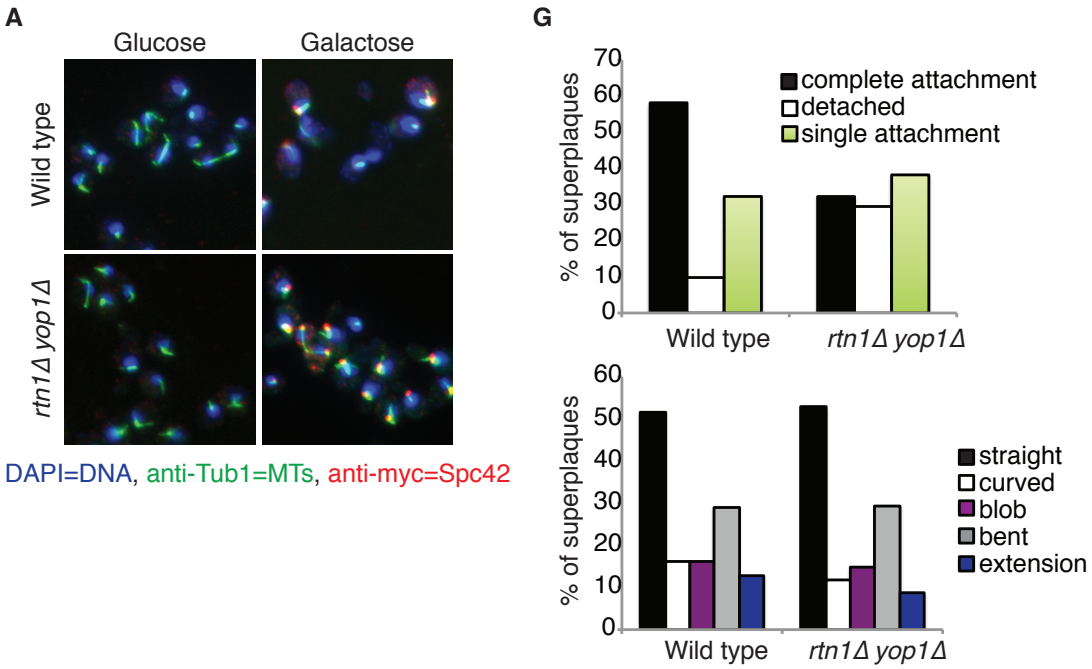
A
Glucose
Galactose
Wild type
rtn1Δ yop1Δ
DAPI=DNA, anti-Tub1=MTs, anti-myc=Spc42
G
% of superplaques
70
60
50
40
30
20
10
0
complete attachment
detached
single attachment
Wild type
rtn1Δ yop1Δ
% of superplaques
60
50
40
30
20
10
0
straight
curved
blob
bent
extension
Wild type
rtn1Δ yop1Δ

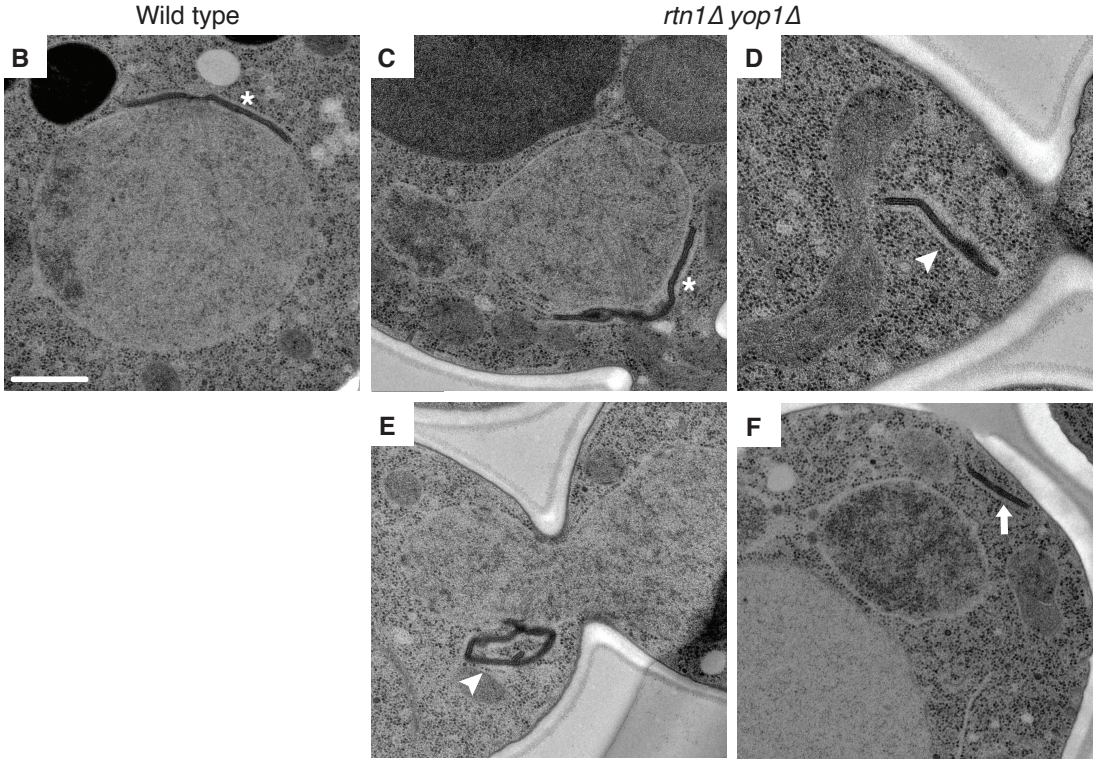
Wild type
rtn1Δ yop1Δ
B
C
D
E
F

Figure 2.4: **Deletion of reticulons affects superplaque formation**.
Contributed by Jennifer Friederichs and Sue Jaspersen from the laboratory of Sue Jaspersen. Parental (SLJ1433) and *rtn1Δ yop1Δ* (SLJ3828) were grown overnight in YEP + 2% raffinose at 30°C until they were in early log-phase then divided into two cultures. In one culture, glucose was added to a final concentration of 2% while the other was treated with 2% galactose to induce expression of *myc-SPC42*. After 4 h of continued growth at 30°C, cultures where harvested and examined by indirect immunofluorescence microscopy and by EM. (A) Microtubules (green) and myc-Spc42 (red) were labeled using α-Tub1 and α-myc antibodies, respectively. DNA (blue) was visualized using DAPI. Bar, 5 μm. (B-F) NE-associated superplaque structures were examined by EM, and analyzed in 31 wild type and 34 *rtn1Δ yop1Δ* SPB/superplaque structures (G). Asterisks indicate SPB superplaques with complete attachment, arrowheads at superplaques with single attachment, and arrows at superplaques completely detached from nucleus. Scale bar B-E, 500 nm.

Microtubule structure of wild type and *rtn1Δ yop1Δ* cells in arrested and released cells was observed using indirect immunofluorescence for α-alpha tubulin or direct fluorescence microscopy of GFP-Tub3 to determine if there were defects in the microtubule cytoskeleton. As reported (MILLER and ROSE 1998), in wild type cells with α-factor treatment, the late G1 arrest point in wild type cells was characterized by frequent alignment of the SPB with the shmoo extension and astral microtubules that extend into the shmoo. However, the α-factor arrested microtubules of *rtn1Δ yop1Δ* cells appeared to have a minor spindle positioning defect (Table 2.1). SPBs were more frequently misoriented away from the shmoo in *rtn1Δ yop1Δ* cells compared to wild type, 12.6% and 7.4% respectively. This suggests a possible impairment of cytoplasmic microtubules. Further analysis of this phenotype by treatment of cells with HU, which results in a S-phase arrest in wild type cells with a short bar-like spindle positioned at the bud neck, revealed additional defects in *rtn1Δ yop1Δ* cells (Figure 2.5A). A single bright focus of GFP-Tub3 fluorescence was observed in the mother cells of HU arrested *rtn1Δ yop1Δ* cells (Figure 2.5A), suggesting that loss of *RTN1* and *YOP1* function is associated not only with a defect in nucleation of cytoplasmic microtubules needed for spindle positioning but also with a defect in the formation of a bipolar spindle. Furthermore, prolonging HU treatment of *rtn1Δ yop1Δ* cells for up to six hr did not increase the percentage of cells with wild type short spindles (data not shown).

To determine if *rtn1Δ yop1Δ* mutants have a defect in spindle formation, I treated cells with nocodazole, which inhibits spindle formation, and assessed the ability of the spindle to repolymerize following removal of the nocodazole. Wild type and

	Wild type	*rtn1Δ yop1Δ*
Microtubules positioned in shmoo	335 (92.6%)	384 (87.3%)
Microtubules positioned away from shmoo	27 (7.4%)	56 (12.6%)
Total	362	440

Table 2.1: ***rtn1Δ yop1Δ* cells have mild SPB positioning defects upon α-factor arrest.**
Parental (YOL183) or *rtn1Δ yop1Δ* (SWY3811) cells expressing GFP-Tub3 arrested with a-factor. Cells were fixed to preserve GFP fluorescence and imaged and scored based on proximity of SPB and microtubules to the shmoo; p-value= 0.00012.

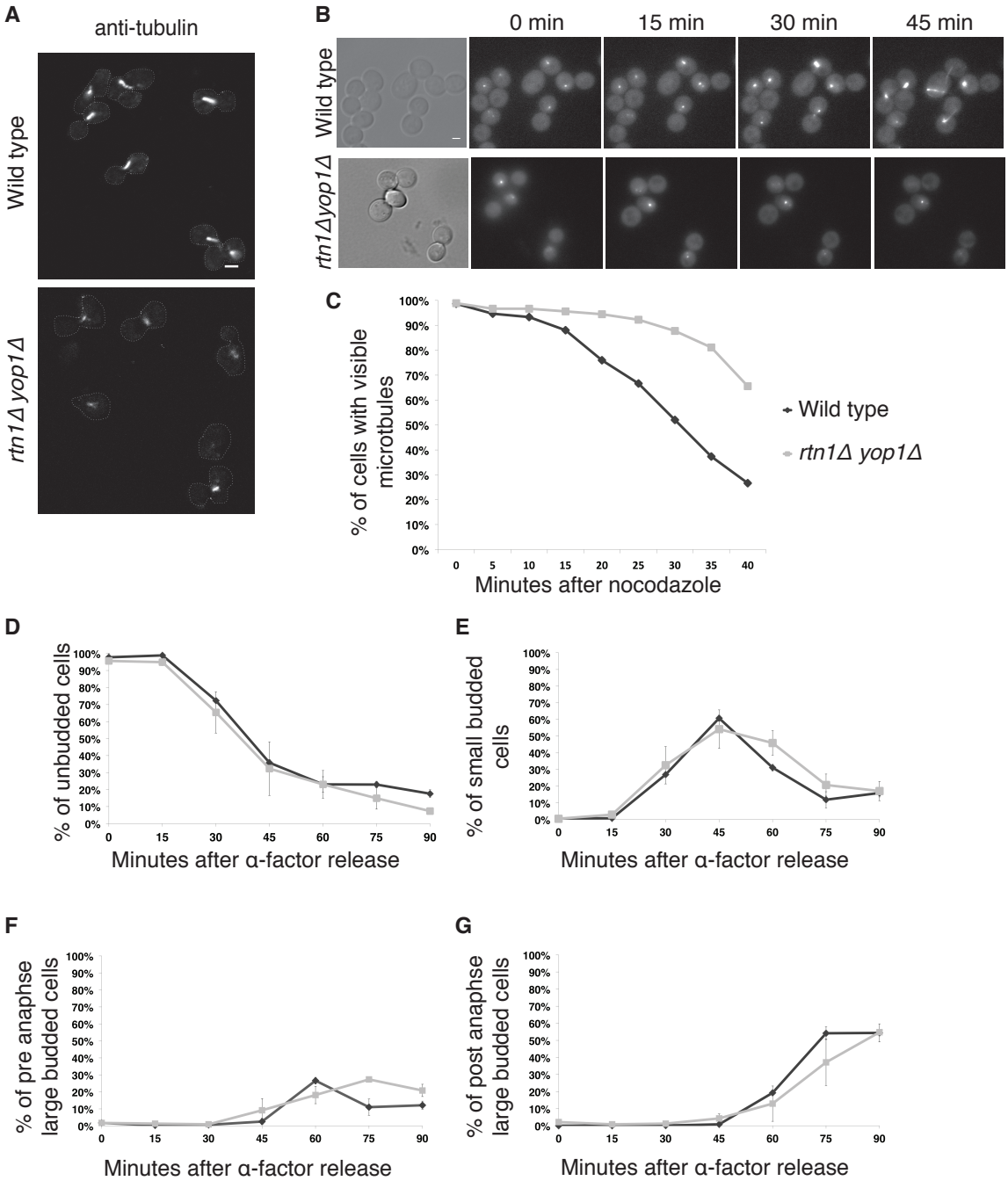
A
anti-tubulin
Wild type
rtn1Δ yop1Δ
B
0 min
15 min
30 min
45 min
Wild type
rtn1Δyop1Δ
C
% of cells with visible microtbules
Minutes after nocodazole
Wild type
rtn1Δ yop1Δ
D
% of unbudded cells
Minutes after α-factor release
E
% of small budded cells
Minutes after α-factor release
F
% of pre anaphse large budded cells
Minutes after α-factor release
G
% of post anaphse large budded cells
Minutes after α-factor release

Figure 2.5: **Mitotic arrest leads to collapsed spindles and reduced microtubule function in *rtn1Δ yop1Δ* cells.**
(A) Microtubules in parental wild type (YOL183) or *rtn1Δ yop1Δ* (SWY3811) cells arrested with 200 mM HU were detected by indirect α-tubulin immunofluorescence and laser scanning confocal microscopy. Scale Bar, 2 μm Contributed by Renee Dawson from the laboratory of Susan Wente. (B) Direct fluorescence of GFP-Tub3 was visualized following nocodazole or α-factor arrest in GFP-Tub3 (SWY4617) or *rtn1Δ yop1Δ* GFP-Tub3 (SW4935) cells. DIC, differential interference contrast. Scale bar, 2 μm. (C) Time-lapse images were scored for release from nocodazole arrest as the percentage of cells exhibiting of microtubule re-polymerization. (F-G) Time-lapse images were scored for release from α-factor arrest based on bud index and position of SPBs within the cells.

rtn1Δ yop1Δ GFP-Tub3 cells were arrested in G2/M with nocodazole. Time course imaging on agarose pads was conducted of individual cells following release. Wild type cells showed re-polymerization of microtubules by 15 min after nocodazole washout. However, re-polymerization in *rtn1Δ yop1Δ* cells was delayed until approximately 30 min (Figure 2.5B,C). This significant delay in *rtn1Δ yop1Δ* cells was not due to growth defects since release from α-factor arrest was not delayed in *rtn1Δ yop1Δ* cells compared to wild type (Figure 2.5D-G). We concluded that *rtn1Δ yop1Δ* cells have altered microtubule dynamics.

Because cytoplasmic microtubules are critical for spindle positioning along the mother-daughter axis, we speculated that *rtn1Δ yop1Δ* cells were defective in nucleation or maintenance of cytoplasmic microtubules (HOEPFNER *et al.* 2002; MOORE *et al.* 2009; WINEY and BLOOM 2012). To further analyze the microtubules of *rtn1Δ yop1Δ,* we imaged cells expressing GFP-Tub1 and Tub4-mCherry by live cell microscopy. The GFP-Tub1 localization results were consistent with the GFP-Tub3 data; however, the cytoplasmic microtubules were more easily observed with GFP-Tub1 (Figure 2.6A). From these images, we found that short spindles nucleated cytoplasmic microtubules that went towards the bud. Strikingly, as the spindles elongated, cytoplasmic microtubules were present less frequently in the *rtn1Δ yop1Δ* cells (52.4% compared to 83.7% in wild type). To determine if *rtn1Δ yop1Δ* cells were deficient in cytoplasmic microtubules nucleation, TEM micrographs of cells under HPF/FS conditions were analyzed. Similar to our other TEM observations (Figure 2.1B-D), *rtn1Δ yop1Δ* SPBs were frequently flanked by NPCs (12 of 17) and associated with some type of detached NE structure (12 of 17)

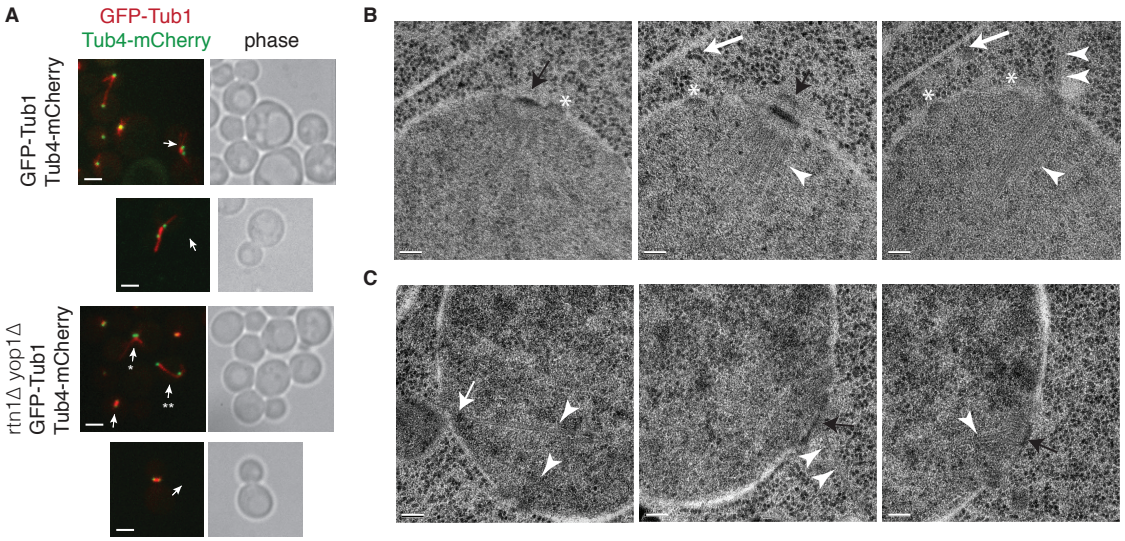

Figure 2.6: ***rtn1Δ yop1Δ* cells have defects in cytoplasmic microtubules.** Contributed by Jinjing Chen and Sue Jaspersen from the laboratory of Sue Jaspersen. (A) Asynchronous cultures of parental wild type (SLJ3996) or *rtn1Δ yop1Δ* (SLJ3994) cells expressing GFP-Tub1 and Tub4-mCherry were grown to early log phase and imaged. Cells were analyzed for the presence or absence of cytoplasmic microtubules and length of spindles. Arrows point to duplicated SPBs in large budded cells. Single asterisk indicates a cell with duplicated poles and cytoplasmic microtubules that go toward bud and mother. The double asterisk indicates a cell with spindle elongation in the mother. (B-C) Asynchronous *rtn1Δ yop1Δ* cells were processed by HPF/FS and imaged by EM. Arrows point to SPBs. Asterisk indicates NPC in close proximity to SPB. Arrowheads point to nuclear and cytoplasmic microtubules. White arrows point to electron-dense structure present in the nucleoplasm associated with nuclear microtubules (B) and to an electron dense structure resembling the satellite (C). Scale bar, 100nm.

(Figure 2.6 B-C). Also, *rtn1Δ yop1Δ* SPBs often lacked visible cytoplasmic microtubules (8 of 17) compared to wild type (1 of 10); however, all were associated with nuclear microtubules. Taken together, we concluded that *rtn1Δ yop1Δ* cells have defects in nuclear positioning caused by insufficient cytoplasmic microtubules.

Rtn1 and Yop1 impact proper spindle function

Since *rtn1Δ yop1Δ* cells exhibit spindle defects during HU arrest and following release from G2/M, cell viability assays were performed to determine if these defects in spindle morphology result in compromised spindle function, chromosome segregation errors and ultimately cell death. The *rtn1Δ yop1Δ* cells were arrested with HU for 6 hr, released into the cell cycle, and then plated on YPD plates. Compared to wild type, *rtn1Δ yop1Δ* cells had 50% reduced viability after HU treatment (Figure 2.7A). Overall, these results suggested that when arrested in S-phase, *rtn1Δ yop1Δ* cells are vulnerable to reduced spindle integrity, resulting in increased cell death.

We also speculated that *rtn1Δ yop1Δ* cells would exhibit defects in SPB function in untreated cells. GFP-Tub3 was used to observe the spindles in an asynchronously growing population of *rtn1Δ yop1Δ* cells. There was no increase in the number of *rtn1Δ yop1Δ* cells with extra SPBs or evidence of non-functional SPBs that did not nucleate microtubules (Figure 2.6B). However, the overall *rtn1Δ yop1Δ* population harbored an increase in large budded cells with pre-anaphase spindles (spindles of less than 2 micrometers) (Figure 2.7B, C). Furthermore, when compared to wild type, the pre-anaphase spindles in *rtn1Δ yop1Δ* cells were more

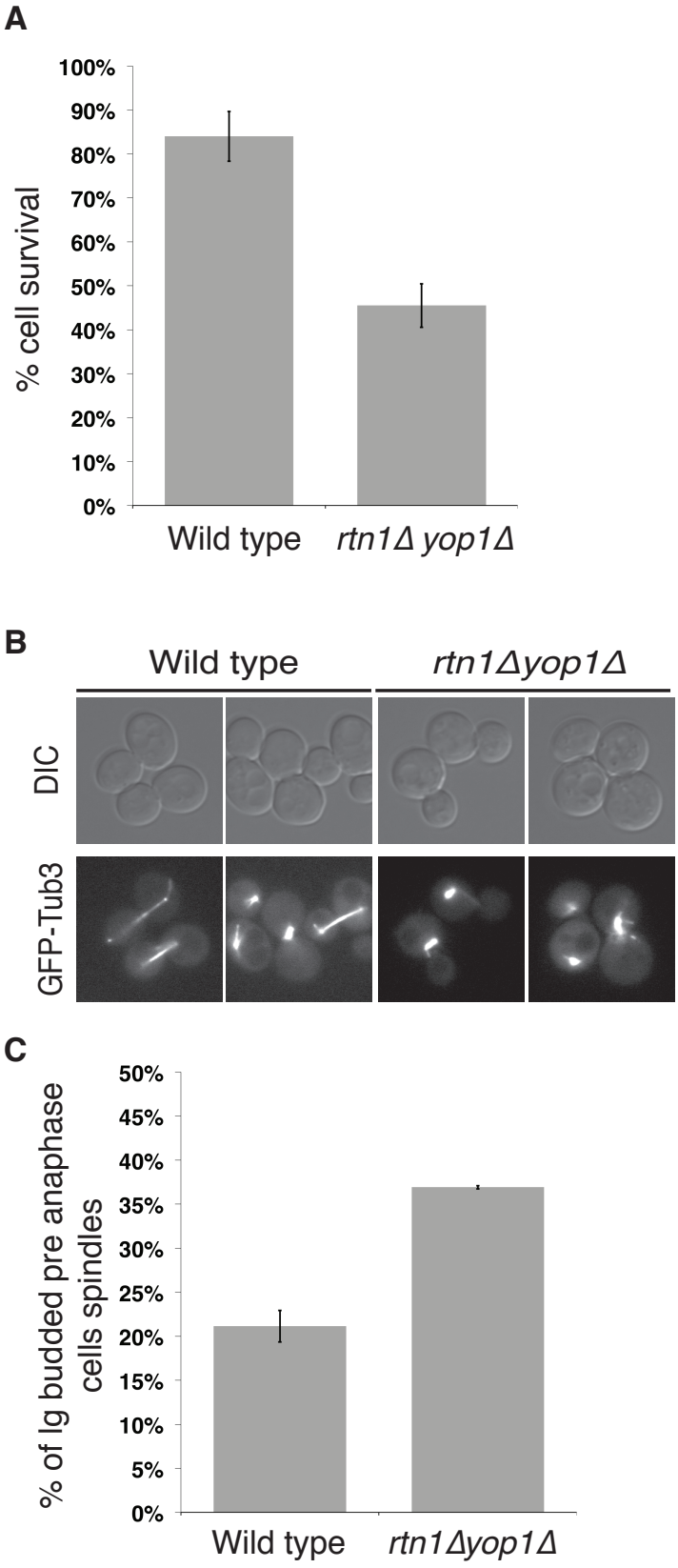
A
100%
90%
80%
70%
60%
50%
40%
30%
20%
10%
0%
% cell survival
Wild type
rtn1Δ yop1Δ
B
Wild type
rtn1Δyop1Δ
DIC
GFP-Tub3
C
50%
45%
40%
35%
30%
25%
20%
15%
10%
5%
0%
% of lg budded pre anaphase cells spindles
Wild type
rtn1Δyop1Δ

Figure 2.7: ***rtn1Δ yop1Δ* cells exhibit functional defects in spindle positioning.** (A) Parental wild type (YOL183) and *rtn1Δ yop1Δ* (SWY3811) cells were arrested with 200mM HU. Cell viability following HU arrest was measured by colony formation after 3 days growth. (B) Live cell direct fluorescence microscopy was conducted with GFP-Tub3 and *rtn1Δ yop1Δ* GFP-Tub3 cells grown to early log phase at 23°C. Scale bar, 2μm. (C) Bud index was scored in DIC images of parental GFP-Tub3 (SWY4616, n = 423) and *rtn1Δ yop1Δ* GFP-Tub3 (SWY4877, n=750).

frequently misaligned within the mother bud (Figure 2.7B). Thus, *rtn1Δ yop1Δ* cells exhibited poor spindle function in asynchronous cells, likely due to reduced SPB integrity and the defects in the cytoplasmic microtubules.

Overexpression of SPB insertion factors specifically rescues rtn1Δ yop1Δ spindle defects

Previously, we demonstrated that NPC clustering in the *rtn1Δ yop1Δ* cells is rescued by the overexpression of *NDC1* or *POM152* (DAWSON *et al.* 2009). Pom152 and Ndc1 interact in a complex in the NPC, and they have partially overlapping roles in NPC assembly (MADRID *et al.* 2006). To determine if altered NPC assembly/function was indirectly impacting SPBs, the shortened misaligned spindles phenotype was assessed by live cell microscopy in *rtn1Δ yop1Δ GFP-TUB3* cells overexpressing *NDC1* or *POM152.* Compared to empty vector, overexpression of *NDC1* rescued both of the SPB defects observed in *rtn1Δ yop1Δ* cells, as reflected by reduced numbers of large budded cells with short spindles (Figure 2.8A) and wild type levels of properly oriented pre-anaphase spindles (Figure 2.8B). In contrast, overexpression of *POM152* did not have the same effect on spindle defects in *rtn1Δ yop1Δ* cells (Figure 2.8A,B), and the decrease in the average percent of short or misaligned spindles was not significant (p-values of 0.20 and 0.13, respectively).

Since overexpression of *POM152* inhibits wild type cell growth (WOZNIAK *et al.* 1994), it is of note that decreased growth rate was not observed in *rtn1Δ yop1Δ* cells (Figure 2.9). Importantly, overexpression of *NDC1* rescued the mild growth

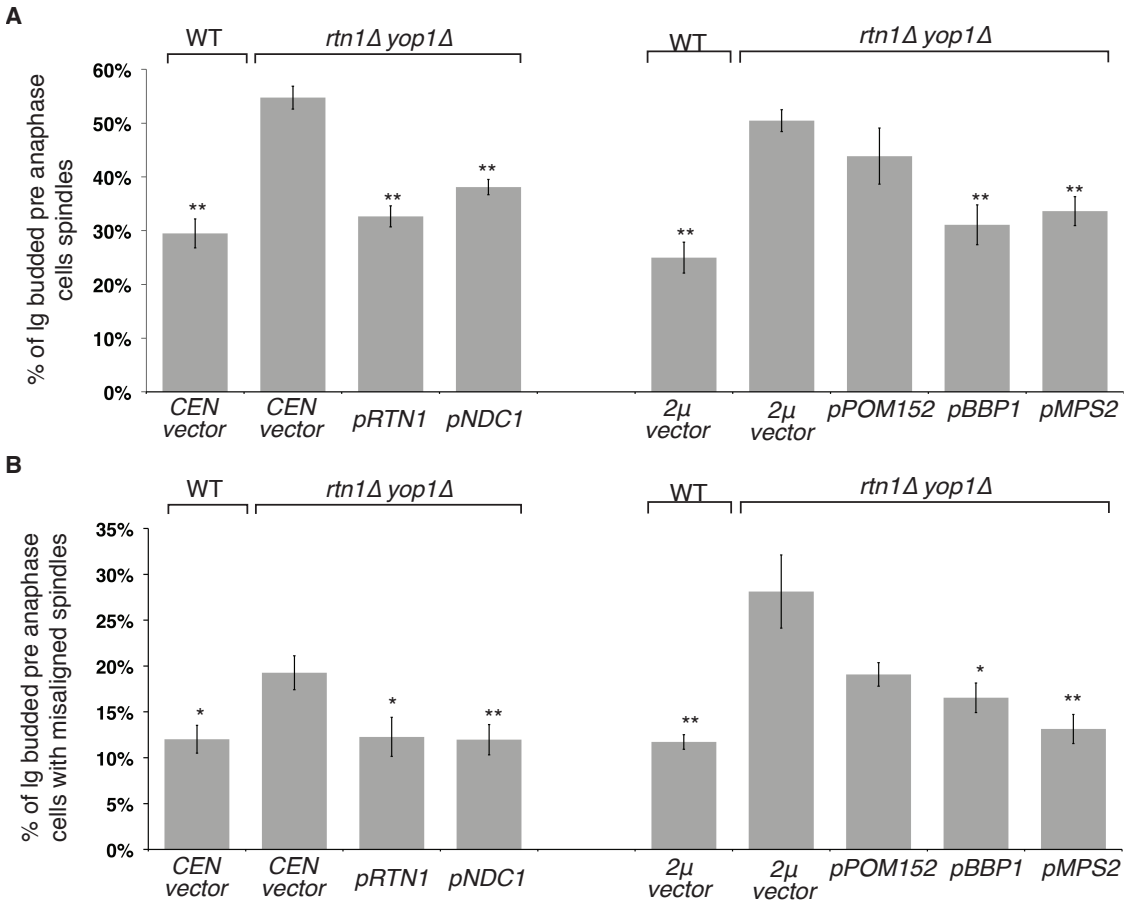

Figure 2.8: **Overexpression of SPB insertion factors rescues *rtn1Δ yop1Δ* defect**. Parental wild type GFP-Tub3 and *rtn1Δ yop1Δ* GFP-Tub3 cells transformed with plasmids expressing *NDC1*, *RTN1*, *POM152*, *BBP1*, *MPS2*, or empty vector were grown to mid-log phase at 30°C and visualized by live cell direct fluorescence microscopy. (A) Cells were scored for bud index by quantification of DIC images and cell cycle position by spindle stage (parental + pRS315, n=1251; + pRS425; n=1483; SWY4877 + pRS315, n=409; +pRSS425; n=2372; + pNDC1; n=2073; + pRTN1, n=2095; + pPOM15; n=904; + pBBP1, n=792; + pMPS2, n=2475). (B) Large budded cells with pre-anaphase spindles were further characterized by orientation of their spindle. Error bars indicate standard error. The asterisk and double asterisk denotes statistical significance (P-value < 0.04, P-value <0.01 respectively) by student's t-test.

defect of *rtn1Δ yop1Δ* cells whereas *POM152* overexpression did not (Figure 2.9), suggesting that the compromised growth of *rtn1Δ yop1Δ* cells reflects the reduced fidelity of SPB function. Overall, overexpression of either *NDC1* or *POM152* rescued NPC clustering in *rtn1Δ yop1Δ* cells (DAWSON *et al.* 2009); however, only *NDC1* overexpression rescued the *rtn1Δ yop1Δ* spindle defect. Thus, simply rescuing the NPC clustering defect did not rescue the SPB defect, suggesting the *rtn1Δ yop1Δ* effect was not an indirect overall NPC perturbation impact.

Proper targeting of Ndc1 to SPBs occurs by its association with other SPB insertion factors at the NE (WINEY *et al.* 1991; SCHRAMM *et al.* 2000; KUPKE *et al.* 2011). Bbp1 and Mps2 are SPB–specific proteins that interact with Ndc1 and play roles in SPB insertion and stability (WINEY *et al.* 1991; MUÑOZ-CENTENO *et al.* 1999; SCHRAMM *et al.* 2000). I hypothesized that overexpressing *BBP1* or *MPS2* would rescue the *rtn1Δ yop1Δ* spindle defects but not the NPC clustering defect. By examining GFP-Tub3, I found that SPB defects were rescued in *rtn1Δ yop1Δ* cells overexpressing *BBP1* or *MPS2* (Figure 2.10A, B). For *BBP1* overexpression, the numbers of large budded cells that had not completed mitosis (31% versus 50% for *rtn1Δ yop1Δ* alone) and the proportion with misoriented anaphase spindles (17% versus 28% for *rtn1Δ yop1Δ* alone) were clearly reduced. Likewise, in the population of cells overexpressing *MPS2*, there were fewer large budded cells that had not completed mitosis (34%) and a lower proportion with misoriented anaphase spindles (13%). Indeed, the spindle defect rescue levels in the *BBP1* and *MPS2* experiments were similar to that found with overexpressing *NDC1*. However, NPC clusters were still present in *rtn1Δ yop1Δ* cells overexpressing *BBP1* or *MPS2*

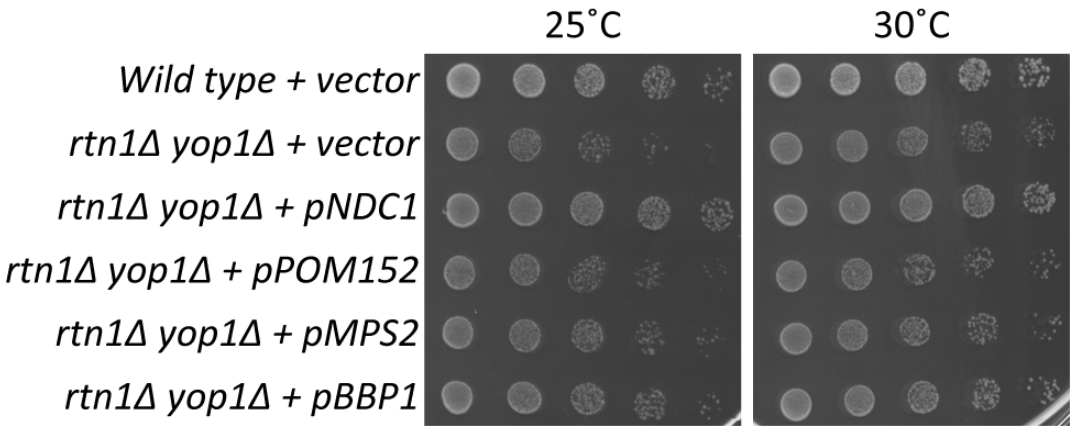

Figure 2.9: **Overexpression of *NDC1* results in rescue of *rtn1Δ yop1Δ growth* defects.**
Parental or *rtn1Δ yop1Δ* cells were transformed with plasmids expressing *NDC1*, *POM152*, *MPS2*, *BBP1*, or empty vector and grown to early log phase at 30°C in synthetic media lacking leucine. Strains were tested for growth at 25°C and 30°C.

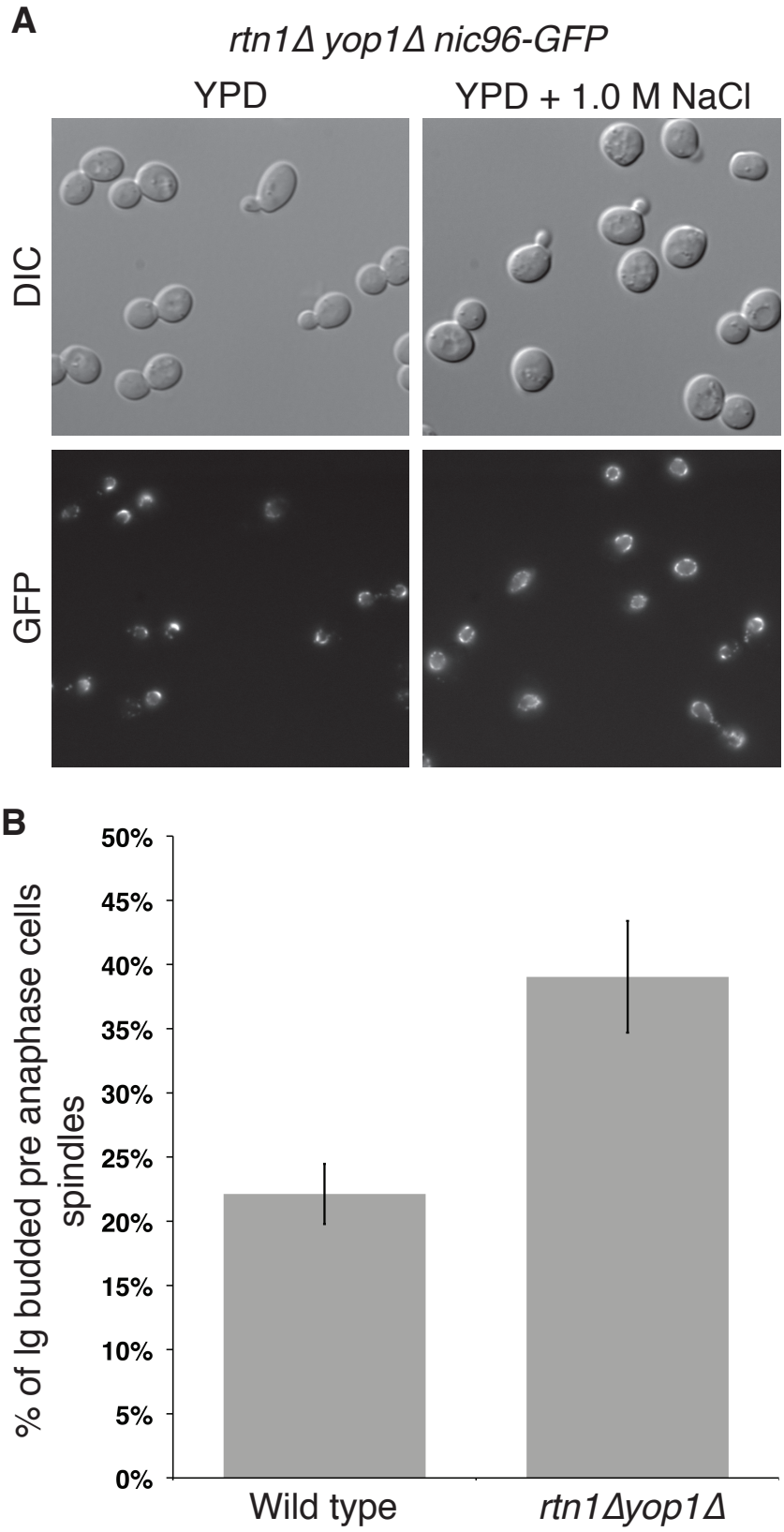
A
rtn1Δ yop1Δ nic96-GFP
YPD
YPD + 1.0 M NaCl
DIC
GFP
B
% of lg budded pre anaphase cells spindles
50%
45%
40%
35%
30%
25%
20%
15%
10%
5%
0%
Wild type
rtn1Δyop1Δ

Figure 2.10**: Growth in high osmolarity only reduces NPC clusters in *rtn1Δ yop1Δ cells.***
(A) Asynchronous cultures of *rtn1Δ yop1Δ nic96-GFP* cells (SWY4725) were grown to log phase at 23°C in YPD. After shifting to YPD alone (control) or YPD + 1.0M NaCl, cells were grown at 23°C for an additional 5 hr and imaged. (B) Asynchronous cultures of parental and *rtn1Δ yop1Δ* cells endogenously expressing *GFP-TUB3* (SWY4616 and SWY4877, respectively) were grown to log phase at 23°C in YPD. After shifting to YPD + 1.0M NaCl, cells were grown at 23°C for an additional 5 hr and imaged. Cells were scored for bud index by quantification of DIC images and cell cycle position by spindle stage (SWY4616: n=171; SWY4877: n=233) p-value = 0.041.

(data not shown). Thus, rescue of the *rtn1Δ yop1Δ* spindle defects by overexpression of SPB anchoring components was specific. These results indicated that the NPC and SPB defects are separable and both potentially the result of defects or insufficiencies in NE membrane proteins.

We speculated that the underlying cause for the *rtn1Δ yop1Δ* mutant phenotypes might be a perturbation in the function of shared SPB and NPC component(s). Ndc1 has roles at both SPBs and NPCs (WINEY *et al.* 1993; CHIAL *et al.* 1998; LAU *et al.* 2004). Two other NE membrane proteins, Brr6 and Apq12, have also been linked to both NPC biogenesis and SPB insertion (SCARCELLI *et al.* 2007; HODGE *et al.* 2010; SCHNEITER and COLE 2010; TAMM *et al.* 2011). To test for specificity, *BRR6* and *APQ12* overexpression was analyzed. Overproduction of neither Brr6 nor Apq12 altered the SPB or NPC defects in *rtn1Δ yop1Δ* cells (data not shown). Thus, the *rtn1Δ yop1Δ* cells had NPC and SPB defects that are separate from the lipid homeostasis defects and membrane fluidity function associated with *BRR6* and *APQ12*. Moreover, *NDC1* overexpression was unique in rescuing both the SPB and NPC defects.

High osmolarity reduces NPC clustering but not spindle defects of rtn1Δ yop1Δ cells

To further test the functional separation of NPC and SPB defects in cells, I analyzed my mutant cells for defects in SPB function and NPC clustering after growth of cells in high osmolarity media (1M NaCl). Strikingly, the percentage of *rtn1Δ yop1Δ* cells with distinct NPC clusters was reduced in high osmolarity media

from 71% to 22% (Figure 2.10A). This differed from a previous report for the *nup120Δ* clustering mutant wherein high osmolarity rescues growth and nucleocytoplasmic transport defects but not NPC clustering (HEATH *et al.* 1995). However, while growth of *rtn1Δ yop1Δ* cells in high osmolarity (1M NaCl) rescued NPC clustering, it did not rescue the observed SPB defects (Figure 2.10B). These results again highlighted differential NPC and SPB effects in the *rtn1Δ yop1Δ* cells. Previous work has shown that high osmolarity results in the increased *RTN2* expression, which could compensate for the loss of Rtn1 and Yop1 at NPCs (DE CRAENE *et al.* 2006b; ROMERO-SANTACREU *et al.* 2009).

Rtn1 and Yop1 interact with Ndc1

Based on the genetic and functional connections, we investigated whether Rtn1 and/or Yop1 physically interact with integral membrane proteins of the NPC and/or SPB. Rtn1 and Yop1 interact by co-immunoprecipitation (VOELTZ *et al.* 2006). Furthermore, based on a published large scale split ubiquitin-based two hybrid screen, Yop1 interacts with both Pom33 and Pom34 (MILLER *et al.* 2005). Using the split ubiquitin two hybrid assay, we used a candidate approach to identify other possible Yop1 interaction partners. Remarkably, Pom34, Pom152 and Ndc1 were all positive for interaction with Yop1. However, Yop1 did not interact with either Nbp1 or Mps3, two proteins involved in SPB insertion, using this system (Figure 2.11A) (ARAKI *et al.* 2006; FRIEDERICHS *et al.* 2011).

Using immunoprecipitation assays, we further examined the interaction between Ndc1 and Rtn1. Lysates of yeast cells exogenously expressing *NDC1-TAP*

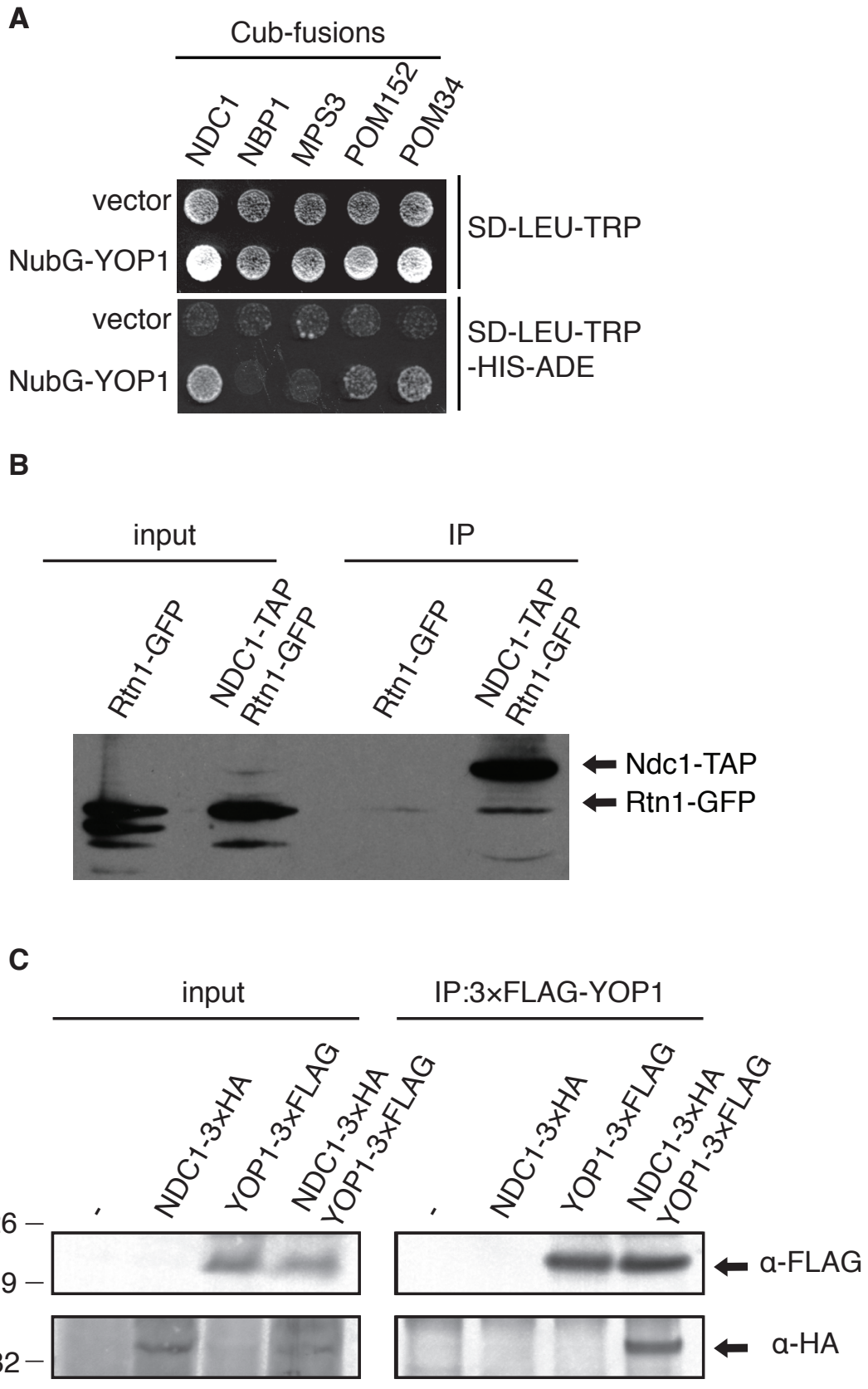
A
Cub-fusions
NDC1
NBP1
MPS3
POM152
POM34
vector
NubG-YOP1
SD-LEU-TRP
vector
NubG-YOP1
SD-LEU-TRP
-HIS-ADE
B
input
IP
Rtn1-GFP
NDC1-TAP
Rtn1-GFP
Rtn1-GFP
NDC1-TAP
Rtn1-GFP
Ndc1-TAP
Rtn1-GFP
C
input
IP:3×FLAG-YOP1
-
NDC1-3xHA
YOP1-3xFLAG
NDC1-3xHA
YOP1-3xFLAG
-
NDC1-3xHA
YOP1-3xFLAG
NDC1-3xHA
YOP1-3xFLAG
26
19
82
α-FLAG
α-HA

Figure 2.11**: Rtn1 and Yop1 interact with Ndc1 and NPC components.**
(A) Contributed by Jingjing Chen and Sue Jaspersen from the laboratory of Sue Jaspersen. Split ubiquitin yeast two-hybrid vectors containing a *LEU2* marker and the C-terminal region of ubiquitin (Cub) fused to *NDC1*, *NBP1*, *MPS3*, *POM152*, or *POM34* (baits) were expressed in SLJ5572 and tested for their ability to interact with the N-terminal region of ubiquitin (NubG) fused to Yop1 or the N-terminal region of ubiquitin alone in a *TRP1* vector (preys). Interaction of bait and prey proteins lead to cleavage of the split ubiquitin and release of a transcription factor, which activates reporter genes such as *HIS3* and *ADE2*. (B) Lysates were prepared from wild type, Ndc1-TAP Rtn1-GFP and Rtn1-GFP cells and immunoprecipitated with IgG-coated sepharose beads. Analysis of cell lysates and immunoprecipitated proteins by western blotting with α-GFP antibodies showed that Ndc1-TAP binds to Rtn1-GFP. (C) Contributed by Jingjing Chen and Sue Jaspersen from the laboratory of Sue Jaspersen. Lysates were prepared from wild type, Ndc1-3xHA, Yop1-3xFLAG, and Ndc1-3xHA Yop1-3xFLAG cells and immunoprecipitated with α-FLAG antibodies. Analysis of cell lysates and immunoprecipitated proteins by immunoblotting with α-FLAG and α-HA antibodies showed that Ndc1-3xHA binds to Yop1-3xFLAG. Positions of molecular mass markers (KDa) are indicated to the left.

and *RTN1-GFP* were incubated with IgG-sepharose beads. By immunoblotting analysis, Rtn1-GFP was co-isolated with Ndc1-TAP (Figure 2.11B). Similarly, lysates of yeast cells exogenously expressing Ndc1-3xHA and Yop1-3XFLAG were incubated α-FLAG affinity matrix and bound samples were analyzed by immunoblotting. As shown, Yop1-3xFLAG and Ndc1-3xHA were co-isolated (Figure 2.11C). Overall, these data showed that Rtn1 and Yop1 physically interact with Ndc1 and other membrane components of the NPC.

DISCUSSION

Previously, we defined a role for Rtn1 and Yop1 in nuclear pore and NPC biogenesis (DAWSON *et al.* 2009). Building on this, here we demonstrate novel functions of Rtn1 and Yop1 at the NE by discovering links to SPB morphology and microtubule dynamics. We conclude that the lack of Rtn1 and Yop1 perturbs Ndc1 function, an essential factor required for both SPB and NPC assembly. This is based on a complementary set of genetic, cell biological and biochemical data. We find that *rtn1Δ yop1Δ* cells have structural and functional defects in SPBs, in the SPB-associated microtubule spindles and cytoplasmic microtubules, and in SPB superplaque formation. Overproduction of either Ndc1 or components involved in anchoring the SPB to the NE rescues the SPB defects in *rtn1Δ yop1Δ* cells. Furthermore, although increasing Ndc1 levels also rescues the NPC defects in *rtn1Δ yop1Δ* cells, overproducing NPC specific or SPB specific components only rescues the defects in their respective complex. Interestingly, Rtn1 and/or Yop1 physically

interact with Ndc1. We conclude that Rtn1 and Yop1 facilitate proper Ndc1 function in the NE at NPCs and SPBs.

Together with our prior work, *rtn1Δ yop1Δ* mutants have clear defects in the structure of both NPCs and SPBs. In addition to the NPC clusters, the NE in *rtn1Δ yop1Δ* cells also has partial NPC-like structures present on only the INM or ONM surface (DAWSON *et al.* 2009). Interestingly, the aberrant lobular SPB structures in *rtn1Δ yop1Δ* cells are not similar to other reported SPB morphological defects (Figure 2.1). The *rtn1Δ yop1Δ* mutant cells also have altered spindle function, indicative of defects in SPB migration due to insufficient or defective cytoplasmic microtubules (Figure 2.5-2.7). Although gross defects in insertion, such as monopolar spindles, are not observed, our data does suggest that the connections of the SPB to the NE are altered. Upon *SPC42* overexpression, a greater proportion of the superplaques in *rtn1Δ yop1Δ* cells are partially or fully disconnected from the NE (Figure 2.4). We speculate that both the NPC and SPB defects in *rtn1Δ yop1Δ* cells reflect decreased stability of the respective structure/complex in the NE.

Ndc1 is to date the only known factor common to both NPCs and SPBs. Based on the work here, we propose that Rtn1 and Yop1 are also common effectors of both NPCs and SPBs. We have previously shown that Rtn1 and Yop1 colocalize to NPC clusters in *nup133Δ* cells (DAWSON *et al.* 2009); however, there is no evidence of physical association of Rtn1 and Yop1 with SPBs. General changes to the lipid and protein composition of the NE are one of several possibilities by which the absence of Rtn1 and Yop1 could affect NPC and SPB stability. Alternatively, several pieces of evidence indicate that the *rtn1Δ yop1Δ* effect is directly perturbing NPCs and/or

SPBs. The SPB is associated with NPC clusters in *rtn1Δ yop1Δ* cells to a greater extent than it is in other NPC clustering mutants *nup133Δ* and *nup120Δ* (Figure 2.1F,G). Furthermore, the gene specificity in the overexpression suppression analysis is intriguing and indicates that the *rtn1Δ yop1Δ* defects are possibly not due to a general perturbation in NPC or the NE. Overexpression of *POM152* rescues the NPC clustering defect but does not rescue the SPB defects in *rtn1Δ yop1Δ* mutants. Likewise, overexpression of *MPS2* or *BBP1* results in rescue of spindle defects, but not NPC clustering. Interestingly, these multicopy suppressors of the *rtn1Δ yop1Δ* phenotypes are physical or genetic interactors of Ndc1/*NDC1.* Moreover, elevated Ndc1 levels rescue both the SPB and NPC defects in the *rtn1Δ yop1Δ* mutant. Based on this genetic data and the physical interaction between Ndc1 and Rtn1/Yop1, we speculate that Ndc1 function is potentially controlled by Rtn1 and/or Yop1.

Others have provided key data supporting a role for Rtns and Yop1/DP1 in stabilizing membrane curvature. Membrane reconstitution assays in the presence of purified Yop1 result in the formation of stable membrane tubules (HU *et al.* 2008), and in *rtn1Δ rtn2Δ yop1Δ* cells the ER structure is specifically altered (WEST *et al.* 2011). However, whereas all tubular ER is dramatically altered in *rtn1Δ yop1Δ* cells, the overall structural properties of the NE are not altered (DAWSON *et al.* 2009). We speculate that the *rtn1Δ yop1Δ* defects in NPCs and SPBs are due to highly localized or highly temporal defects in stabilizing membrane structures at NPCs and/or SPBs. Moreover, the Rtns and Yop1/DP1 could serve to facilitate the function of other proteins directly involved in the respective membrane association of NPCs and SPBs (see below). During NPC assembly, both positive and negative membrane curvature

are predicted to occur for the INM and ONM to fuse (ANTONIN 2009). The Rtns and Yop1/DP1 are proposed to function in the NE and stabilize the highly curved nuclear pore membrane during these early NPC biogenesis steps (DAWSON *et al.* 2009). The physical interactions between Rtn1 and Yop1 with Ndc1 (Figure 2.7B,C) and other membrane components of the NPC (Figure 2.7A (CHADRIN *et al.* 2010)) provide a plausible mechanism by which these proteins might be colocalized or recruited to nuclear pore membranes.

Our working model for how Rtn1 and/or Yop1 mediate NPC biogenesis extends directly to two alternative scenarios for how Rtn1 and/or Yop1 might impact SPB assembly. SPBs also require membrane curvature maintenance, with specific membrane changes required during SPB duplication and migration. First, it is possible that Rtn1 and Yop1 function with Ndc1 at both NPCs and SPBs (Figure 2.12A). Loss of Rtn1 and Yop1 might result in the need for increased levels of Ndc1 at both complexes to allow proper function. As such, both NPCs and SPBs are defective or not correctly assembled without additional Ndc1. Second, alternatively, it is possible that Rtn1 and Yop1 function with Ndc1 only at the NPC (Figure 2.12B). In this case, in the absence of Rtn1 and Yop1, increased levels of Ndc1 are sequestered by NPCs and potentially titrated away from SPBs. It is possible that overexpression of *MPS2* or *BBP1* rescues the SPB in *rtn1Δ yop1Δ* cells due to Mps2 and Bbp1 having overlapping functions with Ndc1 at the SPB, or due to physical interactions between these proteins resulting in Ndc1 being more efficiently targeted away from the NPC to the SPB. This second model places NPC and SPB assembly as acting antagonistically in terms of Ndc1 function.

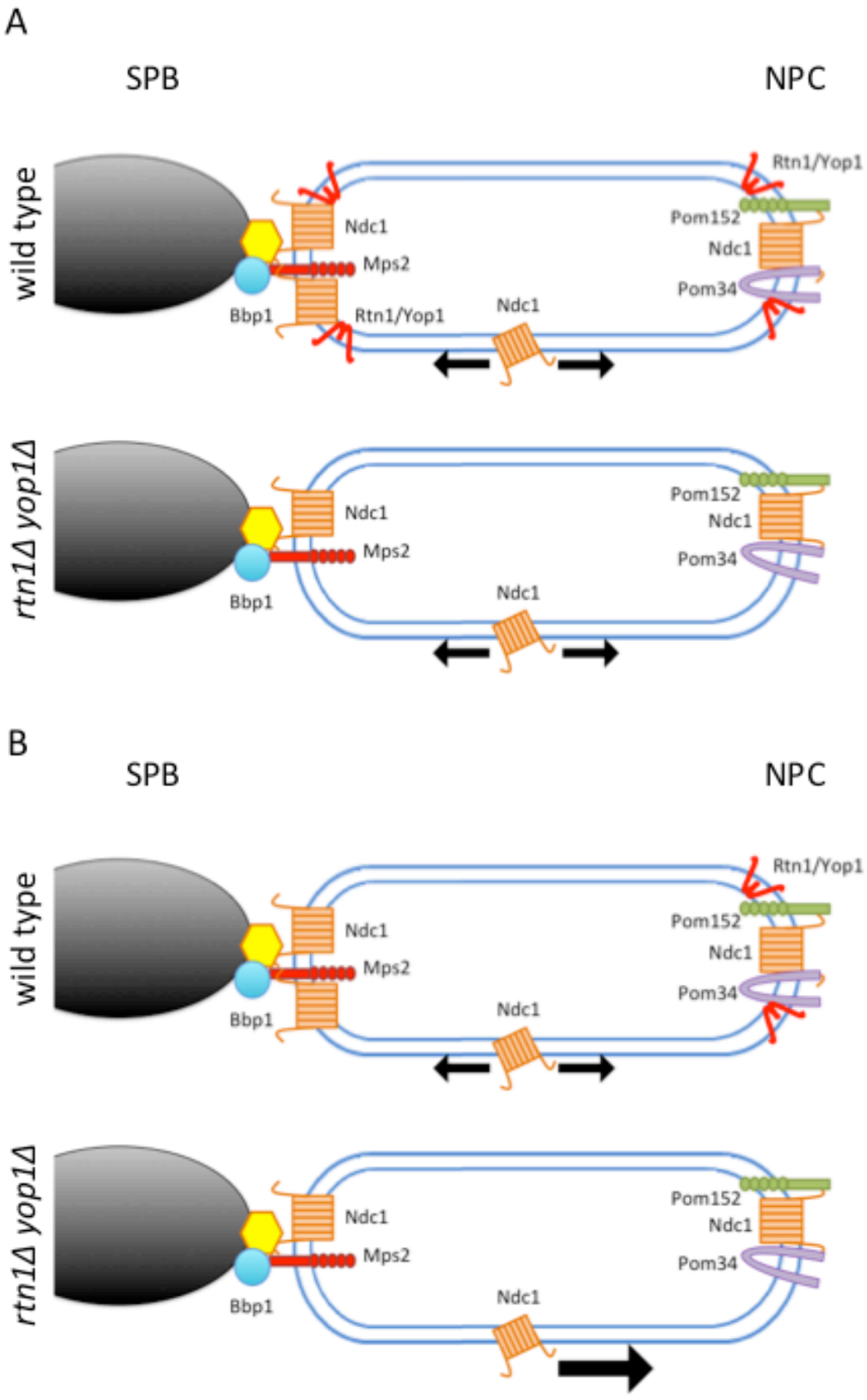
A
SPB
NPC
wild type
Ndc1
Mps2
Bbp1
Rtn1/Yop1
Ndc1
Pom152
Ndc1
Pom34
Rtn1/Yop1
rtn1Δ yop1Δ
Ndc1
Mps2
Bbp1
Ndc1
Pom152
Ndc1
Pom34
B
SPB
NPC
wild type
Ndc1
Mps2
Bbp1
Ndc1
Rtn1/Yop1
Pom152
Ndc1
Pom34
rtn1Δ yop1Δ
Ndc1
Mps2
Bbp1
Ndc1
Pom152
Ndc1
Pom34

Figure 2.12**: Models of Rtn1 and Yop1 function at NPCs and SPBs.**
(A) Model 1: Rtn1 and Yop1 function with Ndc1 at both NPCs and SPBs. Loss of Rtn1 and Yop1 results in defective NPCs and SBPs either via deficient recruitment of Ndc1 to these complexes or deficient stability of membrane structure. (B) Model 2: Rtn1 and Yop1 function with Ndc1 only at the NPC. Loss of Rtn1 and Yop1 results in less stable NPC insertion an increased requirement for Ndc1 at NPCs. Ndc1 sequestration at NPCs results in less Ndc1 available for SPBs, resulting in defects in SPB function.

It has been previously suggested that a feedback mechanism exists in response to defects in SPB duplication, with this resulting in antagonistic roles of the NPC and SPB complexes (WITKIN *et al.* 2010). Many SPB assembly mutants, including *ndc1-1* and *mps2-1*, are suppressed by specific deletions in genes encoding NPC components (CHIAL *et al.* 1998; SEZEN *et al.* 2009; WITKIN *et al.* 2010; FRIEDERICHS *et al.* 2011). Interestingly, proper Ndc1 levels are critical for cell survival, as illustrated by its haploinsufficiency and overexpression phenotypes leading to defects in SPB duplication (CHIAL *et al.* 1999). Our data, along with these studies, supports a model of competition between SPBs and NPCs for a common limiting component, Ndc1.

Since Ndc1 is thought to be targeted to SPBs and NPCs through specific physical interactions with other membrane proteins (ONISCHENKO *et al.* 2009), loss of *POM152* or *POM34* could result in a shift of Ndc1 recruitment to SPBs, which might aid in SPB assembly. Such a model of Ndc1 altered recruitment would suggest that competition for Ndc1 leads to antagonism of SPBs and NPCs.

Evidence exists to indicate that this antagonism between NPCs and SPBs is regulated within the cell. Inhibition of Pom34 translation by the Smy2-Eap1-Scp160-Asc1 (SESA) network is sufficient to rescue the temperature sensitive insertion defects of *mps2-2* cells (SEZEN *et al.* 2009). It is intriguing to consider that linking SPB and NPC assembly/function by such a mechanism might allow control of nuclear pore formation and number during specific cell cycle stages and restrict SPB duplication in the G1 phase of the cell cycle.

CHAPTER III

NUCLEAR PORE COMPLEX INTEGRITY REQUIRES LNP1, A REGULATOR OF CORTICAL ER.

INTRODUCTION

In eukaryotic cells, the nuclear envelope (NE) and endoplasmic reticulum (ER) are part of the same continuous membrane system and yet harbor distinct functions. The intrinsic connection is apparent in higher eukaryotes during open mitosis when the NE is absorbed into the ER, and the NE is reformed through the restructuring of cortical ER once mitosis is completed (HETZER 2010b).

Accordingly, proteins found in the ER are also present in the outer nuclear membrane (ONM) of the NE, whereas the inner nuclear membrane (INM) of the NE has a unique protein composition. Several ER proteins play distinct roles in the ER versus in the NE at NPCs, the 60 MDa assemblies embedded in NE pores that allow nucleocytoplasmic exchange (AITCHISON and ROUT 2012). To date, in *S. cerevisiae,* these include Sec13, Rtn1, Yop1, Pom33, and Per33 (HSIA *et al.* 2007; DAWSON *et al.* 2009; CHADRIN *et al.* 2010; CASEY *et al.* 2012; ZHANG and OLIFERENKO 2014). It is also intriguing that the structures of many nuclear pore complex (NPC) proteins (Nups) resemble the ER coat proteins that bind to and support the membrane curvature

---

This chapter is adapted from "Nuclear pore complex integrity requires Lnp1, a regulator of cortical ER" Amanda K Caesy, Shuliang Chen, Peter Novick, Susan Ferro-Novick, & Susan R. Wente". Submitted to *Molecular Biology of the Cell* on Jan 28, 2015".

during vesicle formation (BROHAWN *et al.* 2008). Further study of the connections between ER and NE membrane components is required to understand this focal point of cell physiology.

Work to date indicates that the proteins with distinct roles at the ER and NPC are specifically involved in NPC biogenesis and structure. In metazoans, NPCs are formed through two processes: post-mitotic biogenesis and interphase *de novo* biogenesis. The stepwise assembly of NPCs during post-mitotic assembly is well defined. After mitosis, as the NE reforms from the cortical ER, sites for NPC assembly are seeded by the ELYS/Nup107 complex on the chromatin. Pore membrane proteins (Poms) of the NPC are recruited as the NE reforms, stabilizing the pore into which other Nups assemble (HETZER *et al.* 2005; ANTONIN *et al.* 2008; DOUCET and HETZER 2010; DOUCET *et al.* 2010). During *de novo* assembly, the intact double membrane of the NE must fuse to allow the formation of a nascent pore. Only one pore membrane protein, Ndc1, is individually essential for *de novo* NPC assembly (CHIAL *et al.* 1998; MANSFELD *et al.* 2006; STAVRU *et al.* 2006). However, the mechanistic steps of the fusion event have been difficult to define potentially due to functional redundancies.

S. cerevisiae is a robust model system for analyzing *de novo* assembly as Nups are highly conserved and the yeast undergoes closed mitosis with all NPCs forming *de novo (ANTONIN et al. 2008; DOUCET and HETZER 2010)*. It is speculated that Poms, peripheral membrane-associated Nups, and changes in lipid composition all contribute to membrane deformation during NE fusion (ANTONIN *et al.* 2008; DOUCET and HETZER 2010; TALAMAS and HETZER 2011; VOLLMER *et al.* 2012). As the

membranes of both nascent pores and fully formed NPCs contain positive and negative curvature, membrane-bound proteins with curvature stabilizing properties might provide necessary support to nuclear pores. Our previous studies identified Rtn1 and Yop1, proteins required for ER tubule formation, as having a role in *S. cerevisiae* NPC assembly. Furthermore, *in vitro* NPC assembly assays using *Xenopus* extracts found that Rtn1 and Yop1 may promote NPC biogenesis (DAWSON *et al.* 2009; CASEY *et al.* 2012). A model was proposed wherein Rtn1 and Yop1 facilitate NE fusion via interactions with NPC membrane proteins and/or stabilize membrane structures during assembly. Once fusion has occurred, structural NPC components further stabilize the highly curved surface of the nascent pore and provide a scaffold onto which other Nups are incorporated (TALAMAS and HETZER 2011).

Environments of high curvature also exist at three-way junctions in reticulated ER. Previously, we identified Lnp1 as a regulator of ER tubule structure. In *S. cerevisiae*, loss of Lnp1 results in regions of collapsed cortical ER as well as regions of highly reticulated ER (CHEN *et al.* 2012). Recently, we found that the presence of mammalian Lnp1 at three way junctions in the ER stabilizes and decreases the mobility of these structures (CHEN *et al.* 2014). However, the mechanism by which Lnp1 leads to this stability is unknown. Interestingly, Lnp1 co-precipitates with and genetically interacts with Rtn1 and Sey1. Furthermore, when Sey1 is inactivated, Lnp1 accumulates on the NE (CHEN *et al.* 2012), which suggests a nuclear role for Lnp1. Thus, we tested whether Lnp1 or Sey1 play a role in NPC assembly.

In this report, I find that in addition to the anticipated ER/NE defects in *lnp1Δ rtn1Δ* mutants, there are distinct defects in NPC organization and nuclear shape. The *lnp1Δ* and *sey1Δ* mutants also exhibit synthetic genetic interactions with mutants in genes encoding key structural components of the NPC. I also find that the C-terminal region of Lnp1 is cytoplasmic and dimerizes *in vitro*. This dimerization is required for proper ER morphology; however, it does not appear necessary for NPC function. Interestingly, I observe functional connections between Lnp1 and Rtn1 at NPCs as well as both Sey1-dependent and -independent effects of Lnp1 on NPCs. These results provide important mechanistic context for Lnp1 function. We conclude that Lnp1 plays a key role in NPC integrity independent of ER functions.

MATERIALS AND METHODS

Yeast strains and plasmids

All strains and plasmids used in this study are listed in Table C1 and Table D1 (Appendix C and D). Unless otherwise noted, yeast genetic techniques were performed by standard procedures described previously (SHERMAN *et al.* 1986). All strains were cultured in either rich (YPD: 1% yeast extract, 2% peptone, and 2% dextrose) or complete synthetic minimal (CSM) media lacking appropriate amino acids with 2% dextrose. Kanamycin resistance was selected on medium containing 200ug/ml G418 (US Biological). Yeast were serially diluted and spotted onto agar plates to assay fitness and temperature sensitivity as previously described (TRAN *et al.* 2007).

Plasmid pSW3906 was generated by subcloning genomic DNA fragments containing promoter, coding sequence and 3'-UTR into the *BamHI* and *PstI* sites of pRS425. DNA fragments of *LNP1* were isolated by PCR amplification with Phusion (New England Biolabs) using primers *5'-ATGCGGATCCTGCGTGGCTGTGTCGA-3'* and *5'-ATCGCTGCAGCCGCCGCAGAAGGCAG-3'*. Plasmid pSW4029 was generated by subcloning genomic DNA fragments containing promoter, and coding sequence of *LNP1* into the *SacI* and *SacII* sites of pRS425. DNA fragments of LNP1-GFP were isolated by PCR amplification of *LNP1-GFP:HIS5* from the yeast GFP collection (HUH *et al.* 2003) with Phusion (New England Biolabs) using *primers 5'-ATGCGAGCTCTGCGTGGCTGTGTCGAGATT-3'* and *5'-GGCCGCGCCCGCGGGCCCTATTTGTATAGTTCATCC-3'*. Plasmid pSW3975 was generated by subcloning genomic DNA fragments containing the coding sequence of amino acids 104-278 of *LNP1* into the *EcoRI* and *SalI* sites of pMAL-cRI expression vector. DNA fragments were isolated by PCR amplification using primers *5'-GCTAGAATTCCGCAAGTTGGCAAAACTCCG-3'* and *5'-GCTAGTCGACTCATTTTGTTTTTTCCTTCTCCGAC-3'*. Plasmids pSW4032, pSW4071, and pSW4087 were generated by PCR amplification and blunt end ligation of pSW4029, pSW3975, and pSW3906, respectively, using primers *5'-GATTTTTTTGAAGGGAGAG-3*' and *5'-AACCACAAAATAGACGAAGTAAAGG-3*'.

Plasmids pSW4000 and pSW4001 were generated using the Gibson Assembly Method (New England Biolabs). pSW4000 was generated with DNA fragments of *myc-SUC2-myc* coding sequence PCR amplified from pSW3190 using primers *5'-*

ATATAGAGCTCCTACAGGTCCTCCTCTGAGATCAGCTTCTGCTCGCATTTTACTTCCCTTACT TGG-3' and *5'-*

AATTAGAGCTCTGCGAGCAGAAGCTGATCTCAGAGGAGGACCTGATGACAAACGAAACTAGC GATAG-3' and *LNP1* coding sequence using primers *5'-*

CCTCTGAGATCAGCTTCTGCTCGCAGAGCTCTAATTGTTTTGTTTTTTCCTTCTCCG-3' and *5'- CTGATCTCAGAGGAGGACCTGTAGGAGCTCTATATCTGATTTTGCGTTAGAATAACTACG -3'* into pRS315. pSW4001 was generated with DNA fragments of Rtn1 coding sequence using primers *5'-*

AAAAAAAATGAAAAAAAAAAACTGTTAATTTTTTTTTTTACTGATTTACAAATTCCTTG -3' and *5'-*

TGTTGTTGGGCTTGGCTATGTTGAGCTGAGGCGGACATATTTGCGTGTGTGAATATGGCCGT AATGGCCACTCTGC-3' and linearized pR3-N.

Immunoprecipitation

Yeast cells grown to early-log phase were harvested and resuspended in spheroplasting buffer (1.4 M sorbitol, 50 mM NaPi (pH 7.4), 50 mM 2-mercaptoethanol, 10μg/OD_{600} Zymolyase-100T). The resuspended cells were incubated at 37°C for 30 min, pelleted through a chilled sorbitol cushion (1.7 M sorbitol, 20 mM HEPES, pH 7.4), and the pellet was lysed in lysis buffer (25 mM HEPES, 150 mM KCl, 5 mM $MgCl_2$, 1 mM DTT, 1 mM PMSF, 1x protease inhibitor, 1% Digitonin, pH 7.4) using a dounce homogenizer (40 strokes). The lysate was centrifuged at 37,000 × g for 20 min at 4°C, and the protein concentration of the supernatant was measured using the Bradford assay.

The protein concentration of the lysate was adjusted to 2 mg/ml with lysis buffer, and 1.0 ml of the lysate was incubated overnight at 4°C with 20 μl of α-FLAG antibody (Clone M2, Sigma, F 1804). Thirty microliters of a 50% slurry of Protein G agarose beads (Thermo) was added to the lysate and incubated at room temperature for 2 hr. The beads were pelleted at 5000 rpm for 30 sec, and washed three times with 1 ml of cold lysis buffer that contained 0.2% digitonin, and heated to 100°C in sample buffer (62.5 mM Tris-HCl, 2% SDS, 5% 2-mercaptoethanol, 10% glycerol, 0.002% bromophenol, pH 6.8) for 5 min. The eluted protein was subjected to SDS-PAGE and immunoblotted with α -HA (1:2000 dilution, Clone HA.11, Covance, MMS-101R) antibody. The secondary antibodies used were goat α-mouse IgG-HRP (1:10,000 dilution, Promega W402B).

Membrane yeast two-hybrid system

Bait and prey plasmids were co-transformed into wild type or mutant reporter strains. Transformants were spotted onto CSM-Leu-Trp, CSM-Leu-Trp-His-Ade, and CSM-Leu-Trp-His-Ade+12mM 3-AT and analyzed for growth after 4 days at 25°C.

Fluorescence Microscopy

To measure the organization of NPCs across the NE, asynchronous cell populations expressing Nic96-GFP were imaged using a microscope (BX50; Olympus) equipped with a motorized stage (Model 999000, Ludl), a UPlanF1 100× NA 1.30 oil immersion objective, and digital charge coupled device camera (Orca-

R2; Hamamatsu). Images were collected and scaled using Nikon Elements and processed with ImageJ or Photoshop 12.0 software. The aggregation index of each nuclei was determined as previously described (NIEPEL *et al.* 2013) using the Oval Profile Plot plug-in (http://rsbweb.nih.gov/ij/plugins/oval-profile.html) of ImageJ.

To image the ER, asynchronous cell populations expressing Sec61-GFP were imaged by widefield microscopy using a Delta Vision OMX (Applied Precision) using a 60x NA 1.42 oil immersion objective. Images were deconvolved using softWoRx® software, and scaled using ImageJ or Photoshop 12.0 software.

For immunofluorescence, cells were fixed in 3.7% formaldehyde and 10% methanol for 10 min and processed as previously described (STRAWN *et al.* 2004). Samples were incubated with affinity purified rabbit α-Nup116C (1:50) (IOVINE *et al.* 1995), and chicken α-GFP (ASW54)(1:2000) at 4°C overnight. The α-GFP antibody was generated in chickens against purified 6xHIS-GFP recombinant protein (Covance, Inc). IgY was purified from egg yolks using the IgY EggsPress purification system (Gallus Immunotech Inc Cary, North Carolina).Bound antibodies were detected by incubation with Alexa Fluor 594-conjugated α-rabbit (1:500) and Alexa Fluor 488-conjugated α-chicken (1:200). Cells were imaged using a Leica TCS SP5 confocal microscope using a 63X (1.4 NA) oil-immersion objective.

Electron Microscopy

Asynchronous cells were grown in YPD at 25°C to early log phase and processed as previously described (Dawson et al 2009). Grids were examined on a CM-12 120-keV electron microscope (FEI). Images were acquired with MegaPlus ES

4.0 camera (Advanced Microscopy Techniques) and processed with ImageJ and Photoshop 12.0 software.

Endoglycosidase H treatment

Wild type cells were transformed with pSW3190, pSW3192, or pSW4000. Transformants were grown in CSM-Leu to early log phase. Cells were harvested, and samples were processed as previously described (Miao et al 2005). Samples were precipitated with TCA and analyzed by immunoblotting.

Biochemical Analysis of Recombinant Proteins

MBP-Lnp1$_{Cterm}$ and MBP-Lnp1$_{CtermDznfn}$ were expressed in BL21-RIL (DE3) cells (Stratagene). Bacteria were pelleted and lysed by sonication in buffer (20mM HEPES pH7.5, 145mM NaCl, 5mM KCl, 10μM ZnSO4). Affinity purification with amylose resin (New England Biolabs) was performed with the soluble fraction of lysates according to manufacturer recommendations. Proteins were further purified by size exclusion chromatography with a S200 column (GE Healthcare). Sedimentation velocity analytical ultracentrifugation and analysis was performed as previously described (FOLKMANN *et al.* 2013).

RESULTS

lnp1Δ rtn1Δ cells have defects in NPC organization

To determine if Lnp1 or Sey1 have a role in NPC structure or assembly, I tested if loss of either Lnp1 or Sey1 disturbs NPC organization. Whereas NPCs are

distributed throughout the NE in wild type cells, NPCs with structural and/or assembly defects aggregate in the NE as clusters (BELGAREH and DOYE 1997; BUCCI and WENTE 1997). To visualize NPCs, wild type and mutant cells endogenously expressing Nic96-GFP were imaged by wide field microscopy (Figure 3.1A). The distribution of NPCs in the NE was determined by measuring the aggregation index of individual nuclei (Figure 3.1B), with a higher aggregation index indicating a greater degree of NPC disorder within the NE (NIEPEL *et al.* 2013). While a subset of the cell population in *rtn1Δ* mutants displayed a minor NPC clustering defect, the localization of Nic96-GFP in *lnp1Δ* and *sey1Δ* mutants was indistinguishable from wild type. However, the localization of Nic96-GFP in *lnp1Δ rtn1Δ* mutants displayed a more severe clustering defect than *rtn1Δ* alone. The *rtn1Δ sey1Δ* double mutant did not exhibit an increase in NPC clustering. Furthermore, the aggregation index of *lnp1Δ rtn1Δ sey1Δ* compared to *lnp1Δ rtn1Δ* was unaltered, indicating that the role of Sey1 as an Lnp1 antagonist is not involved in this process (Figure 3.1A and 3.1B).

To further investigate the NPC aggregation defect in the *lnp1Δ rtn1Δ* mutant, the nuclei and NPCs of these cells were examined by thin section transmission electron microscopy (TEM). TEM images of *lnp1Δ rtn1Δ* cells revealed misshapen nuclei with small clusters of NPCs, consistent with live cell microscopy data (Figure 3.1A and Figure 3.2). Previously, we reported that some of the NPC-like structures in *rtn1Δ yop1Δ* cells were not evenly anchored into the NE by association with only the INM or ONM and that spindle pole bodies were also deformed (DAWSON *et al.* 2009; CASEY *et al.* 2012). However, I did not observe these defects in *lnp1Δ rtn1Δ* cells.

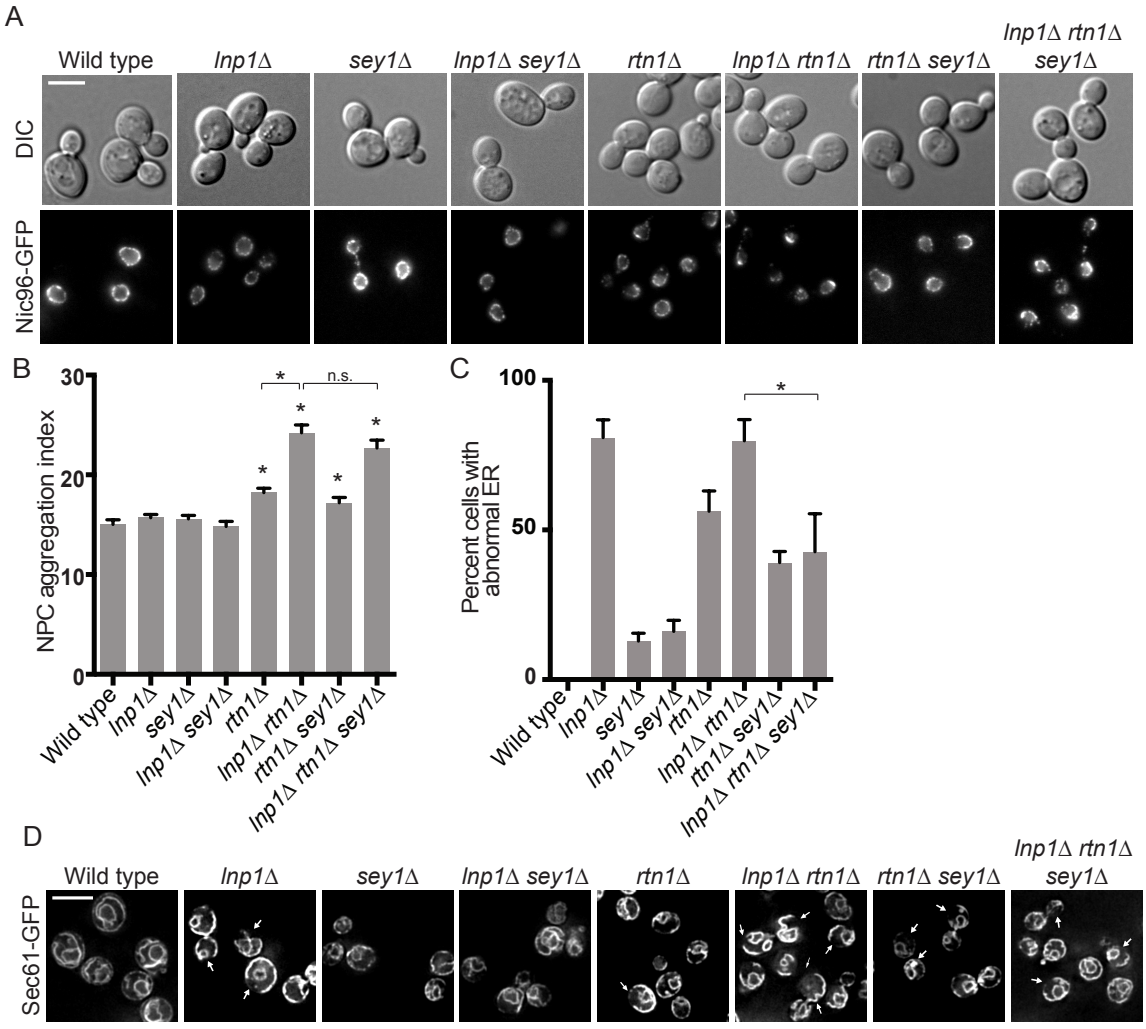

Figure 3.1: ***lnp1Δ rtn1Δ* cells have defects in NPC organization.**
(A) Parental or mutant cells expressing Nic96-GFP were grown to early log phase at 25°C and were visualized by fluorescence microscopy. Scale bar, 5 μm. (B) The aggregation indexes of Nic96-GFP-expressing cells were determined. Error bars represent standard error. Asterisk denotes statistical significance (P-value <0.01). n.s. detones no statistical significance. (C) The percentages of cells with abnormal ER morphology were quantified from images of Sec61-GFP expressing cells. Error bars represent standard error. Asterisk denotes statistical significance (P-value <0.01) by student's t-test. (D) Parental or mutant cells expressing Sec61-GFP were grown to early log phase at 25°C and were visualized by fluorescence microscopy. Scale bar, 5 μm. Arrows indicate regions of collapsed cortical ER.

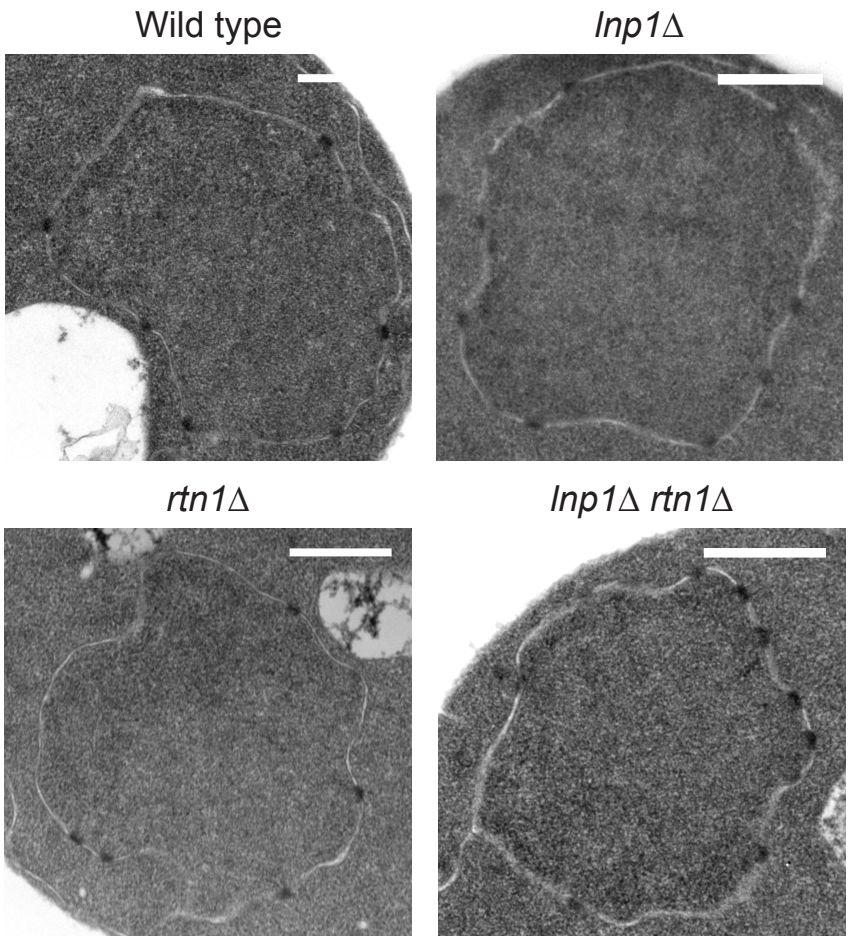

Figure 3.2: **TEM of nuclear pores in *lnp1Δ rtn1Δ* cells.**
Parental, *lnp1Δ*, *rtn1Δ, or lnp1Δ rtn1Δ* cells were grown to early log phase at 23°C and processed for TEM. Scale bar, 500 nm.

Since *rtn1Δ, lnp1Δ,* and *sey1Δ* mutants have ER morphology defects (HU *et al.* 2009; ANWAR *et al.* 2012; CHEN *et al.* 2012), I asked if the defects in NPC organization correlated with abnormal ER morphology. Wild type and mutant cells endogenously expressing Sec61-GFP were imaged by wide field microscopy and visually assessed for defects in ER morphology (Figure 3.1C and 3.1D). As previously reported, the ER of *lnp1Δ* cells was abnormal, with large regions of collapsed cortical ER (CHEN *et al.* 2012). Furthermore, I observed an enhanced ER defect in *lnp1Δ rtn1Δ* cells that was partially rescued in the *lnp1Δ rtn1Δ sey1Δ* mutants. Though *rtn1Δ sey1Δ* cells have defects in ER morphology, with reduced ER tubules and increased ER sheets, these mutants do not have an increase in NPC aggregation (Figure 3.1A-D). Taken together, these results indicated that Lnp1 could play a role in NPC and NE organization independent of its role in ER structure.

Lnp1 and Sey1 localize to the NE and physically interact with shared ER and NPC components.

To determine if Lnp1 and Sey1 are steady-state components of NPCs, I examined Lnp1-GFP and Sey1-GFP localization in NPC clustering mutants. For structural components of the NPC, in NPC clustering mutants, localization shifts from throughout the NE rim to predominantly in the NPC cluster (Figure 3.3A). Wild type and *nup133Δ* mutant cells endogenously expressing Lnp1-GFP, Sey1-GFP or Rtn1-GFP were grown to log phase, fixed, and labeled by indirect immunofluorescence with α-GFP and α-Nup116 antibodies. As previously described (DAWSON *et al.* 2009), Rtn1-GFP localized to both the cortical ER and to the NPC

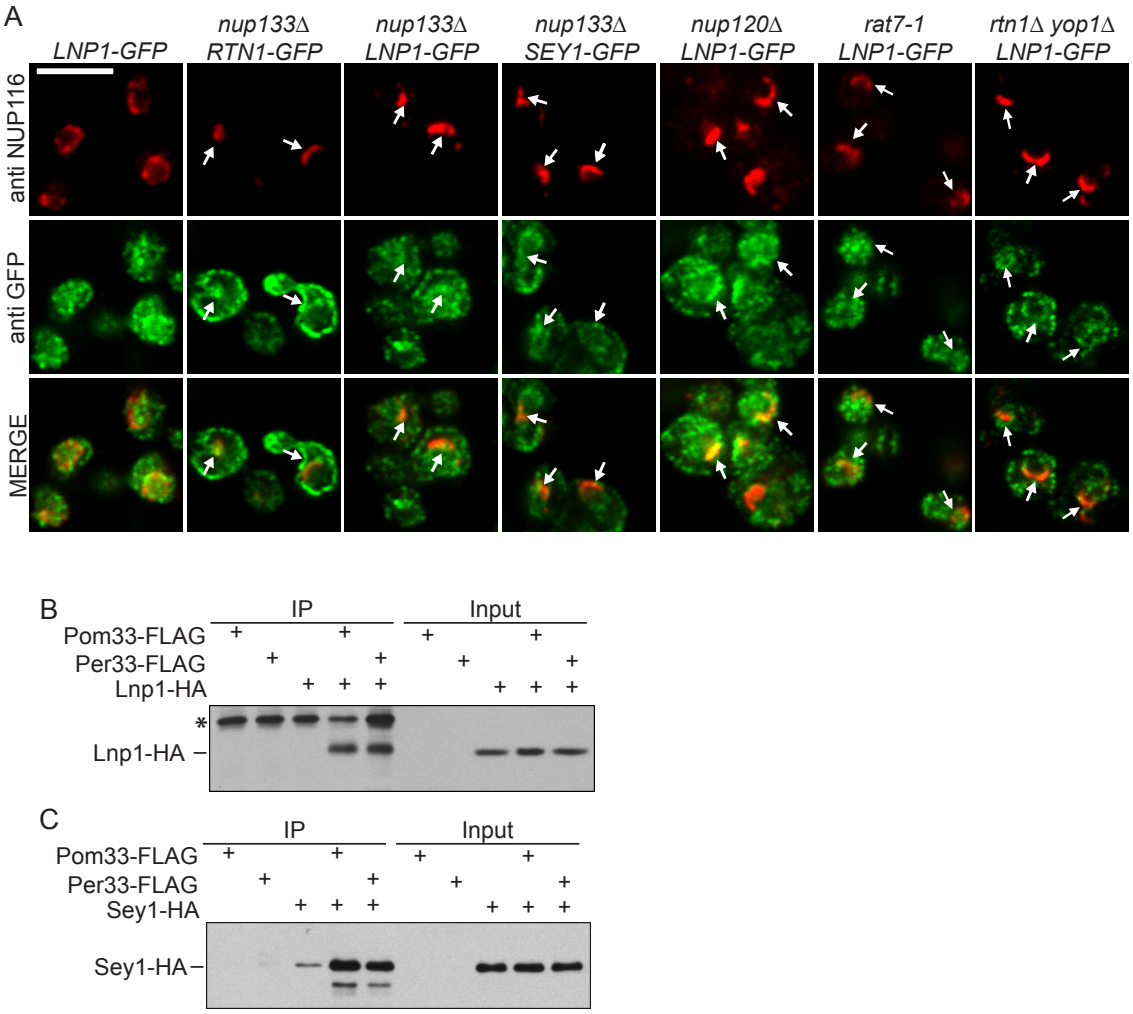

Figure 3.3: **Lnp1 and Sey1 localize to the NE and physically interact with shared ER and NPC components.**
(A) Indirect immunofluorescence microscopy was performed with cells using chicken α-GFP and rabbit α-Nup116C antibodies. Arrows indicate NPC clusters. (B) Contributed by Shuliang Chen from the laboratory of Susan Ferro-Novick. Yeast lysates were prepared from cells expressing Pom33-FLAG, Per33-FLAG, Lnp1-HA, Pom33-FLAG and Lnp1-HA, or Per33-FLAG and Lnp1-HA. Lysates were immunoprecipitated with α-FLAG affinity matrix and blotted using α-HA antibodies. Asterisk indicates contaminant band. (C) Contributed by Shuliang Chen from the laboratory of Susan Ferro-Novick. Yeast lysates were prepared from cells expressing Pom33-FLAG, Per33-FLAG, Sey1-HA, Pom33-FLAG and Sey1-HA, or Per33-FLAG and Sey1-HA. Lysates were immunoprecipitated with α-FLAG affinity matrix and blotted using α-HA antibodies.

clusters in *nup133Δ* cells (Figure 3.3A). In wild type cells, Lnp1-GFP and Sey1-GFP primarily localize as puncta in the tubular ER and NE (CHEN *et al.* 2012). In *nup133Δ* mutants, Lnp1-GFP and Sey1-GFP localization in the ER was not noticeably altered (Figure 3.3A). In addition, both continued to be localized throughout the NE including the NPC cluster region (although the signal was not enriched at the clusters). The same localization results were observed in *nup120D* and *rat7-1* clustering mutants (Figure 3.3A). Thus, unlike Rtn1, Lnp1 and Sey1 were not stably associated with clustered NPCs. Interestingly, in *rtn1Δ yop1Δ* mutants Lnp1-GFP localization was markedly perturbed. Without a highly branched ER network, Lnp1-GFP was more evenly distributed throughout the ER and NE in *rtn1Δ yop1Δ* cells; moreover, the localization of Lnp1-GFP at NPC clusters was diminished (Figure 3.3A, Figure 3.4). This suggested that the localization of Lnp1 to areas of the NE with NPC clusters is dependent on Rtn1 and Yop1.

We next tested whether the association of Lnp1 with NE-NPC regions was due to physical interactions. Both Lnp1 and Sey1 physically interact with Rtn1 and Yop1 by co-immunoprecipitation (CHEN *et al.* 2012). Here we focused on association of Lnp1 and Sey1 with Pom33 and Per33, other ER components that have roles at the NPC (CHADRIN *et al.* 2010). Pom33 and Per33 have strong connections to NPC organization in both *S. cerevisiae* and *S. pombe* (CHADRIN *et al.* 2010; ZHANG and OLIFERENKO 2014). Lysates of yeast cells endogenously expressing Pom33-FLAG or Per33-FLAG and either Lnp1-HA or Sey1-HA were incubated with α-FLAG affinity matrix. Immunoblots of bound samples revealed that Pom33-FLAG and Per33-FLAG are co-isolated with both Lnp1-HA and Sey1-HA (Figure 3.3B and 3.3C). Taken

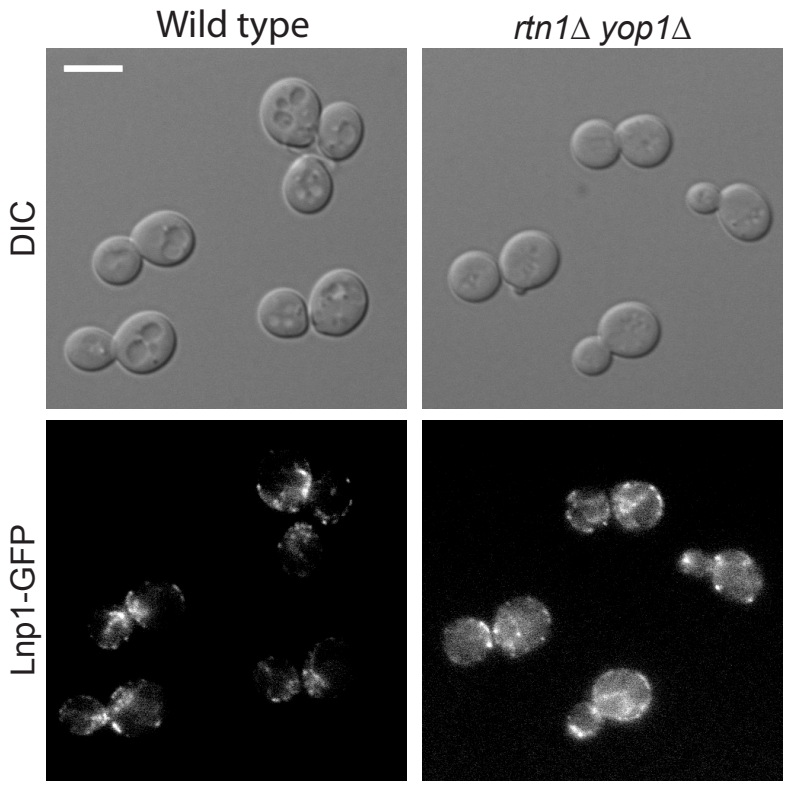

Figure 3.4: **Live cell localization of Lnp1-GFP.**
Parental and *rtn1Δyop1Δ* cells expressing Lnp1-GFP were grown to early log phase at 25°C and were visualized by fluorescence microscopy. Scale bar, 5 μm.

together, Lnp1 and Sey1 were biochemically and cell biologically linked to the NE and NPC components.

lnp1Δ and *sey1Δ* mutants genetically interact with mutants in genes of the Nup84 subcomplex.

To further understand the role of Lnp1 and Sey1 in the NE, the growth phenotypes were analyzed for *lnp1Δ* and *sey1Δ* mutants in combination with different *nup* mutants. The NPC is organized within the NE pore in an apparent eightfold rotational symmetry perpendicular to the membrane plane. Distinct general domains include the nuclear basket, cytoplasmic filaments, and a central core structural scaffold surrounding a central channel. The core NPC scaffold consists of a series of inner, outer and luminal rings connected by linker complexes (ALBER *et al.* 2007b; AITCHISON and ROUT 2012). A panel of mutants was tested, including those genes encoding membrane-bound components of the NPC (*pom33Δ , per33Δ* , *pom152Δ*, *pom34Δ*), structural Nups in the Nup84 (vNup107) subcomplex (*nup133Δ*, *nup120Δ*, *nup84Δ*, *nup85Δ*, *nup145ΔN*, *nup145Δ302*), membrane-binding components of the inner ring (*nup53Δ, nup59Δ*), and nups that directly participate in nucleocytoplasmic transport (*nup100Δ, rat7-1*) (Table 1). To determine if the combinatorial mutants displayed enhanced growth defects, strains were assayed by growth on rich media at a range of temperatures. Whereas *pom33Δ* and *per33Δ* mutants do not have growth defects alone (CHADRIN *et al.* 2010), the *lnp1Δ pom33Δ*, *lnp1Δ per33Δ*, *sey1Δ pom33Δ*, and *sey1Δ per33Δ* double mutants displayed synthetic fitness defects at higher temperatures (Figure 3.5A and Table

Table 3.1: **Genetic interactions with *lnp1Δ* and *sey1Δ***

	lnp1Δ	***sey1Δ***
pom33Δ	synthetic sick	synthetic sick
rtn1Δ pom33Δ	no effect	-
rtn1Δ yop1Δ pom33Δ	synthetic sick	-
per33Δ	synthetic sick	synthetic sick
rtn1Δ per33Δ	synthetic sick	-
rtn1Δ yop1Δ per33Δ	synthetic sick	-
pom152Δ	no effect	-
pom34Δ	no effect	-
pom152Δ pom34Δ	no effect	-
ndc1-4	no effect	synthetic sick
nup53Δ	no effect	no effect
nup59Δ	no effect	no effect
nup53Δ nup59Δ	no effect	no effect
rat7-1 (nup159)	no effect	no effect
nup100Δ	no effect	no effect
nup133Δ	no effect	synthetic sick
nup120Δ	synthetic sick	synthetic sick
nup145ΔN	synthetic sick	no effect
nup145Δ302	synthetic sick	rescue
nup84Δ	synthetic sick	synthetic sick
nup85Δ	synthetic sick	synthetic sick

3.1). In addition, the growth defects of *rtn1Δ yop1Δ per33Δ* and *rtn1Δ yop1Δ pom33Δ* triple mutants were enhanced when combined with *lnp1Δ* (Figure 3.5A and Table 3.1).

Based on the genetic and physical interactions for Lnp1 and Sey1 with Rtn1 and Yop1, I predicted that *lnp1Δ* would genetically interact with mutants in genes encoding NPC components in a manner similar to that found for the *rtn1Δ yop1Δ* double mutant (DAWSON *et al.* 2009). However, major differences in the genetic interaction profiles of *rtn1Δ* and *lnp1Δ* were observed. Notably, all mutants of the Nup84 subcomplex tested (*nup133Δ*, *nup120Δ*, *nup84Δ*, *nup85Δ*, *nup145ΔN*, *nup145Δ302*) had enhanced growth defects in combination with *lnp1Δ* whereas other NPC mutants (*pom34Δ pom152Δ*, *nup53Δ nup59Δ*, *nup100Δ*, *rat7-1*) had no enhanced growth defect with *lnp1Δ* Table 1). Interestingly, *sey1Δ* also genetically interacted with *nup133Δ*, *nup120Δ*, and *nup84Δ* in a similar manner to *lnp1Δ*. Furthermore, an *lnp1Δ sey1Δ nup133Δ* triple mutant exhibited partial rescue of growth defects compared together *lnp1Δ nup133Δ* or *sey1Δ nup133Δ* double mutants (Figure 3.5B). Overall, the observed genetic interactions revealed novel relationships between Lnp1, Sey1, Rtn1, and Yop1 in NE and NPC function.

The function of Lnp1 and Sey1 at NPCs is coupled with the interaction between Rtn1 and the NPC

Previously, we reported that Rtn1 and Yop1 physically interact with NPC components, including the pore membrane protein Ndc1 (CASEY *et al.* 2012). To test

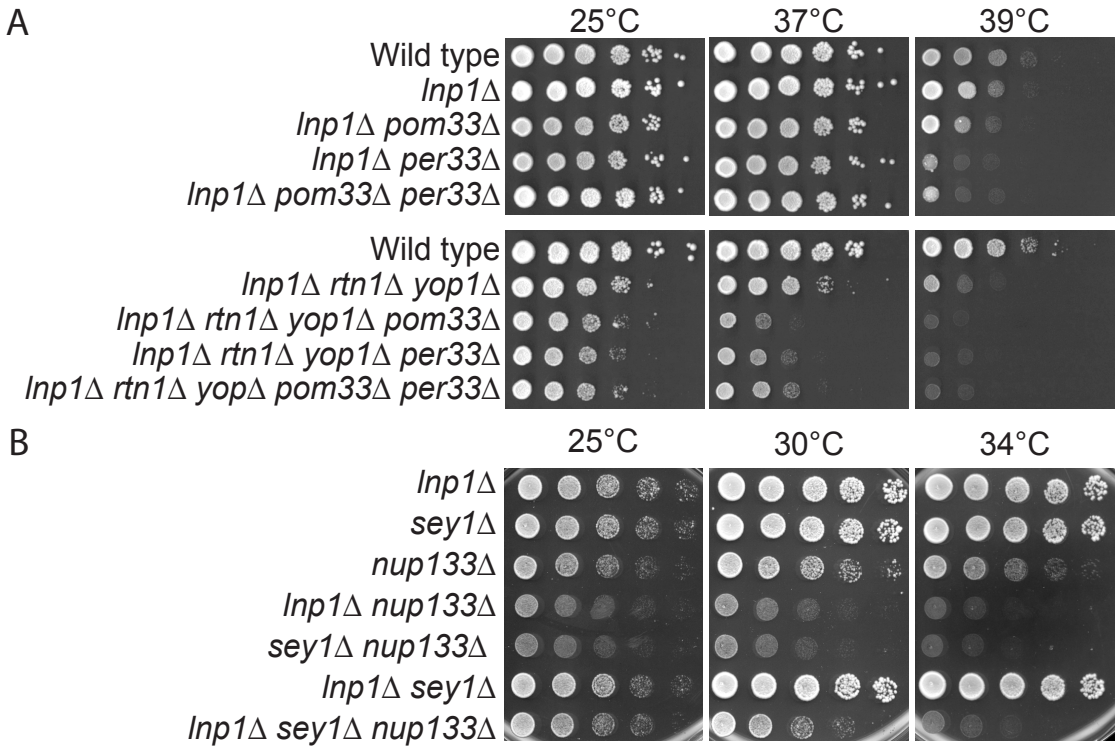

Figure 3.5: ***lnp1Δ* and *sey1Δ* mutants genetically interact with mutants in genes of the Nup84 subcomplex.**
(A) Contributed by Shuliang Chen from the laboratory of Susan Ferro-Novick. *lnp1Δ pom33Δ* and *lnp1Δ rtn1Δ yop1Δ pom33Δ* mutants have enhanced growth defects. Yeast strains were grown at 25°C and five-fold serially diluted onto plates of rich media incubated at the listed temperatures. (B) *lnp1Δ nup133Δ* and *sey1Δ nup133Δ* mutants have enhanced growth defects. Yeast strains were grown at 25°C and five-fold serially diluted onto plates of rich media incubated at the temperatures indicated.

whether *lnp1Δ* and *sey1Δ* impact the recruitment of Rtn1 to NPCs, I used a split ubiquitin yeast two-hybrid system to monitor the interaction between Rtn1 and Ndc1. Rtn1 tagged with the amino- (N-)terminal region of ubiquitin (NubG) was co-expressed with Ndc1 tagged with the carboxy- (C-)terminal region of Ubiquitin (Cub) and the LexA-VP16 transcription factor. A close physical interaction between the bait (Ndc1-Cub) and prey (NubG-Rtn1) proteins leads to cleavage of the split ubiquitin from the bait and release of the LexA-VP16 transcription factor. Once released, the LexA-VP16 transcription factor can activate reporter genes *HIS3* and *ADE2* (SNIDER *et al.* 2010). Activation of these reporter genes was assayed by growth on synthetic media lacking histidine and adenine. To increase the stringency of the physical interaction threshold, the histidine biosynthesis competitive inhibitor 3-aminotriazole (3-AT), was added to growth medium to increase the baseline level of *HIS3* expression required for cell survival.

We assayed for interaction between Cub-Ndc1 and NubG-Rtn1 in wild type, *lnp1Δ*, and *sey1Δ* reporter strains (Figure 3.6A). All three strains grew on media lacking histidine and adenine; however, addition of 12mM 3-AT to the growth medium resulted in loss of growth of the *sey1Δ* reporter strain. This indicated that *sey1Δ* mutants exhibit a decreased interaction between NubG-Rtn1 and Cub-Ndc1. I tested whether the interaction between Cub-Ndc1 and Yop1-NubG was similarly affected; however, no changes in the interaction between Ndc1 and Yop1 were observed in *lnp1Δ* and *sey1Δ* mutants (Figure 3.6A).

Because *lnp1Δ rtn1Δ* mutants had defects in NPC organization and loss of Sey1 altered the Rtn1 and Ndc1 interactions, I hypothesized that overexpression of

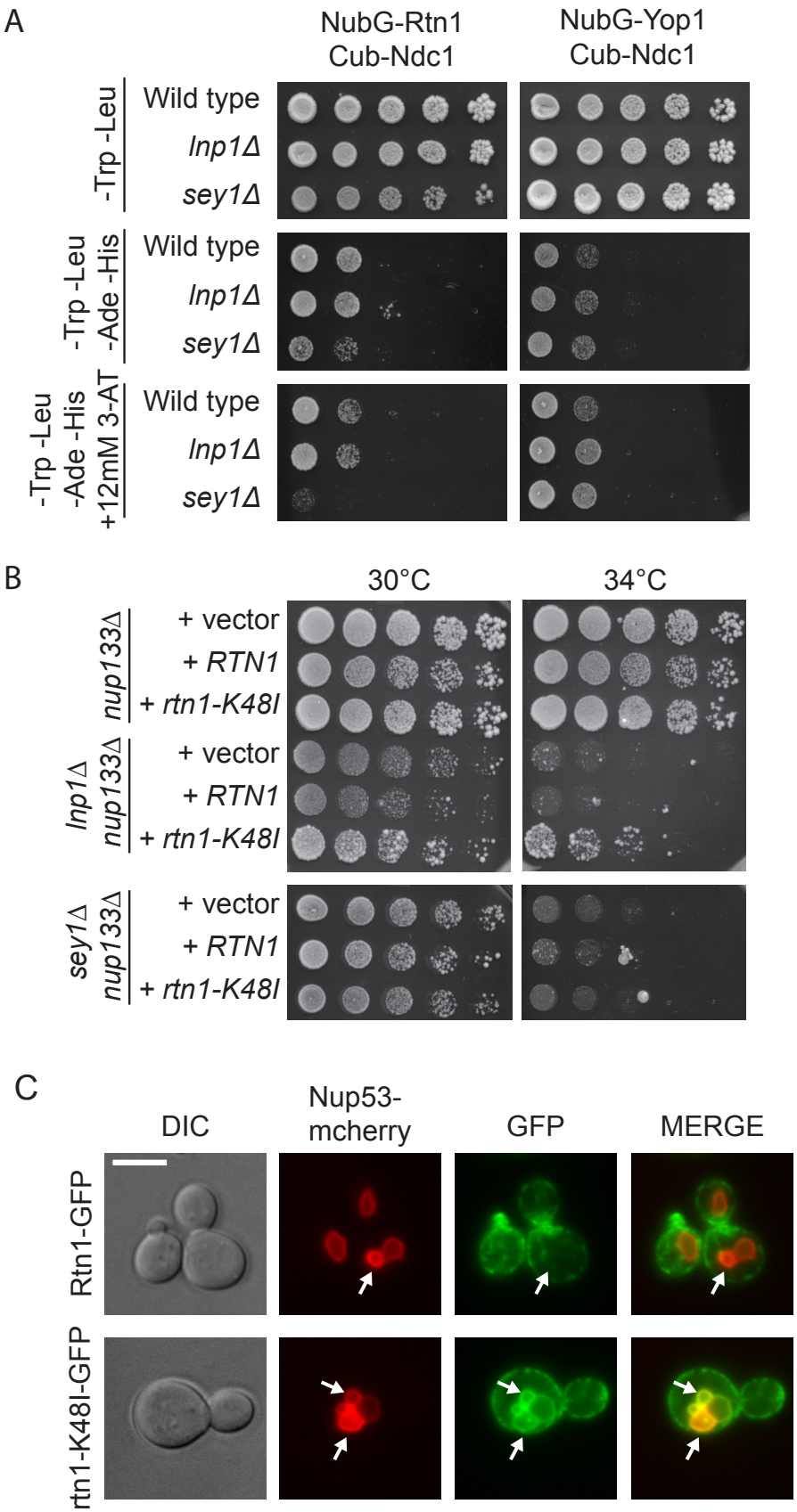
A
NubG-Rtn1
Cub-Ndc1
NubG-Yop1
Cub-Ndc1
-Trp -Leu
Wild type
Inp1Δ
sey1Δ
-Trp -Leu
-Ade -His
Wild type
Inp1Δ
sey1Δ
-Trp -Leu
-Ade -His
+12mM 3-AT
Wild type
Inp1Δ
sey1Δ
B
30°C
34°C
nup133Δ
+ vector
+ RTN1
+ rtn1-K48I
Inp1Δ nup133Δ
+ vector
+ RTN1
+ rtn1-K48I
sey1Δ nup133Δ
+ vector
+ RTN1
+ rtn1-K48I
C
DIC
Nup53-mcherry
GFP
MERGE
Rtn1-GFP
rtn1-K48I-GFP

Figure 3.6: **The function of Lnp1 and Sey1 with NPCs is coupled with the interaction between Rtn1 and the NPC.**
(A) Split ubiquitin yeast two-hybrid vectors containing genes encoding either NubG-Yop1 or NubG-Rtn1 (preys) were expressed in wild type or mutant strains and tested for interaction with Ndc1-Cub (Bait). Presence of both bait and prey plasmids was detected on SCM-Leu-Trp. Interaction of bait and prey was assayed by growth on SCM-Leu-Trp-His-Ade with and without 3-AT. (B) Overexpression of *rtn1-K48I* results in rescue of *lnp1Δ nup133Δ, nup133Δ lnp1Δ nup133Δ*, and *sey1Δ nup133Δ* mutants were transformed with plasmids encoding *RTN1, rtn1-K48I,* or empty vector and grown to early log phase at 25°C and five-fold serially diluted onto SCM-Leu plates at the indicated temperatures. (C) Cells expressing either Rtn1-GFP or rtn1-K48I-GFP were grown to early log phase at at 25°C, induced for overexpression of Nup53-mcherry for 8 hr, and visualized by fluorescence microscopy. Arrows indicate nuclear karmellae. Scale bar, 5 μm.

RTN1 might rescue growth defects observed in *lnp1Δ nup133Δ* mutants and *sey1Δ nup133Δ* mutants. I also tested overexpression of the *rtn1-K48I* mutant which localizes primarily to the NE and is observed to be deficient in self-oligomerization and in ER tubule stabilization (HU *et al.* 2008; SHIBATA *et al.* 2008) but not in NPC function (DAWSON *et al.* 2009). Overexpression of *RTN1* did not alter the growth defect of *lnp1Δ nup133Δ* or *sey1Δ nup133Δ* mutants. However, overexpression of the *rtn1-K48I* mutant specifically rescued the growth defect of *lnp1Δ nup133Δ* mutants, but not *nup133Δ sey1Δ* mutants (Figure 3.6B).

Because the rtn1-K48I protein is deficient in self-oligomerization and is more mobile in the ER (SHIBATA *et al.* 2008), I hypothesized that this mutant would also have increased mobility in the NE. To test this, I compared Rtn1-GFP and rtn1-K48I-GFP for their ability to accumulate Nup53-induced intranuclear karmellae. Upon *NUP53* overexpression, the nuclei of many cells accumulate flattened intranuclear membranes. Membrane components of the NPC associate within these intranuclear karmellae (MARELLI *et al.* 2001). Whereas Rtn1-GFP did not associate with these structures (n=30), I found that the rtn1-K48I-GFP was localized to 66% of Nup53 karmellae observed (n=33) (Figure 3.6C). Taken together, these results suggest that the rtn1-K48I protein is localized through the NE more effectively than wild type.

The zinc finger domain of Lnp1 mediates dimerization is required for ER but not NPC function

The human ortholog of Lnp1 contains two N-terminal trans-membrane domains with both the N- and C-terminus extending into the cytoplasm.

Furthermore, the human homolog of Lnp1 is N-myristoylated, and the N-myristolation is necessary for its function in ER morphology (MORIYA *et al.* 2013). However, *S. cerevisiae* Lnp1 does not contain this N-myristolyation motif (MORIYA *et al.* 2013), indicating key differences between these homologs. To determine the topology of yeast Lnp1, it was tagged at the C-terminus with Suc2 flanked by myc tags for antibody detection. Suc2 is a target for glycosylation within the ER lumen. If the C-terminus of Lnp1 localizes to the ER lumen, the Suc2 tag will be glycosylated and treatment with Endoglycosidase H (EndoH) will result in a decrease in the molecular mass. Pom152-myc-Suc2-myc and Pom34-myc-Suc2-myc were used as positive and negative controls for glycosylation, respectively (MIAO *et al.* 2006). Lysates were treated with EndoH, precipitated and analyzed by immunoblotting (Figure 3.7A). While EndoH digestion of Pom152-myc-Suc2-myc resulted in a reduction of molecular mass, digestion of Lnp1-myc-Suc2-myc and the negative control did not, indicating that the C-terminus of Lnp1 is located in the cytoplasm and not in the ER/NE lumen. This predicted topology is consistent with that reported for human Lnp1 (MORIYA *et al.* 2013).

The C-terminal Lnp1 region contains a zinc finger motif that has a critical yet unknown role in ER function (CHEN *et al.* 2012). Many proteins involved in mediating ER morphology self-interact as a key element in their function (VOELTZ *et al.* 2006; HU *et al.* 2008; SHIBATA *et al.* 2008; ANWAR *et al.* 2012).

We hypothesized that the Lnp1 zinc finger motif mediates dimerization between Lnp1 molecules. To test this hypothesis, the oligomeric state of the purified recombinant C-terminus (amino acids 104-278) of Lnp1 fused to MBP (MBP-

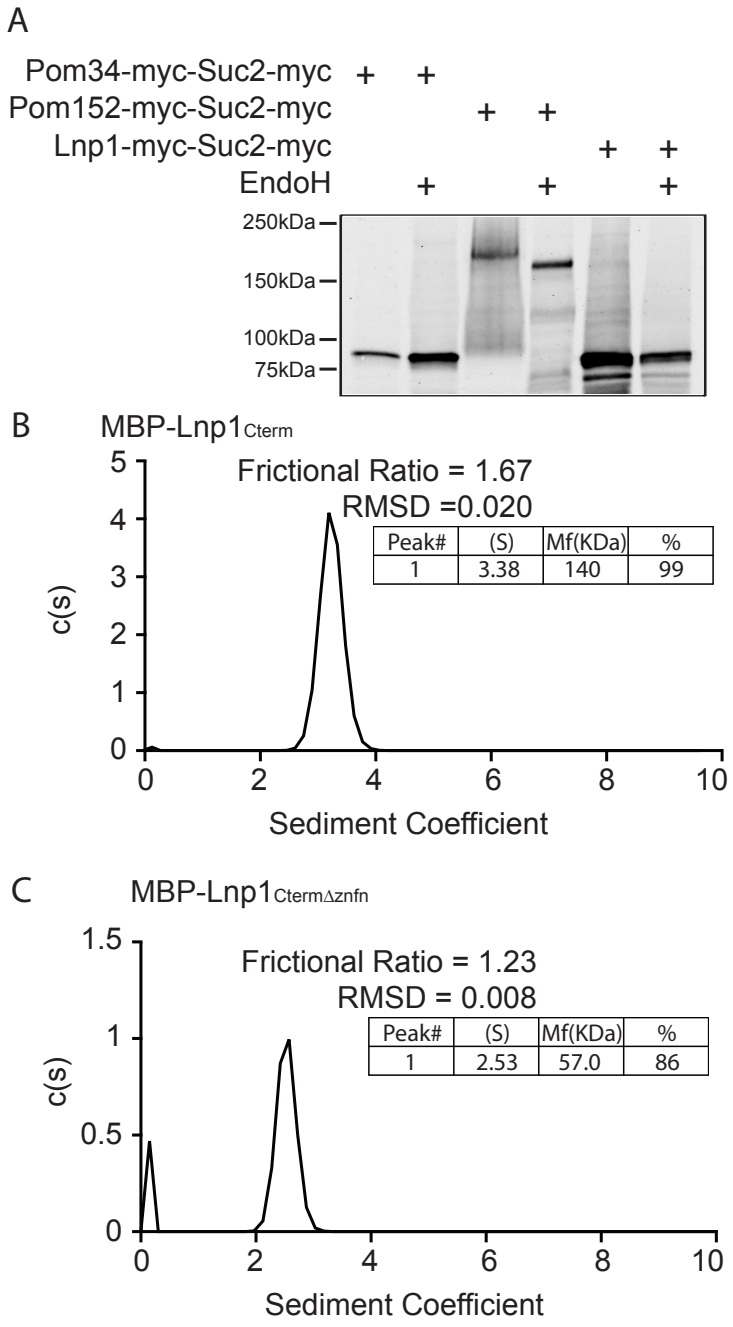

Figure 3.7: **The C terminal zinc finger domain of Lnp1 is required for dimerization *in vitro.***
(A) Lysates from cells expressing Pom34-myc-Suc2-myc, Pom152-myc-Suc2-myc, or Lnp1-myc-Suc2-myc were either mock digested or treated with EndoH and analyzed by immunoblotting with mouse α-Myc antibody. (B-D) Sedimentation velocity analytical ultracentrifugation was performed with recombinant MBP-Lnp1$_{Cterm}$ and MBP-Lnp1$_{Cterm\Delta znfn}$. Determined molecular masses are given for major species.

Lnp1$_{Cterm}$) was analyzed by analytical ultracentrifugation (Figure 3.7B). This revealed that MBP-Lnp1$_{Cterm}$ behaved as a dimer *in vitro*. To determine if the zinc finger motif of Lnp1 was responsible for the *in vitro* dimerization of MBP-Lnp1$_{Cterm}$, I tested purified recombinant MBP-Lnp1$_{Cterm\mathbf{D}znfn}$, which lacks the zinc finger motif (amino acids 221-248). Interestingly, analytical ultracentrifugation showed that MBP-Lnp1$_{Cterm\mathbf{D}znfn}$ migrated as a monomer (Figure 3.7C). I concluded that the zinc finger motif of Lnp1 is required for the dimerization of Lnp1.

To determine if the zinc finger motif is required for NE localization, plasmids encoding full-length Lnp1-GFP and *lnp1Δ*znfn-GFP were expressed in wild type cells. Localization was assessed by epifluorescence widefield microscopy. Both Lnp1-GFP and *lnp1Δ*znfn-GFP localized similarly in the ER, thus the zinc finger motif of Lnp1 was not required for its proper localization within the cell (Figure 3.8A). As the zinc finger motif is required for the function ofLnp1 in ER morphology (CHEN *et al.* 2012), I next analyzed whether the zinc finger motif dimerization domain is important for the function of Lnp1 at NPCs. Surprisingly, exogenous expression of either *pLNP1* or *plnp1Δznfn* rescued the growth defect of *lnp1Δ nup133Δ* mutants to the same degree (Figure 3.8B). Next, I tested if exogenous expression of *lnp1Δznfn* could rescue the NPC aggregation defects of *lnp1Δ rtn1Δ NIC96-GFP* mutants.

Indeed, both *pLNP1* and *plnp1Δznfn* decreased the NPC aggregation index in *lnp1Δ rtn1Δ NIC96-GFP* mutants to levels consistent with *rtn1Δ NIC96-GFP* alone (Figure 3.8C and 3.8D). As a control for the requirement of the Lnp1 zinc finger motif in ER morphology, *lnp1Δ SEC61-GFP* cells expressing *pLNP1* or *plnp1Δznfn* plasmids were assayed for ER morphology defects. Compared to empty vector,

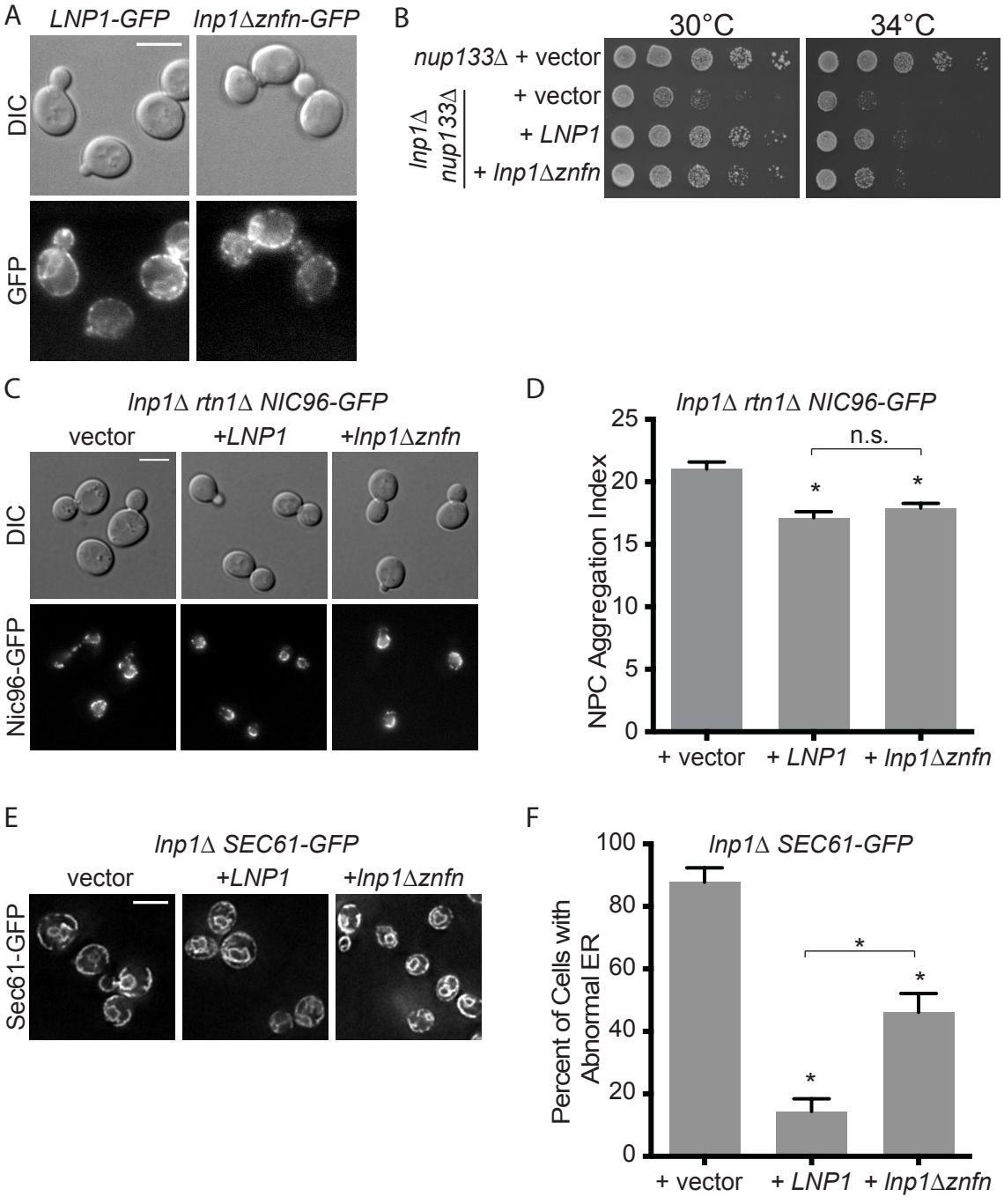
A
LNP1-GFP
lnp1Δznfn-GFP
DIC
GFP
B
30°C
34°C
nup133Δ + vector
lnp1Δ nup133Δ + vector
+ LNP1
+ lnp1Δznfn
C
lnp1Δ rtn1Δ NIC96-GFP
vector
+LNP1
+lnp1Δznfn
DIC
Nic96-GFP
D
lnp1Δ rtn1Δ NIC96-GFP
NPC Aggregation Index
25
20
15
10
5
0
n.s.
*
*
+ vector
+ LNP1
+ lnp1Δznfn
E
lnp1Δ SEC61-GFP
vector
+LNP1
+lnp1Δznfn
Sec61-GFP
F
lnp1Δ SEC61-GFP
Percent of Cells with Abnormal ER
100
80
60
40
20
0
*
*
*
+ vector
+ LNP1
+ lnp1Δznfn

Figure 3.8: **The zinc finger of Lnp1 is not required for NPC function.**
(A) Parental cells exogenously expressing either Lnp1-GFP or *lnp1Δ*znfn-GFP were grown to early log phase at 25°C and were visualized by fluorescence microscopy. Scale bar, 5 μm. (B) Expression of *lnp1Δznfn* results in rescue of *lnp1Δ nup133Δ. lnp1Δ nup133Δ* mutants were transformed with *pLNP1*, *plnp1Δznfn,* or empty vector and grown to early log phase at 25°C, five fold serially diluted, and grown at indicated temperatures.(C) Expression of *lnp1Δznfn* results in rescue of *lnp1Δ rtn1Δ* NPC aggregation. *lnp1Δ rtn1Δ NIC96-GFP* mutants were transformed with *pLNP1*, *plnp1Δznfn,* or empty vector and grown to early log phase at 25°C and imaged. Scale bar, 5 μm. (D) The aggregation indexes of Nic96-GFP expressing cells were determined. Error bars represent standard error. Asterisk denotes statistical significance (P-value <0.01) by student's t-test. (E) Expression of *lnp1Δznfn* is not sufficient to rescue *lnp1Δ* defects in ER. *lnp1Δ SEC61-GFP* mutants were transformed with *pLNP1*, p*lnp1Δznfn,* or empty vector and grown to early log phase at 25°C and imaged. Scale bar, 5 μm. (F) The percentages of cells with abnormal ER morphology were quantified from images of Sec61-GFP expressing cells. Error bars represent standard error. Asterisk denotes statistical significance (P-value <0.01).

pLNP1 rescued the ER defects of *lnp1Δ SEC61*-GFP mutants from 87% to 14%, respectively. However, *plnp1Δznfn* did not rescue the ER defects completely, with 46% of cells displaying ER defects. Thus, the zinc finger domain of Lnp1 is required for the maintenance of ER structure but was not necessary for Lnp1's role in NPC function and organization.

DISCUSSION

This work identifies a novel role for Lnp1 in NPC organization and structure that is connected with Rtn1 function but is independent of the Lnp1 role in ER structure. This conclusion is based on several lines of evidence. First, loss of Lnp1 and Rtn1 in cells results in aggregation of NPCs. This NPC aggregation defect is not rescued by the further loss of Lnp1's antagonist in ER morphology, Sey1, even though *sey1Δ* does rescue the ER defects of *lnp1Δ* mutants. Moreover, general defects in the ER are not sufficient to cause these NPC aggregation defects, as cells lacking Rtn1 and Sey1 exhibit severe defects in ER morphology but do not display defects in NPC organization.

Second, both Lnp1 and Sey1 physically and genetically interact with genes encoding NPC components that have ties to the ER. Recently, *S. pombe* Tts1, the homologue of *S. cerevisiae* Pom33, was found to have roles in NE remodeling during mitosis. Loss of Tts1 results in the accumulation of NPCs in ER/NE junctions at the onset of mitosis (ZHANG and OLIFERENKO 2014). This phenotype parallels our observation that *lnp1Δ* has genetic interactions with *pom33Δ* and *per33Δ*. It is also of note that for all the NPC components tested, *lnp1Δ* and *sey1Δ* appear to only

genetically interact with those that have the most direct ties to the ER. Rtn1, Yop1, Pom33 and Per33 are found within the ER, and the Nup84 subcomplex harbors Sec13 and has evolutionary ties to the COPII coat complex.

Third, loss of Sey1 and Lnp1 have differential impacts on the requirements for Rtn1 at the NPC. Loss of Sey1, but not of Lnp1, results in decreased interaction of Rtn1 with the NPC by yeast two-hybrid analysis. This is interesting when considered with previous work that loss of Sey1 results in increased Lnp1 at the NE as well as an increased physical interaction between Lnp1 and Rtn1. Moreover, overexpression of *RTN1* is not sufficient to rescue the synthetic growth defects of *sey1Δ nup133Δ* mutants. This indicates that loss of Sey1 alters Rtn1's ability to interact with the pore, but increased levels of Rtn1 are not sufficient to overcome the resulting defect. Intriguingly, this defect is not sufficient to cause obvious defects in NPC organization, as Sey1 loss was not associated with NPC aggregation. Perhaps even more intriguing is that overexpression of the *rtn1-K48I* mutant that is defective in oligomerization and ER tubule polymerization rescues synthetic growth defects of *lnp1Δ* mutants but not of *sey1Δ.* The rtn1-K48I altered protein is more mobile in membranes (HU *et al.* 2008; SHIBATA *et al.* 2008) and is localized to Nup53-induced intranuclear karmellae (Figure 4C). Therefore, increased mobility of rtn1-K48I might allow it to rescue the loss of Lnp1 function in the NE.

Finally, Lnp1 dimerization is required for maintenance of ER structure but not for NPC function. I find that the zinc finger domain in the C-terminal Lnp1 domain mediates homodimerization *in vitro*. In concordance with previous studies (CHEN *et al.* 2012), expression of *lnp1Δznfn* does not fully rescue the ER defects

observed in in the ER. However, expression of *lnp1Δznfn* rescues the synthetic genetic interactions of *lnp1Δ* and the NPC aggregation defect of *lnp1Δ rtn1Δ.* Taken together, Lnp1 has distinct and separate roles in ER structure and NPC organization.

There are several possible models for how Lnp1 functions in NPC assembly. The specific *nup* genetic interactions with *lnp1Δ* and *sey1Δ* could be due to a role in stabilizing newly formed pores (Figure 3.9A). Specifically, Lnp1 might mediate Rtn1 function at nascent pores. Nuclear pores contain points of very high membrane curvature in the NE but are surrounded by areas of no curvature. Lnp1 can localize to both flattened and highly curved membranes; however, Rtn1 oligomers are only stably associated with areas of high curvature. Through a physical interaction with Lnp1, the oligomerization of Rtn1 could be modulated to increase mobility of Rtn1 in the NE, allowing Rtn1 to be more easily trafficked to sites of new NPC assembly (Figure 3.9B). This is consistent with the ability of *rtn1-K48I* but not *RTN1* to rescue synthetic growth defects of *lnp1Δ* mutants. Alternatively, changes in the tubular ER network and NE/ER connections could also alter NPC assembly and organization (Figure 3.9C). Decreased connections to the NE could limit the avenues by which membrane proteins are trafficked to the NE. This is consistent with the decreased interaction between Ndc1 and Rtn1 in *sey1Δ* mutants. The antagonistic relationship between Lnp1 and Sey1 might play a role in its functional link to NPCs, though Lnp1 could function independently of Sey1 as well, as indicated by the NPC aggregation data and incomplete rescue of growth defects in *lnp1Δ sey1Δ nup133Δ* mutants.

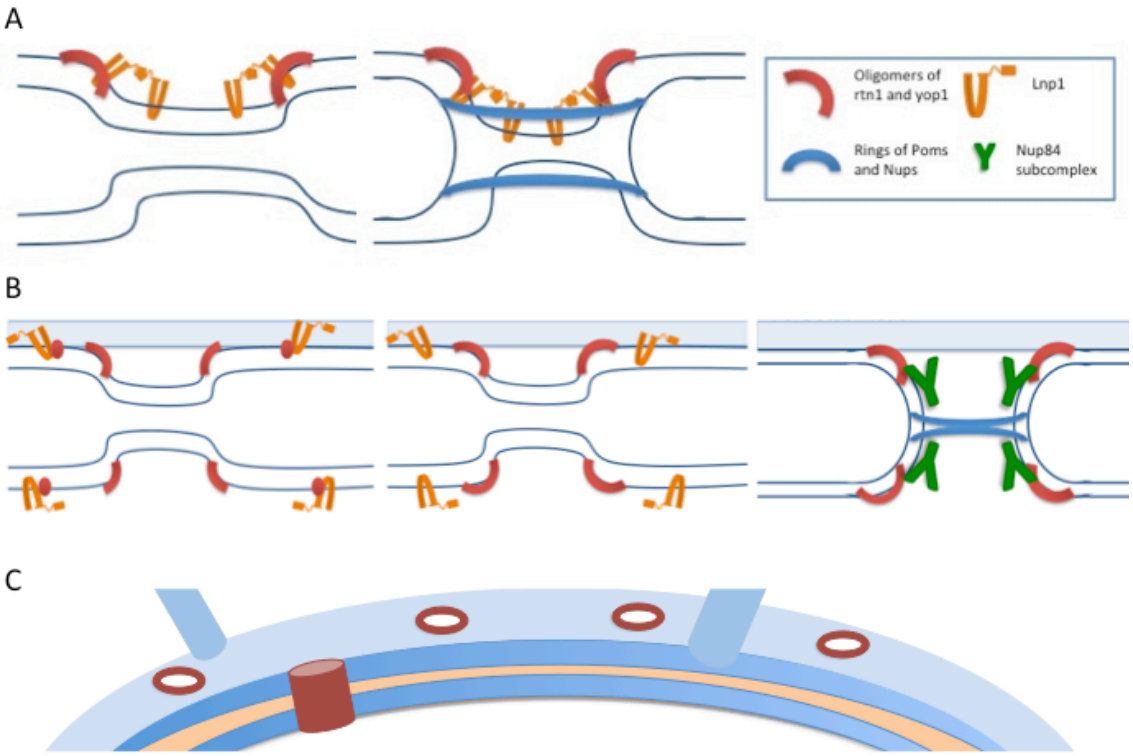

Figure 3.9: **Models for Rtn1 and Lnp1 function at the NPC.**
(A) Model 1: Lnp1 association with Rtn1 induces and stabilizes negative curvature, leading to stabilization of fusion events.(B) Model 2: Lnp1 association with Rtn1 inhibits Rtn1 oligomerization, leading to more efficient recruitment of Rtn1 to NPCs (C) Model 3: The proper maintenance of NE/ER junctions is important for NE homeostasis and NPC assembly

The ER and NE are an interconnected membrane system with a variety of distinct cellular functions. Here we build on the paradigm of individual proteins having different functions dependent on different cellular membrane environments: ER versus NE. The roles of Rtn1, Lnp1, and Sey1 in the ER are intimately linked with the fusion of curved membrane tubules. Whereas the mechanism by which Sey1 mediates fusion is understood, the mechanism(s) by which Lnp1 functions in the ER is not understood. Both *rtn1-K48I* and *lnp1Δznfn* mutants rescue NPC specific but not ER specific defects, indicating separate roles at these distinct locations. Further determination of Lnp1 and Rtn1 mechanisms in modulation ER tubules may result in further insights into the function of these proteins in NPC biogenesis.

CHAPTER IV

DISCUSSION AND FUTURE DIRECTIONS

The NE and ER perform separable essential functions, yet are components of the same contiguous lipid membrane system with a common evolutionary history. Several ER proteins are required for proper NPC structure and function. In particular, Rtn1 and Yop1 stabilize cortical ER tubules and mediate early steps in NPC biogenesis (DAWSON *et al.* 2009). In my studies in chapter 2, I uncovered roles for Rtn1 and Yop1 in NPC and SPC structural integrity and found physical and genetic links to Ndc1 at the NPC. In chapter 3, I identified a specific function in NPC stability for Lnp1 and Sey1, proteins required for proper cortical ER formation. These conclusions are based on a combination of genetic, cell biologic and biochemical data in *S. cerevisiae*. Although I identified roles for Rtn1, Yop1, and Lnp1 at the NPC, the mechanisms by which these proteins affect NPC assembly and stability are not completely determined. Further studies of the mechanisms of Rtn1, Yop1, and Lnp1 at the pore will provide insights into NPC biogenesis and the organization of the pore membrane and further refine our models of Lnp1 and Rtn1 function at the NPC (Figure 2.12 and Figure 3.9).

Mapping of physical interactions of Rtn1 and Yop1 with the NPC

Previously, we identified several physical connections between Rtn1 and Yop1 and the NPC. In NPC clustering mutants, Rtn1 and Yop1 localize to NPCs;

furthermore, both Rtn1 and Yop1 interact with membrane components of the NPC by split ubiquitin yeast two-hybrid analysis. Physical interactions between Rtn1, Yop1, and Ndc1, a required transmembrane component of the NPC, have also been observed by co-immunoprecipitation from crude cell lysates. These findings indicate that Rtn1 and Yop1 are present in the pore membranes of NPCs, potentially via a physical interaction with Ndc1.

Because Ndc1 forms multiple distinct complexes with several membrane-associated proteins at the pore membrane (MADRID *et al.* 2006; FLEMMING *et al.* 2009; ONISCHENKO *et al.* 2009), it is unclear whether the physical interactions of Rtn1 and Yop1 with Ndc1 are direct. Several Poms and membrane-associated Nups could mediate the interaction between Rtn1, Yop1, and Ndc1. I propose to test the necessity of each Ndc1-interacting Pom and Nup for Rtn1 and Yop1 association with Ndc1 and NPCs. Using split ubiquitin yeast two-hybrid interactions of Ndc1-Yop1 and Ndc1-Rtn1 as readouts, I can systematically delete the genes for each pore membrane component in my yeast two-hybrid reporter strain and assay for changes in this interaction.

Because of the functional redundancy of the pore components, it is possible that several Poms could be sufficient for Rtn1 and Yop1 interaction with Ndc1, thus combinations of nulls should be tested as well. Furthermore, if a loss of interaction between Ndc1 and Rtn1 or Yop1 is found, I will confirm this both by co-immunoprecipitation studies and by colocalization of Rtn1 and Yop1 to NPCs. Truncation mutants of *RTN1* and *YOP1* yeast two-hybrid constructs can also be utilized to identify the required interaction domains of these proteins. Preliminary

studies of *pom34Δ* and *pom152Δ* yeast two-hybrid reporter strains indicate that neither of these Poms are necessary for the Ndc1-Yop1 or Ndc1-Rtn1 interaction.

Because Ndc1 is required for cell viability and mutations in *NDC1* affect both NPC and SPB function, *in vivo* testing of Ndc1 interactions with Rtn1 and Yop1 are challenging. However, *in vitro* binding assays with Ndc1-TAP purifications and recombinant Rtn1 or Yop1, full length or truncated, could further define any direct interactions between these proteins. A similar strategy with Ndc1-TAP purifications was used to identify direct interactions between Ndc1, Nup53, and Nup59 (ONISCHENKO *et al.* 2009).

Competitive Binding of Lnp1 and Ndc1 for Rtn1

In a *sey1Δ* mutant, the yeast two-hybrid interaction between Ndc1 and Rtn1 is reduced (Figure 3.6A); however, there is no current evidence to suggest that Sey1 is found at the NPC at steady state. Remarkably, *sey1Δ* mutants also result in the increased localization of Lnp1 to the NE and an increased physical association by co-immunoprecipitation between Rtn1and Lnp1 (CHEN *et al.* 2012). This correlation could suggest that Lnp1 and Ndc1 compete for binding of Rtn1. Antagonism between these two complexes could mediate Rtn1 levels and function at nuclear pores and ER/NE junctions.

Whereas overexpression of *NDC1* is toxic to cells (MADRID *et al.* 2006), overexpression of *LNP1* is tolerated well. Increased expression of *LNP1-GFP* also results in increased localization of Lnp1-GFP to the NE in a similar manner as sey1*Δ* mutants. If increased levels of Lnp1 results in decreased association of Rtn1 with

Ndc1, this would support the hypothesis that Lnp1 and Ndc1 compete for binding of Rtn1. Furthermore, since neither Lnp1 nor Rtn1 are required for viability, mutational analysis of the interactions between Lnp1 and Rtn1 could provide clues to understanding the nature of Rtn1's interaction with Lnp1, Ndc1, and the NPC.

Effects of Lnp1 association on Rtn1 mobility in membranes

Whereas Rtn1 and Yop1 are found at NPCs, it is unclear how these proteins are trafficked to nuclear pores. Both Rtn1 and Yop1 preferentially localize to regions of positive curvature in membranes as immobile oligomers. Nuclear pores are islands of curvature in an otherwise flat membrane, which poses a challenge for the recruitment of Rtn1 and Yop1 to these membrane structures. One possibility is that Rtn1 and Yop1 oligomerization could be disrupted via a physical interaction of another protein that acts as an escort in the NE. Since Lnp1 can localize to both flat and curved membranes and associates with Rtn1, Lnp1 is a potential candidate for this function. Furthermore, an *rtn1-K48I* mutant that is defective in oligomerization and that has increased mobility is able to rescue growth defects of *lnp1Δ* mutants (Figure 3.6B). If Lnp1 mediates Rtn1 mobility, overexpression of *LNP1* or loss of *SEY1* in which the physical interaction between Rtn1 and Lnp1 is increased should result in increased mobility of Rtn1 by fluorescence recovery after photobleaching (FRAP) and increased localization of Rtn1 to the NE.

Alternatively, Pom33 and Per33 association with Rtn1 could be responsible for Rtn1 trafficking to the NPC. Pom33 and Per33 both physically interact with Rtn1 and Lnp1 (CHADRIN *et al.* 2010). Recently, physical interactions between TMEM33,

the mammalian homolog of Pom33, and reticulons were identified; furthermore, exogenous expression of TMEM33 was found to suppress the over-reticulation phenotypes associated with overexpression of Rtn4C in cell culture (URADE *et al.* 2014). Further defining these potential complexes and their effect on Rtn1 function lead to a better understanding of how Pom33, Per33, and Lnp1 may regulate Rtn1 in the ER and at the nuclear pore.

Localization of ER shaping proteins in the NE

Nuclear import of Nups is required for proper NPC assembly (D'ANGELO *et al.* 2006). Thus nuclear pore formation is thought of as a symmetric event with both the INM and ONM playing similar roles in pore formation. Whereas it has been confirmed that the ER shaping proteins Rtn1, Yop1, Lnp1, and Sey1 are present in the ONM, the presence of these proteins in the INM has not been established. Data from our lab indicate that Rtn1, Yop1, Lnp1, and Sey1 do have the potential to localize to the INM. Upon *NUP53* overexpression, the nuclei of many cells accumulate flattened intranuclear membranes. Membrane associated Nups, Poms, and INM proteins associate within Nup53 induced intranuclear karmellae (MARELLI *et al.* 2001). I have found that Lnp1-GFP is able to localize to these karmellae structures. Although wild type Rtn1-GFP and Yop1-GFP do not efficiently localize to these structures, I predict that this is most likely due to Rtn1 and Yop1's affinity for curved membranes and inability to stability associate with flattened membranes (HU *et al.* 2008; SHIBATA *et al.* 2008; SHIBATA *et al.* 2010). This hypothesis is supported by the oligomerization mutant *rtn1-K48I* (SHIBATA *et al.* 2008), which is

able to accumulate in Nup53 induced karmellae (see Figure 3.6C). However this is not definitive evidence for the normal physiological residence of Rtn1, Yop1, and Lnp1 in the INM.

Due to the high abundance of Rtn1 and Yop1 within the ER and ONM, traditional methods of INM localization by immuno-gold TEM labeling may be challenging. Super-resolution imaging methods such as stochastic optical reconstruction microscopy (STORM) or structured illumination microscopy (SIM) can be used to resolve the INM and ONM in some instances. By co-labeling cells with a fluorescent lumenal marker and tagging the cytoplasmic domains of Rtn1, Yop1, and Lnp1 with fluorescent protein tags, sufficient resolution could be obtained using super-resolution imaging techniques to determine if these proteins normally reside in the INM. However, enrichment of Rtn1 and Yop1 at the pore membranes of nuclear pores could confound these studies, as this would occlude the definition of a clear lumenal layer between membranes. Furthermore, the high abundance of Rtn1, Yop1, and Lnp1 in the ER and NPC combined with potentially low working amounts in the INM could also obscure exclusion from the INM and an asymmetric localization of protein. Another method to test for the presence of an INM pool of Rtn1, Yop1, and Lnp1 is the utilization of reporter protein fusions. For example, tagging a non-lumenal domain of these ER proteins with a transcription factor lacking an NLS could provide readouts for the nuclear localization that is not dependent upon or limited by available microscopy techniques.

Determining the localization of Rtn1, Yop1, and Lnp1 in the NE may shed light on the mechanisms of NE fusion and NPC assembly. Establishment of INM

populations of Rtn1 and Yop1 would provide evidence for a symmetric model of pore formation. However, a completely asymmetric distribution of membrane ER proteins may be used to support asymmetric pore fusion models in which *de novo* pore formation is initiated from one side of the membrane. Such a model would parallel post-mitotic assembly pathway models, in which NPC formation is seeded via Nup interactions with chromatin. Alternatively, asymmetric distribution or Rtn1, Yop1 and Lnp1 could indicate the presence of an INM factor that plays the counterpart to Rtn1, Yop1, and Lnp1 in the ONM. Two such candidates are Heh1 and Heh2, INM proteins with established lumenal interactions with Pom152. Genetic interactions of *heh1Δ* with *rtn1Δ*, *pom34Δ*, and *pom152Δ* also indicate functional interaction between these membrane components (YEWDELL *et al.* 2011). Finally, asymmetric distribution could indicate that Rtn1, Yop1, and Lnp1 do not function in NPC assembly, but do play a role in the stability of NPCs after pore formation. However, this model is not supported by *in vitro* data that showed reticulons are required for pore formation in *Xenopus* extracts (DAWSON *et al.* 2009).

Conservation of ER protein function in ER structure and NPC assembly

The ER functions of the Reticulons, Lnp1, and Sey1 (Atlastin in vertebrates) are well conserved in mammals; however, less is known about the functions of these proteins in NPC formation in vertebrates. Elucidation of the similarities and differences between the roles of Rtn1, Yop1, Lnp1, and Sey1 at the NE could shed light on the conservation of *de novo* NPC assembly mechanisms and NE/ER function as a whole.

Data indicate that the functions for the Reticulon and Yop1/DP1 families of proteins in vertebrate NPC assembly are well conserved. In mammals, there are four genes encoding reticulons, each with multiple splice variants. The transmembrane and C-terminus of the reticulon family is highly conserved; however, the N-terminus of the Reticulons varies greatly (DI SANO *et al.* 2012). These different reticulons have been implicated in the regulation of membrane vesicle trafficking, ER stress homeostasis, calcium homeostatis, and autophagy and have been linked to several diseases including *amyotrophic lateral sclerosis,* Alzheimer's disease, and Parkinson's disease (DI SANO *et al.* 2012). Immuno-depletion of Rtn4a in *Xenopus* egg extracts inhibits *de novo* NPC assembly *in vitro* (DAWSON et al. 2009). Overexpression of *RTN3*, *RTN4*, or *DP1* delays reformation of the NE after mitosis, most likely due to a delay in the removal of reticulons from flattening ER tubules at chromatin (ANDERSON and HETZER 2008). Physical interactions between the reticulons and vertebrate Ndc1 could further define the roles of Rtn1 in NPC assembly and shed light on the functional domains of the reticulon N-terminus.

Both mammalian and *S. cerevisiae* homologs of Lnp1 localize and function at three way junctions in the ER. Knockdown of Lnp1 in mammalian cell culture results in unstable three way junctions in the ER (CHEN *et al.* 2014). This is similar to the *lnp1Δ* phenotype in *S. cerevisiae* (CHEN et al. 2012), but the effect of Lnp1 knockdown on NPCs and NE morphology in vertebrates has yet to be reported. I have found that the zinc finger domain of Lnp1 mediates dimerization in the *S. cerevisiae* protein and is required for Lnp1's function in ER structure but not in NPC stability. If the functions of Lnp1 are highly conserved, I predict that dimerization is

also important for the ER function of vertebrate Lnp1 but not for any NPC specific function of Lnp1. By adding back either wild type or dimerization deficient Lnp1 to Lnp1 knock down cells, differential rescue of ER and NPC defects could be tested. Some evidence suggests that the structure and function of vertebrate Lnp1 may not be identical to that in *S. cerevisiae*. Vertebrate Lnp1 (vLnp1) contains an N-myristoyl modification that is required for Lnp1 function in ER formation; however, this motif is not found in *S. cerevisiae* (MORIYA *et al.* 2013). Whereas the ER function of mammalian Lnp1 may require this N-myristoylation, it is possible that an NPC function of Lnp1 could be independent of this modification as well.

The mechanisms of Sey1 and Atlastin (mammalian ortholog of Sey1) in the ER appear well conserved. Both Sey1 and Atlastin mediate homotypic ER fusion via their GTPase activity and localize to three-way junctions in the ER (RISMANCHI *et al.* 2008; HU *et al.* 2009; PARK and BLACKSTONE 2010). However, there are some key differences between vertebrate Atlastin and Sey1. Recently, the C-terminal tail of Atlastin was found to contain an amphipathic helix that aids in Atlastin mediated membrane fusion (FAUST *et al.* 2015). However, this amphipathic helix does not appear to be conserved in *S. cerevisiae.* Whereas Atlastin is absolutely acquired to mediate fusion of tubules in mammalian cells, *S. cerevisiae* can accomplish fusion of the ER via two distinct mechanisms: via Sey1 mediated fusion and soluble N-ethylmaleimide-sensitive factor attachment protein receptors (SNAREs) (ROGERS *et al.* 2013; ROGERS *et al.* 2014). If ER morphology is directly connected to NPC stability, this could mean that Atlastin knockdown may have a stronger effect on NPC assembly than what is observed in *S. cerevisiae*. Furthermore, additional NPC defects

could be observed in *S. cerevisiae* double mutants where both Sey1 and SNARE function is disrupted.

Because Atlastins and vLnp1 are required to promote proper ER formation, knockdown of either of these proteins results in dramatic defects in ER morphology (RISMANCHI *et al.* 2008) that could confound any NPC specific defects in cells. It is also interesting that both vertebrate Lnp1 and Atlastin contain additional membrane binding motifs not found in *S. cerevisiae,* and these binding motifs are functionally required in the ER (MORIYA *et al.* 2013; FAUST *et al.* 2015). This could indicate that the membrane binding abilities of Lnp1 and Sey1 in *S. cerevisiae* are different. Furthermore, it can be technically challenging to differentiate between defects in *de novo* NPC assembly and post-mitotic NPC assembly at steady state in mammalian cell culture. Immuno-depletion of specific proteins in *Xenopus* extracts has been a powerful tool in the study of NPC assembly and could be applied to Lnp1 and Atlastins. These studies could identify roles for Atlastins and Lnp1 in both *de novo* and post-mitotic NPC assembly.

In vitro recruitment of Nups to curved membranes

In *de novo* NPC assembly, once the NE has fused, it is predicted that additional Poms and structural Nups are recruited to the nascent pore to stabilize regions of curved membranes and provide a molecular scaffold for other NPC components. However, the exact order and mechanism of this recruitment is not well defined. Some NPC components are recruited directly to membranes. These

soluble membrane-binding Nups could be responsible for the recruitment of distinct subcomplexes to nascent pores.

Both Nup53 and Nup59 from *S. cerevisiae* (as well as mammalian Nup53) associate with membranes *in vitro* via dimerization and amphipathic helix domains. Whereas Nup53 and Nup59 can associate with a wider range of membrane curvatures, these proteins also deform membranes *in vitro*, suggesting that they have membrane curvature preferences (VOLLMER *et al.* 2012). Of note, Nup53 and Nup59 may be functionally redundant with Pom152. Nup53, Nup59, and Pom152 compete for binding with Ndc1, and *nup53Δ nup59Δ pom152Δ* triple mutants are lethal (TCHEPEREGINE *et al.* 1999; MARELLI *et al.* 2001; ONISCHENKO *et al.* 2009).

Several components of the inner and outer structural rings of the NPC associate with membrane binding Nups. Using proteins from a fungal thermophile, *Chaetomiaceae thermophilium,* the Hurt lab has characterized the structures and interaction domains of the components of the inner and outer structural rings (AMLACHER *et al.* 2011; THIERBACH *et al.* 2013). The structural Nups of the inner pore ring do not directly interact with one another but are bridged by the linker Nups ctNic96 and ctNup53. ctNup53 directly binds to ctNup192, ctNic96, ctNup170, and ctNup188 via discrete interaction domains (AMLACHER *et al.* 2011). Thus, Nup53 and Nup59 could be a major recruitment factor to nascent pores.

Vertebrate Nup133 contains an ArfGAP1 lipid packing sensor domain (ALPS domain) that is predicted to target the Nup107/160 complex (Nup84 subcomplex in *S. cerevisiae)* to the curved membranes of nascent pores (DRIN *et al.* 2007; HSIA *et al.* 2007; DOUCET *et al.* 2010; DRIN and ANTONNY 2010). The vNup133 ALPS domain

preferentially binds liposomes of about 35nm in diameter *in vitro* (DRIN *et al.* 2007). This curvature is very similar to the 40nm observed diameter the pore membrane (MAIMON *et al.* 2012). In mammalian cells, mutations in the ALPS domain of vNup133 result in mislocalization of the vNup107/160 complex to the cytoplasm and defective NPC assembly, indicating that Nup133 recruitment to membranes is required for interphase NPC assembly (DOUCET *et al.* 2010). Whereas putative ALPS domains have been identified in Nup120 and Nup133 of *S. cerevisiae*, it is not known if these proteins have the same membrane binding properties as vNup133 (KIM *et al.* 2014).

Because Nup53, Nup59, and Nup133 associate with structural Nups and have membrane recruitment potential, they are prime candidates as the major recruiters of the NPC scaffold during *de novo* NPC assembly. To test if Nup53/Nup59 and Nup133 can act as membrane adapters for NPC components, liposomes could be pre-incubated with Nup53 or Nup133 and NPC components of the inner and outer structural rings could be tested for association. Utilization of Nups from *C. thermophilium* may be beneficial for these studies as they are more stable *in vitro* than their *S. cerevisiae* counterparts and are more amendable to individual biochemical purification and to cryo-EM studies (AMLACHER *et al.* 2011; THIERBACH *et al.* 2013). From this, distinct prepore complexes could be identified, and the stepwise association of NPC components and subcomplexes may be determined.

Membrane reconstitution assays in the presence of recombinant Rtn1 or Yop1 result in the formation of membrane tubules of approximately 15nm in diameter (HU *et al.* 2008). Because Rtn1 and Yop1 also have known roles in NPC

structure, it is of interest if the presence of Rtn1 and Yop1 *in vitro* could alter or promote Nup53/Nup59 or Nup133 association to membranes. These Nups could associate along the entire Rtn1 induced tubule or concentrate at the tips of tubules. Alternatively, the presence of other NPC factors with membrane shaping properties could alter the organization of Rtn1 in membranes and inhibit tubule formation. The organization of prepore complexes on liposomes or on Rtn1 induced tubules could further be examined by electron microscopy.

Identification of regulators of NPC number and assembly

Whereas we have limited understanding of the early steps in *de novo* NPC assembly, we know even less about how the number of NPCs in a cell is regulated. The number of NPCs found in the nuclei in metazoans can vary. Furthermore, activation of some cell types, such as lymphocytes can result in the induction of new NPC formation without undergoing mitosis (MAUL *et al.* 1971; MAESHIMA *et al.* 2011). In *S. cerevisiae*, the number of NPCs is linked to the surface area of the nucleus, maintaining a relative constant NPC density in the NE of 11.6 NPCs per μm^2. However, in S phase NPC density increases to 14.6 NPCs per μm^2 (WINEY *et al.* 1997). This indicates a potential cell cycle regulation of NPC assembly. However the mechanism by which NPC number is controlled in *S. cerevisiae* remains unknown.

Whereas some NPC mutants are predicted to alter NPC assembly, we do not have a clear understanding if and how these defects result in decreased NPC numbers. This is due in part to the technical difficulties in measuring accurate NPC number in cell populations. The current standard in the field for the determination

of NPC number involves counting individual NPCs in serially sections of nuclei in TEM micrographs (WINEY *et al.* 1997). Because of the labor-intensive nature of this analysis, the NPC densities of most NPC mutants remain uncharacterized. Furthermore, NPC distribution defects of many NPC mutants can further prevent predicting the number of NPCs based on fluorescence intensity using standard widefield and confocal microscopy techniques. Advances in super-resolution microscopy provide an opportunity to count and measure single pores in the yeast nuclear envelope. Using fluorescently labeled GFP nanobodies, individual pore structures can be identified and counted with STORM (RIES *et al.* 2012). However, this method is also labor intensive and not readily adaptable to larger scale screens.

To identify novel effectors of NPC assembly and NPC number, a method must be developed that does not rely upon the counting of individual nuclei. One possibility is the utilization of known temperature sensitive NPC mutants that can be used to block new NPC assembly. For example, when *nic96-1* cells are shifted to the 37°C, new NPC assembly is blocked due to insufficiency of Nic96 within the cell. Cell divisions after shift to the non-permissive temperature result in daughter cells with fewer NPCs every cell division. After 3 divisions at the 37°C, *nic96-1* cells are reported to go from an average of 105 NPCs per cell (11 NPCs per μm^2) to 16 NPC per cell (1.5 NPCs per μm^2). Remarkably, I have found that the viability of *nic96-1* mutants remains quite high after three divisions at the 37°C if they are shifted back to the permissive temperature. However, after four divisions, *nic96-1* cells do not survive, even after recovery at the permissive temperature, most likely due to insufficient NPCs for nucleocytoplamic transport. Because of this property, *nic96-1*

mutants could be used as a screening tool to identify genes that play a role in NPC assembly or control NPC number, either by crossing *nic96-1* cells with the null collection (reference of SGA) or using overexpression libraries in a multicopy suppressor screen. Candidates from the screen could be tested for increased viability after 4 divisions at 37°C (increased pore number) or decreased viability after 3 divisions (decreased pore number). Overexpression of certain regulators of NPC assembly may result in increased numbers of pores in *nic96-1* cells which would allow these mutants to survive additional rounds of cell divisions at the non permissive temperature.

Though much is known about the organization of soluble Nups in the NPC, there is still much more to learn about the complex interactions between Nups and Poms at the pore membrane. Further analysis of these complex interactions will lead to a better understanding of the organization at the pore membrane and the order of in NPC assembly.

APPENDIX A

NPC motility: shifting gears between fungal nuclear and cytoplasmic organization

In eukaryotic cells, mechanisms that modulate nuclear envelope function are critical for linking cytoplasmic events with nuclear gene expression, and vice versa. At the crux of this regulation are the nuclear pore complexes (NPCs), the large proteinaceous channels embedded in NE pores which mediate essential nucleocytoplasmic exchange of proteins and RNA (WENTE and ROUT 2010). Fifteen years ago, the discovery that *Saccharomyces cerevisiae* NPCs move in the nuclear envelope led to early speculations that such motility might facilitate regulation of transcription by signaling (BELGAREH and DOYE 1997; BUCCI and WENTE 1997). A new study by Steinberg et al. sheds light on a role for cytoskeletal motors in the ATP-dependent movement of fungal NPCs (STEINBERG *et al.* 2012). They also present intriguing connections between NPC motility, nuclear import and export efficiency, and nuclear chromatin organization. Moreover, a tremendous complexity of mechanisms is highlighted by the differences they find for factors controlling NPC motility amongst fungal species (Figure A.1).

The nuclear lamin network is considered a distinguishing element between fungal and metazoan nuclear envelopes. NPCs are not mobile in interphase

---

This chapter is adapted from "Nuclear transport: shifting gears in fungal nuclear and cytoplasmic organization. Amanda K Casey, Susan R. Wente. *Current Biol*. 2012 Oct 9;22(19)."

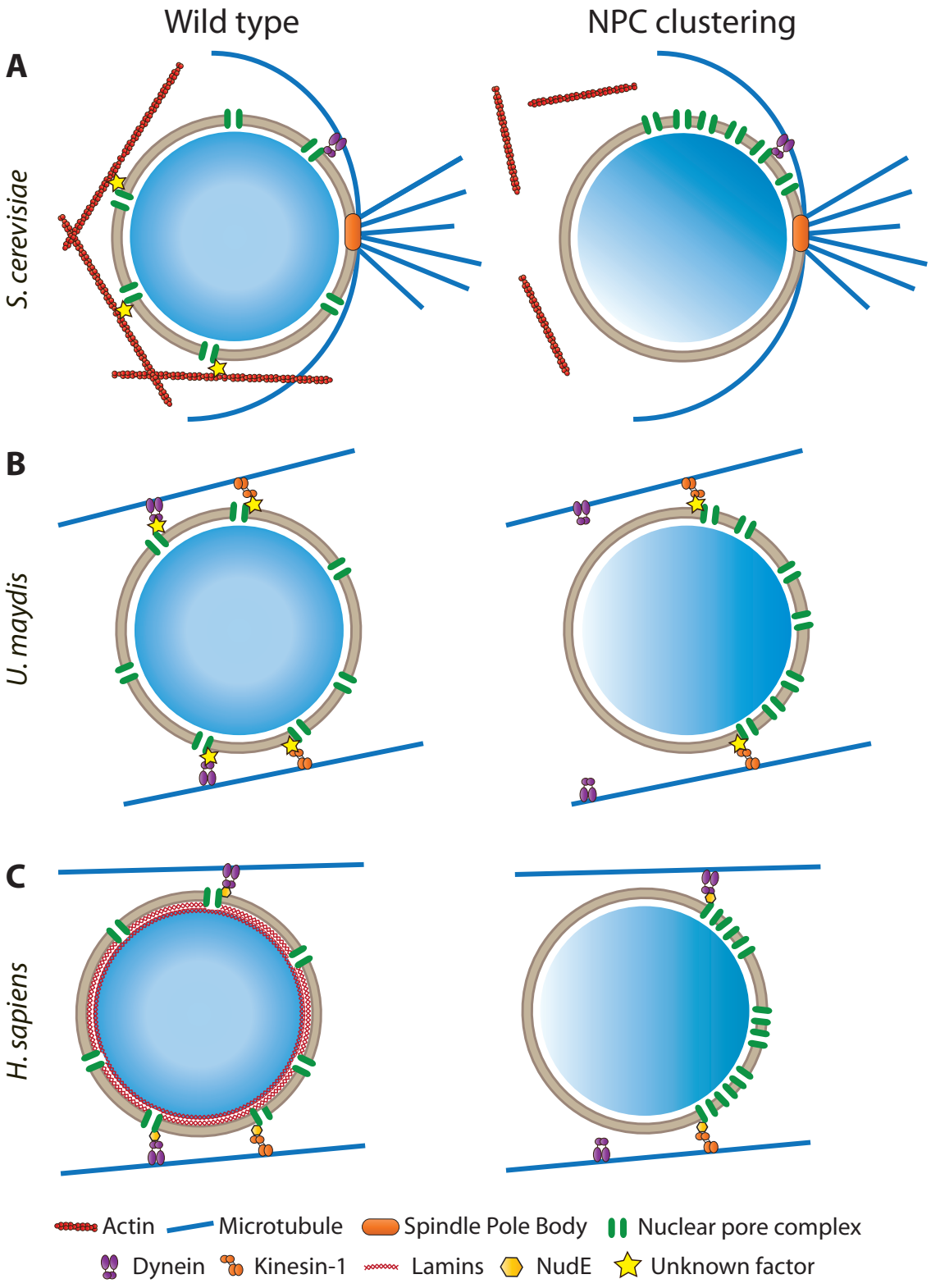
Wild type
NPC clustering
A
S. cerevisiae
B
U. maydis
C
H. sapiens
Actin
Microtubule
Spindle Pole Body
Nuclear pore complex
Dynein
Kinesin-1
Lamins
NudE
Unknown factor

Figure A.1. Model of NPC and nuclear organization
(A) *S. cerevisiae*: Left, actin-dependent NPC motility maintains NPC distribution, whereas microtubules coordinate nuclear migration during closed mitosis with dynein/NPC interactions. Right, disrupting actin alters NPC motility and results in NPC clusters. The membrane-embedded microtubule organizing center (spindle pole body) is shown. (B) *U. maydis*: Left, NPC distribution is maintained through microtubule-dependent NPC motility, with roles for dynein and kinesin-1. Right, loss of microtubule, dynein or kinesin-1 function results in loss of NPC motility and NPC clusters appear. (C) *H. sapiens*: Left, NPC spacing is maintained by the nuclear lamina network. Dynein and kinesin-1 associate with NPCs and are required for cellular nuclear positioning. Right, disruption of the lamina network results in NPC clustering. In all panels, intranuclear blue shading reflects overall chromosomal organization.

metazoan nuclei with an intact lamina (DAIGLE *et al.* 2001), whereas the loss of nuclear lamins perturbs nuclear organization and NPC distribution (LIU *et al.* 2000) (NPCs are clustered in discrete regions instead of being over the entire nuclear surface) (Figure A.1C). In contrast, fungal cells lack a lamin orthologue and have mobile NPCs (Figure A.1A- B) (WENTE and ROUT 2010) (BELGAREH and DOYE 1997; BUCCI and WENTE 1997). Based on this evidence, others speculated that NPC motility in *S. cerevisiae* is due to the lack of a lamina network locking NPCs in place (BELGAREH and DOYE 1997; BUCCI and WENTE 1997). However, whether NPC movement is an active process was unresolved and the mechanism of movement was unclear.

In this report, Steinberg et al. examined the movement of individual NPCs harboring fluorescently tagged NPC proteins (Nups) by live cell microscopy in three different fungal models: *Ustilago maydis, Aspergillus nidulans, and S. cerevisiae* (STEINBERG *et al.* 2012). The percentage of NPCs with directed motility and the velocity of motile NPCs are similar in all three species. Strikingly, NPC motility is dependent upon ATP (based on reversible inhibition by cyanide *m*-chlorophenyl-hydrazone (CCCP) treatment) and distinct cytoskeletal elements. Of note, the different fungal models have contrasting requirements for microtubules and actin filaments. In *U. maydis* and *A. nidulans*, NPC motility requires the microtubule network (with the microtubule destroying drug benomyl eliminating movement) (Figure A.1B). Furthermore, in *U. maydis*, NPCs move along paths that follow microtubule tracks, suggesting that microtubule motors might provide force for NPC motility. In *S. cerevisiae*, NPC movement and distribution is not altered by the

depletion of microtubules with benomyl; however, depletion of actin filaments with the drug latrunculin A inhibits NPC motility (Figure A.1A). No effect of latrunculin A is observed in *U. maydis* or *A. nidulans*. Overall, although different, some type of cytoskeletal connection and molecular motor is involved in fungal NPC movement through the nuclear envelope (Figure A.1A-B). Exactly how the dynein and kinesin-1 are coupled to the NPCs in *U. maydes* and *A. nidulans* is unknown, and likewise for actin in *S. cerevisiae*.

It is also very exciting that Steinberg et al. find that perturbations in fungal NPC motility coincidentally result in the appearance of NPC clusters (Figure A.1A-B). This is true with inhibitor treatments (CCCP, benomyl, or latrunculin A in the respective model) and in mutant cells with defective cytoskeletal elements. This helps resolve a long-standing question of why NPCs cluster in *S. cerevisiae nup* and nuclear envelope mutants (DOYE *et al.* 1994; WENTE and BLOBEL 1994; AITCHISON *et al.* 1995; GORSCH *et al.* 1995; HEATH *et al.* 1995; BELGAREH and DOYE 1997). Others predicted that NPC clusters result from a loss of motility or factors that prevent aggregation (BELGAREH and DOYE 1997; BUCCI and WENTE 1997), and/or that aberrant NPC-cytoskeletal attachments might play a role (HEATH *et al.* 1995). If motility prevents NPC clustering as indicated by Steinberg et al. (STEINBERG *et al.* 2012), altered NPC-cytoskeletal connections could be the underlying basis for NPC clustering phenotypes.

Does NPC motility play a direct role in nucleocytoplasmic communication or nuclear function? Steinberg et al. find intriguing correlations between chromosomal organization and NPC dynamics (STEINBERG *et al.* 2012). In *U. maydis*, chromosomal

movements frequently coincide with NPC movement, and chromosomal reorganization is also ATP dependent. In addition, loss of microtubule integrity induces chromosomal clustering around the NPCs clusters (Figure A1B). To separate effects on nuclear protein import and export from NPC clustering, they exploit the differential timing of impacts on microtubules versus clustering. In *U. maydis,* transport defects are dependent on NPC cluster formation. They hypothesize that decreased transport efficiency results from the inaccessibility of NPCs in clusters to chromatin free channels in the nucleus. Indeed, many of the reported *S. cerevisiae* NPC clustering mutants accumulate nuclear mRNA (DOYE *et al.* 1994; WENTE and BLOBEL 1994; AITCHISON *et al.* 1995; GORSCH *et al.* 1995; HEATH *et al.* 1995; BELGAREH and DOYE 1997). Of note, Steinberg et al. did not test for mRNA export defects in cells with NPC clustering induced by cytoskeleton perturbations. Others find that nuclear transport and NPC clustering phenotypes are uncoupled in some *nup159* and *nup133* mutants (DOYE *et al.* 1994; GORSCH *et al.* 1995; BELGAREH and DOYE 1997). Thus, this will be an important question to further investigate.

Although a role for the cytoskeleton in NPC motility is novel, it is well established that both fungi and metazoans utilize microtubules and their motors for cellular nuclear positioning (XIANG and FISCHER 2004; STARR 2007). There are some hints that the NPC motility and nuclear movement mechanisms share an origin. Although *S. cerevisiae* NPC motility is actin dependent, its NPCs and microtubule motors have functional connections to nuclear migration (Figure A1). Most recently, *S. cerevisiae* studies showed that the dynein light chain is recruited to ubiquitylated Nup159 at NPCs and this plays a role in nuclear migration (HAYAKAWA *et al.* 2012).

Even though some *nup159* mutants result in NPC clustering (GORSCH *et al.* 1995), specifically disrupting dynein light chain binding does not result in NPC clustering (HAYAKAWA *et al.* 2012). Interestingly, in metazoan cells, centrosome/nuclear proximity is maintained by microtubule tethering of NPCs through Nup133 (BOLHY *et al.* 2011). Further work will be needed to address connections between nuclear positioning and NPC motility.

The physiological importance of NPC motility was speculated on many years ago wherein some suggested that NPC redistribution might aid in gene expression responses to environmental stimuli (BUCCI and WENTE 1997). The Steinberg et al. study now extends this hypothesis. It is known that changes in cellular environments reorganize the cytoskeleton (such as disassembly of the actin cytoskeleton in high osmolarity (CHOWDHURY *et al.* 1992)). Altering the cytoskeleton could in turn alter NPC motility and localization. For metazoans, altering the nuclear lamina will likely also be required to change NPC distribution. Such changes to NPC motility and organization might then impact transcriptionally active genes. In fungi and metazoans, gene loci interactions with Nups are well documented (STRAMBIO-DE-CASTILLIA *et al.* 2010; EGECIOGLU and BRICKNER 2011). Indeed, Steinberg et al. report that loss of NPC motility alters chromosomal organization [4]; yet, future studies will be needed to test if gene transcription is changed when NPC motility is blocked. If so, the field should also carefully re-consider the use of NPC clustering mutants to test gene loci interactions with NPCs. With molecular motors driving motility, the NPCs are uniquely positioned as key players in shifting gears between cytoplasmic and nuclear events.

APPENDIX B

Analysis of Sec13 function in the Nup84 subcomplex

INTRODUCTION

Structural Nups contribute to the stability of the NPC. These components can stabilize the curved surfaces of the NPC, act as adaptors for Poms to the NPC, and provide a scaffold upon which other nups assemble. The Nup84 subcomplex (Nup107 in metazoans) provides such roles in the NPC core. The structure of this subcomplex has been well studied by cryo-EM, protein crystallography, molecular modeling, and recently by super-resolution microscopy (SINIOSSOGLOU *et al.* 2000; LUTZMANN *et al.* 2002; DEVOS *et al.* 2006; BECK *et al.* 2007; HSIA *et al.* 2007; BROHAWN *et al.* 2008; DEBLER *et al.* 2008; BROHAWN and SCHWARTZ 2009; LEKSA *et al.* 2009; FERNANDEZ-MARTINEZ *et al.* 2012; SZYMBORSKA *et al.* 2013; SHI *et al.* 2014).

The Nup84 subcomplex is composed of 7 proteins (Nup84, Nup85, Nup120, Nup133, Nup145C, Sec13, and Seh1) that form a Y-shaped 500kDa structure (SINIOSSOGLOU et al. 2000; LUTZMANN et al. 2002). This complex is organized in the central core of the NPC in a head to tail fashion, forming rings on both sides of the NE (ALBER *et al.* 2007b; SZYMBORSKA *et al.* 2013). Structural modeling indicates that the Nup84 complex is found 16 times in the pore, consisting of 15% of the total mass of the NPC (LUTZMANN *et al.* 2002; ALBER *et al.* 2007a; ALBER *et al.* 2007b).

Many structural subcomplexes of the NPC share several structural properties with COPII coats, and both complexes are hypothesized to be derived from a

common coat ancestor (DEVOS *et al.* 2006; HSIA *et al.* 2007; BROHAWN *et al.* 2008; BROHAWN *et al.* 2009; NEUMANN *et al.* 2010). Both the Nup84 subcomplex and the COPII coat contain β-propellers and α-solenoid domains which are the functional building blocks of many known coatomers. This α-solenoid motif is sometimes referred to as Ancestral Coatomer Element 1 domains (ACE1 domains) (DEVOS *et al.* 2006; HSIA *et al.* 2007; BROHAWN *et al.* 2009). ACE1 domains are divided into distinct regions: the crown, trunk, and tail.

The outer cage of the COPII coat is made up of two proteins: Sec31 and Sec13. Sec31 contains both an ACE1 domain and a β-propeller. The ACE1 domain of Sec31 homo-dimerizes at its crown and the β-propellers of Sec31 form the vertices at of the COPII lattice structure. Sec13 is an open β-propeller with six propeller blades. The seventh blade is completed by Sec31 to form a closed β-propeller. The function of Sec13 in the COPII coatomer is less defined than that of Sec31. Studies show that the requirement for Sec13 in COPII transport can be bypassed by the loss of several asymmetric cargoes (ELROD-ERICKSON and KAISER 1996). Thus, it is predicted that the Sec13 β-propeller provides rigidity and stability to the COPII coat (COPIC *et al.* 2012).

The Nup84 subcomplex contains four β-propellers, two of which are found in ACE1 domain proteins (Nup120 and Nup133), and two of which are open β-propellers (Sec13 and Seh1). Of note, Sec13, a required component of COPII, is also found in the Nup84 Subcomplex (SINIOSSOGLOU *et al.* 2000; LORD *et al.* 2013). In the Nup84 subcomplex, Nup145C completes the seventh blade of the Sec13 β-propeller. The second open β-propeller in this complex, Seh1 is completed by Nup85 (HSIA *et al.* 2007; DEBLER *et al.* 2008). Interestingly, Seh1, is also found with Sec13 in the SEA

coatomer complex, which mediates trafficking to the vacuole in *S. cerevisiae* (DOKUDOVSKAYA and ROUT 2011; DOKUDOVSKAYA et al. 2011).

Since the β-propellers of the Nup84 subcomplex are not needed to form the Y-structure of the complex, the β-propellers could function in other roles of the complex, such as mediating physical interactions between Nup84 subcomplex subunits or other structural Nups. Indeed, crystal structures of both the Nup145C/Sec13 and Nup85/Seh1 complexes reveal oligomerization with each other via highly conserved residues (HSIA *et al.* 2007; DEBLER *et al.* 2008; LEKSA and SCHWARTZ 2010).

Whereas the structural similarities between these two complexes have been studied in detail, the functional and mechanistic similarities between COPII and the Nup84 subcomplex are largely inferred. I hypothesize that the β-propellers of these complexes function in a similar manner. I predict that the Sec13 and Seh1 β-propellers of the Nup84 subcomplex provide stability and rigidity to the NPC structure.

RESULTS

Sec13 bypass mutants results in defects in ER and NPC morphology

To determine if cells lacking Sec13 have defects in NPC or NE structure, Iutilized bypass of Sec13 (*bst*) mutants (ELROD-ERICKSON and KAISER 1996) which are suppressors of *sec13Δ* lethality. To visualize NPCs, cells endogenously expressing Nic96-GFP in two *bst* mutant backgrounds (*bst1Δ sec13Δ* and *emp24Δ sec13Δ)* were imaged by wide field microscopy (Figure B.1A). I imaged cells at the permissive

temperature 23°C as well as cells shifted to the non-permissive temperature 34°C for 4 hr. At 23°C, *bst1Δ sec13Δ* cells displayed an overall normal Nic96-GFP localization and *emp24Δ sec13Δ* mutant cells displayed minor NPC clustering defects and minor cytoplasmic mislocaliztion Nic96-GFP (Figure B.1A). However, when shifted to 34°C, both *bst1Δ sec13Δ* and *emp24Δ sec13Δ* cells displayed abnormal localization of Nic96-GFP, including NPC clusters, abnormal NE morpholgy, and increased mislocalization of Nic96-GFP to the cytoplasm.

To further examine the NPC defect in these mutants, the membranes and NPCs of these cells were examined by thin section transmission electron microscopy (TEM). TEM images of *bst1Δ* and *bst1Δ sec13Δ* mutants shifted to 34°C. Asynchronous cells were grown to early log phase at 23°C and shifted to 34°C for 4 hr. Cells were processed and imaged as previously described (DAWSON *et al.* 2009). Whereas TEM images of *bst1Δ* mutants appeared normal TEM images of *bst1Δ sec13Δ* revealed NPC clustering in the NE, abnormal NE morpholgy, and gross abnormalities in ER membrane architecture (Figure B.1A). Due to the dramatic changes in ER morphology, I concluded that defects in COPII mediated transport at the non-permissive temperature were contributing to the majority of my obsered NPC defects, indicating the *bst* mutant background is not optimal for studing Sec13 funciton in the NPC.

Targeted disruption of Sec13 from the NPC

Continuing mystudies of Sec13's role in the Nup84 subcomplex, I generated a point mutant in *NUP145, nup145-K758P*. Mutation of the lysine 758 to a proline is

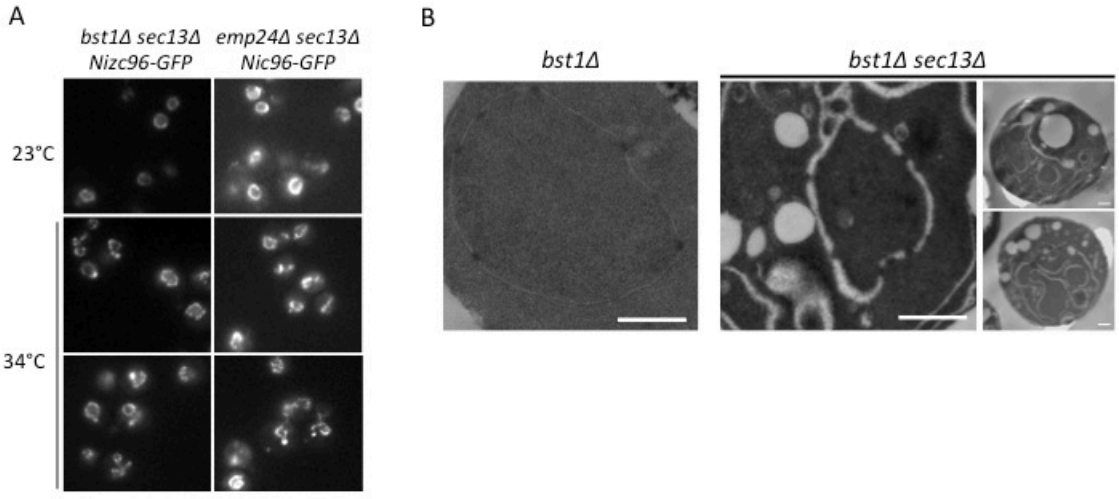

Figure B1: sec13 bypass mutants results in defects in ER and NPC morphology. (A) Cells expressing Nic96-GFP were grown to early log phase at 23°C, shifted to 23°C or 34°C for 4 hr, and visualized by fluorescence microscopy. (B) Cells were grown to early log phase at 23°C, shifted to 34°C for 4 hr, and processed for TEM. Scale bar, 500 nm.

predicted to disrupt β-sheet formation of the seventh blade of β-propeller structure of Sec13, thus disrupting the association of Sec13 to Nup145C but not altering COPII secretion. To generate the *nup145-K758P* plasmid, PCR mutagenesis was performed on pSBYp116 (*pNUP145:LEU2*) using primers *5'-ACAGCCTCGTATACGTTTGCACCCTTTTCAACAGGTTCAA-3'* and *5'-TTGAACCTGTTGAAAAGGGTGCAAACGTATACGAGGCTGT-3'*.

Using a plasmid shuffle strategy, *nup145Δ* mutants were covered either by wild type *pNUP145* or *pnup145-K758P*. I tested the health of *pnup145-K758P* using serial dilution growth assays, and found no defects in growth compared to a p*NUP145* control (Figure B2.A). Next, I tested nup145-K758P for association with Sec13. Pulldowns were performed using IgG-coated lysates from *nup145Δ SEC13-TAP* cells expressing either wild type *pNUP145* or *pnup145-K758P* as previously described (CASEY *et al.* 2012). As predicted, Sec13-TAP pulldowns showed a loss of interaction with nup145-K758P (Figure B2.B).

Next, I tested if targeted loss of physical interaction between Sec13 and Nup145 results in changes in NPC distribution. To visualize NPCs, *pNUP145* or *pnup145-K758P* endogenously expressing Nup159-GFP were imaged by wide field microscopy (Figure 3.2C). Compared to *NUP145*, Nup159-GFP localization appeared unperturbed in the *nup145-K758P* mutant, indicating that Sec13 is not structurally required for NPC assembly.

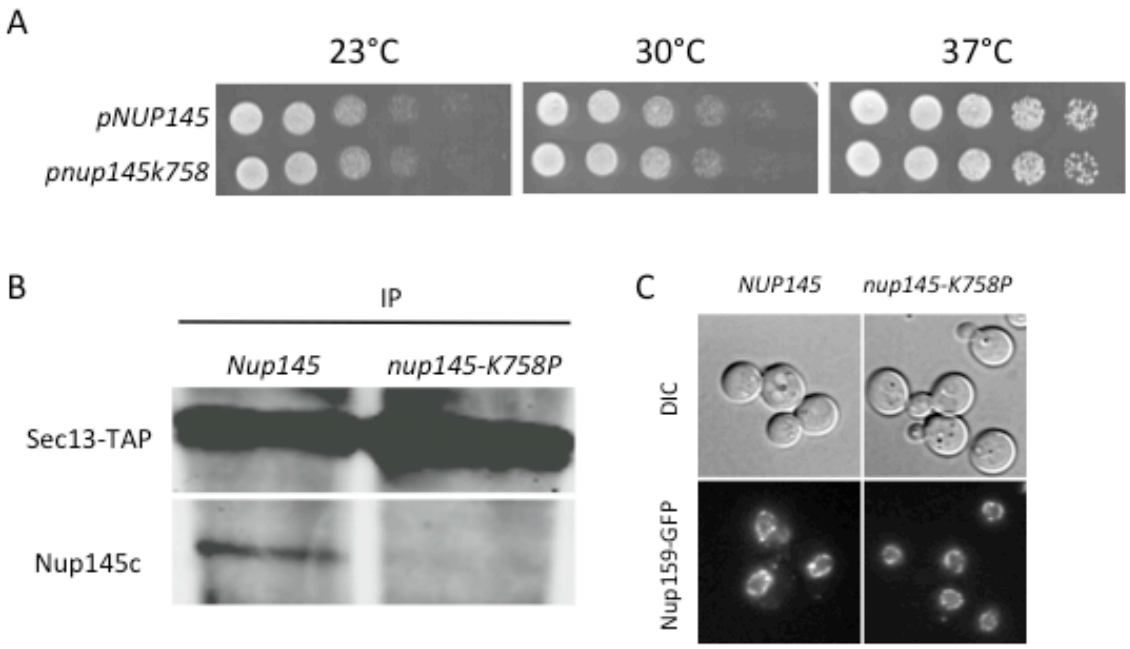

Figure B2: nup145-K758P disrupts Sec13 binding.
(A) *nup145Δ* expressing either *pNUP145* or *pnup145-K758P* were grown to log phase at 23°C, serially diluted, and spot on plates at the temperatures indicated. (B) Lysates were prepared from Sec13-TAPcells and immunoprecipitated with IgG-coated sepharose beads. Analysis of cell lysates and immunoprecipitated proteins by western blotting with α-NUP145C antibodies showed that Sec13-TAP binds to Nup145 but not nup145-K758P. (C) Asynchronous cultures of *nup145Δ NUP159-GFP* cells expressing either *pNUP145* or *pnup145-K758P* were grown to log phase at 23°C in YPD and imaged.

Disruption of Sec13 and Seh1 from the NPC

Because Sec13 and Seh1 are homologs and are predicted to have overlapping functions (HSIA *et al.* 2007), I predicted that combining the Sec13 binding mutant *nup145-K758P* with *seh1Δ* would result in defects in Nup84 subcomplex structure. To test this, I generated *nup145Δ seh1Δ* double mutants that express etiher *pNUP145* or *pnup145-K758P.* I tested the health of *seh1Δ nup145-K758P* using serial dilution growth assays, and found changes in growth compared to *seh1Δ NUP145* or to *nup145-K758P* mutants alone (Figure B3.A).

Next, I tested if *seh1Δ nup145-K758P* mutants resulted in changes in NPC distrubution or Nup localization. To test this, *seh1Δ NUP145* and *seh1Δ nup145-K758P* cells were crossed with a broad array of Nup-GFP reporters, including Nup159-GFP, Mlp1-GFP, Nup133-GFP, Nup188-GFP, and Nic96-GFP. These cells were grown to log phase at 23°C and were imaged by wide field microscopy (Figure 3.3B). Compared to *seh1Δ NUP145*, the localization of all Nup-GFP reporters appeared unaltered in the *seh1Δ nup145-K758P* mutant.

DISCUSSION AND FUTURE DIRECTIONS

In this study, I examined the effects of loss of Sec13-Nup145C binding on NPC structure. I hypothesized that Sec13 and Seh1 provide stability and rigidity to the NPC structure and that loss of these β-propellers would result in instability of Nups in the pore. I generated *nup145-K758P,* a point mutant of *NUP145* that prevents Nup145 association with Sec13. Association is prevented by the inability of the nup145-K758P mutant to form the β-blade needed to complete the β-propeller of

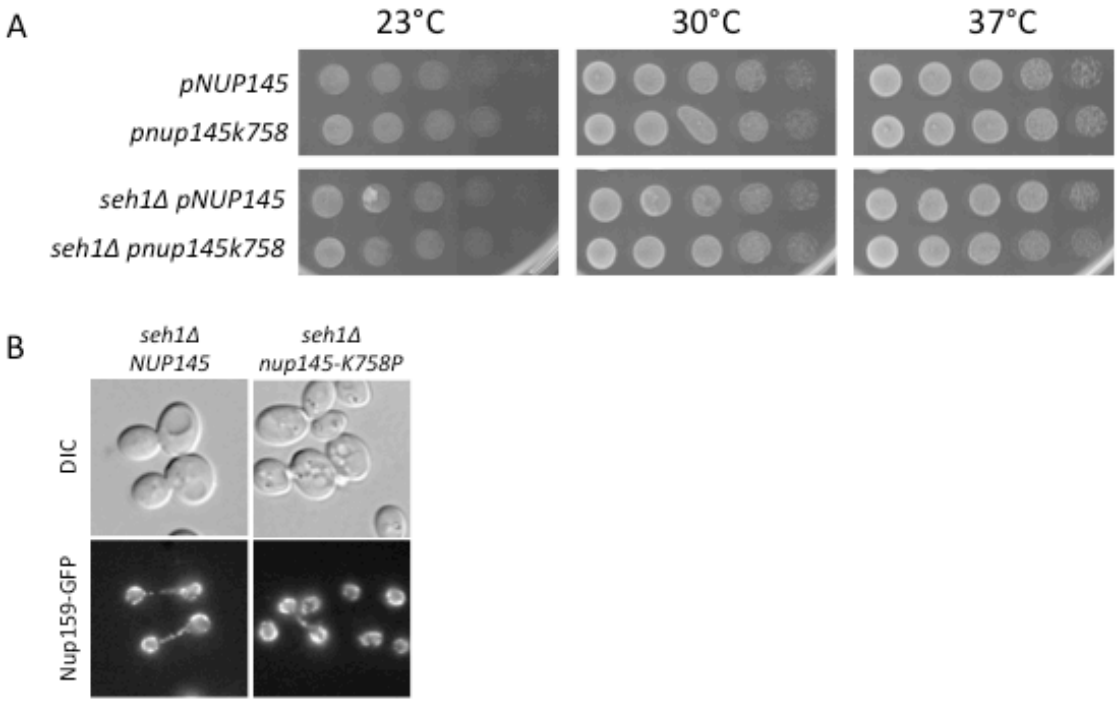

Figure B3: Loss of Sec13 and Seh1 from the NPC does not result in NPC defects. (A) *seh1Δ nup145Δ* expressing either *pNUP145* or *pnup145-K758P* were grown to log phase at 23°C, serially diluted, and spot on plates at the temperatures indicated. (C) Asynchronous cultures of *seh1Δ nup145Δ NUP159-GFP* cells expressing either *pNUP145* or *pnup145-K758P* were grown to log phase at 23°C in YPD and imaged.

Sec13. Furthermore, I confirmed the inability of nup145-K758P to bind Sec13 by coimmunoprecipitation.

I assessed *nup145-K758P* mutants for indications of defective NPCs and observed no defects in growth or Nup localization. Furthermore, I found no defects when *nup145-K758P* mutants were combined with *seh1Δ* as well. This indicates that neither Sec13 nor Seh1 are required at the pore under normal conditions. Recently, the Rout lab further characterized the interaction interfaces of the Nup84 subcomplex through analysis of physical interactions and cryo-EM studies of several Nup domain deletions (FERNANDEZ-MARTINEZ *et al.* 2012; SHI *et al.* 2014). This analysis found that Sec13 and Seh1 are positioned very close to one another in the Y-complex.

My data suggest that loss of Sec13 from the pore does not alter interactions between the Nup84 subcomplex and other NPC components. Another possibility is that the functions of Sec13 and Seh1 are redundant with the β-propeller domains of Nup120 and Nup133. In this case, removal of these β-propeller domains would be necessary to see an effect. However, since β-propellers of Nup120 and Nup133 are integrated into a larger structure, removal of these domains may cause additional defects that would be difficult to separate.

Whereas I tested for physical disruptions at the NPC and defects in growth associated with *nup145-K758P seh1Δ* mutants, I did not test the functionality of the NPC specifically. Sec13 has been implicated in stabilizing the COPII structure, potentially providing additional rigidity to the coat when under strain. The NPC is also under strain such that very large cargoes, e.g. large ribosomal subunits, must be

accommodated for transport in the pore. Crystal structures of some Nups in varying conformations have led some researchers in the nucleocytoplasmic transport field to propose a model in which the NPC may dilate to accommodate these large cargoes (SOLMAZ *et al.* 2013). Sec13 could be an important factor for NPC stability during the accommodation of bulky cargoes through the pore. By testing for defects in specific transport factors or by stressing these specific transport pathways, the function of Sec13 and Seh1 at the NPC could be further determined.

Finally, it is possible that the loss of Sec13 and Seh1 form the Nup84 subcomplex is compensated for by the rearrangement of Nup84 subcomplex subunits within the NPC architecture. If so, the function of Sec13 and Seh1 in the Nup84 subcomplex can be further analyzed by comparing the organization of this complex with and without these members by super-resolution microscopy. Careful STORM analysis of the Nup84 subcomplex has recently defined the orientation of this complex within the NPC (SZYMBORSKA *et al.* 2013). The three dimensional spacing of these components was also determined using this data. By comparing the organization of wild type Nup84 subcomplex and this complex lacking Sec13 and Seh1 using STORM analysis, I may gain further insights into the plasticity and pore stabilizing ability of the Nup84 subcomplex.

APPENDIX C

Table C.1: **Yeast strains used in this study.**

Strain	Genotype	Source
BY4741	*MATa his3Δ1 leu2Δ0 LYS2 met15Δ0 ura3Δ0*	(MORTIMER and JOHNSTON 1986)
BY4742	*MATα his3Δ1 leu2Δ0 lys2Δ0 MET15 ura3Δ0*	(MORTIMER and JOHNSTON 1986)
Bbp1-GFP	*MATa BBP1-GFP:HIS3 his3Δ1 leu2Δ0 met15Δ0 ura3Δ0*	(HUH *et al.* 2003)
Ndc1-GFP	*MATa NDC1-GFP:HIS3 his3Δ1 leu2Δ0 met15Δ0 ura3Δ0*	(HUH *et al.* 2003)
Nic96-GFP	*MATa NIC96-GFP:HIS3 his3Δ1 leu2Δ0 met15Δ0 ura3Δ0*	(HUH *et al.* 2003)
Sec61-GFP	*MATa SEC61-GFP:HIS3 his3Δ1 leu2Δ0 met15Δ0 ura3Δ0*	(HUH *et al.* 2003)
Lnp1-GFP	*MATa LNP1-GFP:HIS3 his3Δ1 leu2Δ0 met15Δ0 ura3Δ0*	(HUH *et al.* 2003)
Rtn1-GFP	*MATa RTN1-GFP:HIS3 his3Δ1 leu2Δ0 met15Δ0 ura3Δ0*	(HUH *et al.* 2003)
NMY32	*his3 200 trp1-901 leu2-3,112 ade2 LYS2::(lexAop)4-HIS3 URA3::(lexAop)8-lacZ ade2::(lexAop)8-ADE2 GAL4*	Dualsystems Biotech
LGY101	*MATα ura3-52 his3Δ200 leu2Δ1 rat7-1(ts)*	(GORSCH *et al.* 1995)
lnp1Δ	*MATa lnp1::KanR his3Δ1 leu2Δ0 met15Δ0 ura3Δ0*	(WINZELER *et al.* 1999)
nup53Δ	*MATa nup53::KanR his3Δ1 leu2Δ0 met15Δ0 ura3Δ0*	(WINZELER *et al.* 1999)
nup59Δ	*MATa nup59::KanR his3Δ1 leu2Δ0 met15Δ0 ura3Δ0*	(WINZELER *et al.* 1999)
nup84Δ	*MATa nup84::KanR his3Δ1 leu2Δ0 met15Δ0 ura3Δ0*	(WINZELER *et al.* 1999)
nup85Δ	*MATa nup85::KanR his3Δ1 leu2Δ0 met15Δ0 ura3Δ0*	(WINZELER *et al.* 1999)
nup100Δ	*MATa nup100::KanR his3Δ1 leu2Δ0 met15Δ0 ura3Δ0*	(WINZELER *et al.* 1999)
nup133Δ	*MATa nup133::KanR his3Δ1 leu2Δ0 met15Δ0 ura3Δ0*	(WINZELER *et al.* 1999)
nup120Δ	*MATa nup120::KanR his3Δ1 leu2Δ0 met15Δ0 ura3Δ0*	(WINZELER *et al.* 1999)
pom152Δ	*MATa per152::KanR his3Δ1 leu2Δ0 met15Δ0 ura3Δ0*	(WINZELER *et al.* 1999)

pom34Δ	*MATa per34::KanR his3Δ1 leu2Δ0 met15Δ0 ura3Δ0*	(WINZELER *et al.* 1999)
pom33Δ	*MATa pom33::KanR his3Δ1 leu2Δ0 met15Δ0 ura3Δ0*	(WINZELER *et al.* 1999)
per33Δ	*MATa per33::KanR his3Δ1 leu2Δ0 met15Δ0 ura3Δ0*	(WINZELER *et al.* 1999)
rtn1Δ	*MATa rtn1::KanR his3Δ1 leu2Δ0 met15Δ0 ura3Δ0*	(WINZELER *et al.* 1999)
sey1Δ	*MATa sey1::KanR his3Δ1 leu2Δ0 met15Δ0 ura3Δ0*	(WINZELER *et al.* 1999)
SLJ001	*MATa bar1::hisG;ura3-1;leu2-3,112;trp1-1;his3-11,15;ade2-1;can1-100;GAL+*	(CASEY *et al.* 2012)
SLJ173	*MATα bar1::hisG;ura3-1;leu2-3,112;trp1-1;his3-11,15;ade2-1;can1-100;GAL+*	(CASEY *et al.* 2012)
SLJ1433	*MATa trp1::GAL-myc-SPC42-TRP1*	(JASPERSEN *et al.* 2002)
SLJ3828	*MATa yop1::HygR rtn1::KanR trp1::GAL-myc-SPC42-TRP1*	(CASEY *et al.* 2012)
SLJ5572	*MATa his3Δ200 trp1-901 leu2-3,112 ade2 LYS2::(lexAop)4-HIS3 ura3::(lexAop)8-lacZ ade2::(lexAop)8-ADE2 GAL4*	(CASEY *et al.* 2012)
SLJ5975	*MATα NDC1-3×HA-HIS3MX6:*	(CASEY *et al.* 2012)
SLJ5976	*MATa YOP1-3×FLAG-KanR*	(CASEY *et al.* 2012)
SLJ5977	*MATα NDC1-3×HA-HIS3MX6 YOP1-3×FLAG-KanR*	(CASEY *et al.* 2012)
SLJ5572	*MATa his3Δ200 trp1-901 leu2-3,112 ade2 LYS2::(lexAop)4-HIS3 ura3::(lexAop)8-lacZ (lexAop)8-ADE2 GAL4*	Dual Biotech NMY51
SWY3810	*MATa rtn1::KanR yop1::KanR ura3Δ0 leu2Δ0 met15Δ0 his3Δ1*	(DAWSON *et al.* 2009)
SWY3811	*MATα rtn1::KanR yop1::KanR ura3Δ0 leu2Δ0 his3Δ1 lys2Δ0*	(DAWSON *et al.* 2009)
Swy4047	*MATα Nup133::KanR RTN1-GFP:HIS3 his3Δ1 leu2Δ0 lys2Δ0 ura3Δ0*	This Study
SWY4522	*MATa NDC1-GFP:HIS3 his3Δ1 met15Δ0 ura3Δ0 leu2Δ0::DsRed-HDEL:LEU2*	(CASEY *et al.* 2012)
SWY4616	*MATα GFP-TUB3 his3Δ1 leu2Δ0 ura3Δ0 met15Δ0*	(CASEY *et al.* 2012)
SWY4617	*MATa GFP-TUB3 his3Δ1 leu2Δ0 ura3Δ0 met15Δ0*	(CASEY *et al.* 2012)
SWY4636	*MATα NDC1-TAP:HIS3 RTN1-GFP:HIS3 his3Δ1 leu2Δ0 ura3Δ0*	(CASEY *et al.* 2012)
SWY4637	*MATa NDC1-TAP:HIS3 RTN1-GFP:HIS his3Δ1 leu2Δ0 ura3Δ0*	(CASEY *et al.* 2012)
SWY4725	*MATα rtn1::KanR yop1::KanR NIC96-GFP:HIS3 met15Δ0 his3Δ1 leu2Δ0 ura3Δ0*	(CASEY *et al.* 2012)
Swy4798	*MATα Nup133::KanR SEY1-GFP:HIS3 his3Δ1 leu2Δ0 met15Δ0 ura3Δ0*	This Study
Swy4802	*MATa rtn1::KanR sey1::KanR his3Δ1 leu2Δ0*	This Study

	ura3Δ0	
SWY4877	*MATα rtn1::KanR yop1::KanR GFP-TUB3 his3Δ1 leu2Δ0 ura3Δ0 met15Δ0*	(CASEY *et al.* 2012)
SWY4878	*MATα rtn1::KanR yop1::KanR GFP-TUB3 his3Δ1 leu2Δ0 ura3Δ0 met15Δ0*	(CASEY *et al.* 2012)
SWY4906	*MATa rtn1::KanR yop1::KanR leu2Δ0::DsRed-HDEL:LEU2 ndc1-GFP:HIS3 ura3Δ0*	(CASEY *et al.* 2012)
SWY4934	*MATa rtn1::KanR yop1::KanR GFP-TUB3 his3Δ1 leu2Δ0 ura3Δ0 lys2Δ0*	(CASEY *et al.* 2012)
SWY4935	*MATa rtn1::KanR yop1::KanR GFP-TUB3 his3Δ1 leu2Δ0 ura3Δ0 met15Δ0*	(CASEY *et al.* 2012)
SWY4950	*MATa rtn1::KanR yop1::KanR BBP1-GFP:HIS3 NIC96-mcherry:HYGB his3Δ1 leu2Δ0 ura3Δ0 lys2Δ0*	(CASEY *et al.* 2012)
SWY4970	*MATa NIC96-mcherry:HYGB BBP1-GFP:HIS3 his3Δ1 leu2Δ0 ura3Δ0*	(CASEY *et al.* 2012)
SWY4971	*MATa nup120::KanR NIC96-mcherry:HYGB BBP1-GFP:HIS3 his3Δ1 leu2Δ0 ura3Δ0*	(CASEY *et al.* 2012)
SWY4972	*MATa rtn1::KanR yop1::KanR SEC63-GFP:HIS3 his3Δ1leu2Δ0::DsRED-HDEL:LEU2 ura3Δ0*	(CASEY *et al.* 2012)
SWY5033	*MATα nup133::KanR NIC96-mcherry:HYGB BBP1-gfp:HIS3 his3Δ1 leu2Δ0 ura3Δ0 lys2Δ0 met15Δ0*	(CASEY *et al.* 2012)
SWY5285	*MATα nup145::KanR his3Δ1 leu2Δ0 ura3Δ0 lys2Δ0 pNUP145:URA3*	This Study
SWY5292	*MATα nup145::KanR Sec13-TAP::HIS3 his3Δ1 leu2Δ0 ura3Δ0 met15Δ0 pNUP145:URA3*	This Study
SWY5356	*MATα nup145::KanR seh1:: his3Δ1 leu2Δ0 ura3Δ0 met15Δ0 pNUP145:URA3*	This Study
SWY5366	*MATα nup145::KanR seh1::KanR NUP53-GFP::HIS3 his3Δ1 leu2Δ0 ura3Δ0 lys2Δ0 met15Δ0 pNUP145:URA3*	This Study
SWY5368	*MATα nup145::KanR seh1::KanR NIC96-GFP::HIS3 his3Δ1 leu2Δ0 ura3Δ0 lys2Δ0 met15Δ0 pNUP145:URA3*	This Study
SWY5368	*MATα nup145::KanR seh1::KanR MLP1-GFP::HIS3 his3Δ1 leu2Δ0 ura3Δ0 lys2Δ0 met15Δ0 pNUP145:URA3*	This Study
SWY5370	*MATα nup145::KanR seh1::KanR NUP159-GFP::HIS3 his3Δ1 leu2Δ0 ura3Δ0 lys2Δ0 met15Δ0 pNUP145:URA3*	This Study
Swy5390	*MATα lnp1::KanR NIC96-GFP:HIS3 his3Δ1 leu2Δ0 ura3Δ0*	This Study
Swy5432	*MATα nup133::KanR LNP1-GFP:HIS3 his3Δ1 leu2Δ0 ura3Δ0*	This Study
Swy5433	*MATα rtn1::KanR yop1::KanR LNP1-GFP:HIS3 his3Δ1 leu2Δ0 ura3Δ0*	This Study

Swy5459	*MATα lnp1::KanR rtn1::KanR his3Δ1 leu2Δ0met15Δ05 ura3Δ0*	This Study
Swy5462	*MATa lnp1::KanR rtn1::KanR NIC96-GFP:HIS3 his3Δ1 leu2Δ0 lys2Δ0 ura3Δ0*	This Study
Swy5463	*MATα lnp1::KanR rtn1::KanR NIC96-GFP:HIS3 his3Δ1 leu2Δ0 met15Δ0 ura3Δ0*	This Study
Swy5464	*MATa lnp1::KanR sey1::KanR NIC96-GFP:HIS3 his3Δ1 leu2Δ0 ura3Δ0*	This Study
Swy5465	*MATα lnp1::KanR sey1::KanR NIC96-GFP:HIS3 his3Δ1 leu2Δ0 ura3Δ0*	This Study
Swy5485	*MATα lnp1::KanR pom152::HIS3 his3Δ1 leu2Δ0 lys2Δ0 ura3Δ0*	This Study
Swy5486	*MATα lnp1::KanR rtn1::KanR his3Δ1 leu2Δ0 lys2Δ0 ura3Δ0*	This Study
Swy5488	*MATα lnp1::KanR pom34:: his3Δ1 leu2Δ0 lys2Δ0 ura3Δ0*	This Study
Swy5489	*MATα lnp1::KanR pom34::HIS3 pom152::HIS3 his3Δ1 leu2Δ0 lys2Δ0 ura3Δ0*	This Study
Swy5534	*MATα rtn1::KanR NIC96-GFP:HIS3 his3Δ1 leu2Δ0 met15Δ0 ura3Δ0*	This Study
Swy5535	*MATα rtn1::KanR NIC96-GFP:HIS3 his3Δ1 leu2Δ0 lys2Δ0 ura3Δ0*	This Study
Swy5563	*MATa lnp1::KanR rtn1::KanR sey1::KanR NIC96-GFP:HIS3 his3Δ1 leu2Δ0 lys2Δ0 ura3Δ0*	This Study
Swy5564	*MATα lnp1::KanR rtn1::KanR sey1::KanR NIC96-GFP:HIS3 his3Δ1 leu2Δ0 lys2Δ0 ura3Δ0*	This Study
Swy5589	*MATα lnp1::loxP-spHIS5 rtn1::KanR his3Δ1 leu2Δ0 lys2Δ0 met15Δ0 ura3Δ0*	This Study
Swy5847	*MATα ura3-52 his3Δ200 leu2Δ1 rat7-1(ts) LNP1-GFP:HIS*	This Study
Swy5869	*MATα lnp1::KanR nup133::KanR his3Δ1 leu2Δ0 met15Δ0 ura3Δ0*	This Study
Swy5918	*MATα lnp1::KanR nup59::KanR his3Δ1 leu2Δ0 met15Δ0 ura3Δ0*	This Study
Swy5919	*MATα lnp1::KanR nup59::KanR his3Δ1 leu2Δ0 met15Δ0 ura3Δ0*	This Study
Swy5926	*MATa lnp1::KanR nup145::KanR his3Δ1 leu2Δ0 lys2Δ0 ura3Δ0 pNup145:URA*	This Study
Swy5931	*MATα nup120::KanR LNP1-GFP:HIS3 his3Δ1 leu2Δ0 met15Δ0 ura3Δ0*	This Study
Swy5932	*MATα lnp1::KanR nup120::KanR his3Δ1 leu2Δ0 met15Δ0 ura3Δ0*	This Study
Swy5957	*MATα lnp1::KanR nup53::KanR nup59::KanR his3Δ1 leu2Δ0 met15Δ0 ura3Δ0*	This Study
Swy5974	*MATa lnp1::KanR nup85::KanR his3Δ1 leu2Δ0 lys2Δ0 ura3Δ0 pNup145:URA*	This Study

Swy5976	*MATα nup53::KanR nup59::KanR his3Δ1 leu2Δ0 lys2Δ0 ura3Δ0*	This Study
Swy5984	*MATa lnp1::KanR nup100::KanR his3Δ1 leu2Δ0 met15Δ0 ura3Δ0*	This Study
Swy5991	*MATa rtn1::KanR sey1::KanR NIC96-GFP:HIS3 his3Δ1 leu2Δ0 met15Δ0 ura3Δ0*	This Study
Swy5992	*MATα rtn1::KanR sey1::KanR NIC96-GFP:HIS3 his3Δ1 leu2Δ0 met15Δ0 lys2Δ0 ura3Δ0*	This Study
Swy5993	*MATa lnp1::KanR nup84::KanR his3Δ1 leu2Δ0 met15Δ0 ura3Δ0 pNup145:URA*	This Study
Swy6015	*MATα lnp1::KanR ura3-52 his3Δ200 leu2Δ1 rat7-1(ts)*	This Study
Swy6017	*MATa nup85::KanR sey1::KanR his3Δ1 leu2Δ0 met15Δ0 ura3Δ0*	This Study
Swy6034	*MATα sey1::KanR NIC96-GFP:HIS3 his3Δ1 leu2Δ0 lys2Δ0 met15Δ0 ura3Δ0*	This Study
Swy6046	*MATa rtn1::KanR sey1::KanR SEC61-GFP:HIS3 his3Δ1 leu2Δ0 ura3Δ0*	This Study
Swy6047	*MATα lnp1::KanR SEC61-GFP:HIS3 his3Δ1 leu2Δ0 lys2Δ0 ura3Δ0*	This Study
Swy6048	*MATα sey1::KanR SEC61-GFP:HIS3 his3Δ1 leu2Δ0 ura3Δ0*	This Study
Swy6049	*MATα lnp1::KanR sey1::KanR SEC61-GFP:HIS3 his3Δ1 leu2Δ0 ura3Δ0*	This Study
Swy6050	*MATα lnp1::KanR rtn1::KanR SEC61-GFP:HIS3 his3Δ1 leu2Δ0 lys2Δ0 ura3Δ0*	This Study
Swy6095	*MATα lnp1::KanR rtn1::KanR sey1::KanR SEC61-GFP:HIS3 his3Δ1 leu2Δ0 ura3Δ0*	This Study
Swy6104	*MATa rtn1::KanR SEC61-GFP:HIS3 his3Δ1 leu2Δ0 lys2Δ0 ura3Δ0*	This Study
Swy6165	*MATα nup84::KanR sey1::KanR his3Δ1 leu2Δ0 lys2Δ0 ura3Δ0*	This Study

APPENDIX D

Table D.1: Plasmids used in this study

Plasmid	Description	Resource
dsRed-HDEL	*trp1::DsRED-HDEL:TRP1* integration plasmid	(BEVIS *et al.* 2002)
pBS35	*mCHERRY/HYGB* integration plasmid	(SHANER *et al.* 2004)
pMal-Cri	MBP expression vector	New England Biosciences
pRS315	*CEN/LEU2*	(SIKORSKI and HIETER 1989)
pRS316	*CEN/URA3*	(SIKORSKI and HIETER 1989)
pRS425	*2u/LEU2*	(CHRISTIANSON *et al.* 1992)
pRS315.NDC1	*NDC1/CEN/LEU2*	(CHIAL *et al.* 1998)
pSBYp116	*CEN/LEU2/NUP145*	(BROHAWN *et al.* 2008)
PSJ906	*SPC42-mCHERRY-HIS/LEU2*	This Study
pSJ1287	*pBT3-STE-Ndc1*	(CASEY *et al.* 2012)
pSJ1469	*pR3N-Yop1*	(CASEY *et al.* 2012)
Psw300	*CEN/HIS3/NUP145Δ302*	(EMTAGE *et al.* 1997)
Psw388	*CEN/HIS3/Nup145ΔN*	(EMTAGE *et al.* 1997)
PSW863	*POM152*/2μ/*LEU2*	(MIAO *et al.* 2006)
Psw3190	*CEN/LEU2/POM34-MYC-SUC2-MYC*	(MIAO *et al.* 2006)
Psw3192	*CEN/LEU2/POM152-MYC-SUC2-MYC*	(MIAO *et al.* 2006)
Psw3420	*CEN/LEU2/RTN1-GFP*	(DAWSON *et al.* 2009)
Psw3421	*CEN/LEU2/rtn1-K48I-GFP*	(DAWSON *et al.* 2009)
PSW3422	*RTN1*/CEN/*LEU2*	(DAWSON *et al.* 2009)
PSW3592	*leu2Δ0::DsRED-HDEL:LEU2* integration cassette	(CASEY *et al.* 2012)
PSW3673	*APQ12*/2μ/*LEU2*	This Study
PSW3674	*BBP1*/2μ/*LEU2*	This Study
PSW3675	*BRR6*/2μ/*LEU2*	This Study
PSW3676	*MPS2*/2μ/*LEU2*	This Study
PSW3844	*CEN/LEU2/nup145K758P*	(BROHAWN *et al.* 2008)
Psw3905	*CEN/LEU2/LNP1*	This Study
Psw3906	*2u/LEU2/LNP1*	This Study
Psw3975	*MBP-LNP1cterm*	This Study
Psw4000	*CEN/LEU2/LNP1-MYC-SUC2-MYC*	This Study
Psw4001	pR3N-RTN1	This Study
Psw4028	*2u/LEU2/RTN1*	This Study
Psw4029	*2u/LEU2/LNP1-GFP*	This Study
Psw4031	*2u/LEU2/rtn1-K48I*	This Study
Psw4032	*2u/LEU2/LNP1Dznfn-GFP*	This Study
Psw4071	*MBP-LNP1ctermDznfn*	This Study
Psw4086	*CEN/LEU2/LNP1Dznfn*	This Study
Psw4087	*2u/LEU2/LNP1Dznfn*	This Study

REFERENCES

Abramoff, M., P. Magelhaes and S. Ram, 2004 Image processing with ImageJ., pp. 36–42. Biophotonics International.

Adams, I. R., and J. V. Kilmartin, 1999 Localization of core spindle pole body (SPB) components during SPB duplication in Saccharomyces cerevisiae. J Cell Biol 145**:** 809-823.

Adams, R. L., and S. R. Wente, 2013 Uncovering nuclear pore complexity with innovation. Cell 152**:** 1218-1221.

Aitchison, J. D., G. Blobel and M. P. Rout, 1995 Nup120p: a yeast nucleoporin required for NPC distribution and mRNA transport. J Cell Biol 131**:** 1659-1675.

Aitchison, J. D., and M. P. Rout, 2012 The Yeast Nuclear Pore Complex and Transport Through It. Genetics 190**:** 855-883.

Alber, F., S. Dokudovskaya, L. M. Veenhoff, W. Zhang, J. Kipper *et al.*, 2007a Determining the architectures of macromolecular assemblies. Nature 450**:** 683-694.

Alber, F., S. Dokudovskaya, L. M. Veenhoff, W. Zhang, J. Kipper *et al.*, 2007b The molecular architecture of the nuclear pore complex. Nature 450**:** 695-701.

Amlacher, S., P. Sarges, D. Flemming, V. van Noort, R. Kunze *et al.*, 2011 Insight into structure and assembly of the nuclear pore complex by utilizing the genome of a eukaryotic thermophile. Cell 146**:** 277-289.

Anderson, D. J., and M. W. Hetzer, 2008 Reshaping of the endoplasmic reticulum limits the rate for nuclear envelope formation. J Cell Biol 182**:** 911-924.

Antonin, W., 2009 Nuclear envelope: membrane bending for pore formation? Curr Biol 19**:** R410-412.

Antonin, W., J. Ellenberg and E. Dultz, 2008 Nuclear pore complex assembly through the cell cycle: regulation and membrane organization. FEBS Lett 582**:** 2004-2016.

Antonin, W., R. Ungricht and U. Kutay, 2011 Traversing the NPC along the pore membrane: targeting of membrane proteins to the INM. Nucleus 2**:** 87-91.

Anwar, K., R. W. Klemm, A. Condon, K. N. Severin, M. Zhang *et al.*, 2012 The dynamin-like GTPase Sey1p mediates homotypic ER fusion in S. cerevisiae. J Cell Biol 197**:** 209-217.

Araki, Y., C. K. Lau, H. Maekawa, S. L. Jaspersen, T. H. Giddings *et al.*, 2006 The Saccharomyces cerevisiae spindle pole body (SPB) component Nbp1p is required for SPB membrane insertion and interacts with the integral membrane proteins Ndc1p and Mps2p. Mol Biol Cell 17**:** 1959-1970.

Baur, T., K. Ramadan, A. Schlundt, J. Kartenbeck and H. H. Meyer, 2007 NSF- and SNARE-mediated membrane fusion is required for nuclear envelope formation and completion of nuclear pore complex assembly in Xenopus laevis egg extracts. J Cell Sci 120**:** 2895-2903.

Beaudouin, J., D. Gerlich, N. Daigle, R. Eils and J. Ellenberg, 2002 Nuclear envelope breakdown proceeds by microtubule-induced tearing of the lamina. Cell 108**:** 83-96.

Beck, M., V. Lučić, F. Förster, W. Baumeister and O. Medalia, 2007 Snapshots of nuclear pore complexes in action captured by cryo-electron tomography. Nature 449**:** 611-615.

Becker, J., F. Melchior, V. Gerke, F. R. Bischoff, H. Ponstingl *et al.*, 1995 RNA1 encodes a GTPase-activating protein specific for Gsp1p, the Ran/TC4 homologue of Saccharomyces cerevisiae. J Biol Chem 270**:** 11860-11865.

Belgareh, N., and V. Doye, 1997 Dynamics of nuclear pore distribution in nucleoporin mutant yeast cells. J Cell Biol 136**:** 747-759.

Bevis, B. J., A. T. Hammond, C. A. Reinke and B. S. Glick, 2002 De novo formation of transitional ER sites and Golgi structures in Pichia pastoris. Nat Cell Biol 4**:** 750-756.

Bian, X., R. W. Klemm, T. Y. Liu, M. Zhang, S. Sun *et al.*, 2011 Structures of the atlastin GTPase provide insight into homotypic fusion of endoplasmic reticulum membranes. Proc Natl Acad Sci U S A 108**:** 3976-3981.

Bischoff, F. R., C. Klebe, J. Kretschmer, A. Wittinghofer and H. Ponstingl, 1994 RanGAP1 induces GTPase activity of nuclear Ras-related Ran. Proc Natl Acad Sci U S A 91**:** 2587-2591.

Blobel, G., 2010 Three-dimensional organization of chromatids by nuclear envelope-associated structures. Cold Spring Harb Symp Quant Biol 75**:** 545-554.

Bolger, T. A., A. W. Folkmann, E. J. Tran and S. R. Wente, 2008 The mRNA export factor Gle1 and inositol hexakisphosphate regulate distinct stages of translation. Cell 134**:** 624-633.

Bolhy, S., I. Bouhlel, E. Dultz, T. Nayak, M. Zuccolo *et al.*, 2011 A Nup133-dependent NPC-anchored network tethers centrosomes to the nuclear envelope in prophase. J Cell Biol 192**:** 855-871.

Brohawn, S. G., N. C. Leksa, E. D. Spear, K. R. Rajashankar and T. U. Schwartz, 2008 Structural evidence for common ancestry of the nuclear pore complex and vesicle coats. Science 322**:** 1369-1373.

Brohawn, S. G., J. R. Partridge, J. R. Whittle and T. U. Schwartz, 2009 The nuclear pore complex has entered the atomic age. Structure 17**:** 1156-1168.

Brohawn, S. G., and T. U. Schwartz, 2009 Molecular architecture of the Nup84-Nup145C-Sec13 edge element in the nuclear pore complex lattice. Nat Struct Mol Biol 16**:** 1173-1177.

Bucci, M., and S. R. Wente, 1997 In vivo dynamics of nuclear pore complexes in yeast. J Cell Biol 136**:** 1185-1199.

Burns, L. T., and S. R. Wente, 2012 Trafficking to uncharted territory of the nuclear envelope. Curr Opin Cell Biol 24**:** 341-349.

Burns, L. T., and S. R. Wente, 2014 From hypothesis to mechanism: uncovering nuclear pore complex links to gene expression. Mol Cell Biol 34**:** 2114-2120.

Byers, B., and L. Goetsch, 1974 Duplication of spindle plaques and integration of the yeast cell cycle. Cold Spring Harb Symp Quant Biol 38**:** 123-131.

Byers, B., and L. Goetsch, 1975 Behavior of spindles and spindle plaques in the cell cycle and conjugation of Saccharomyces cerevisiae. J Bacteriol 124**:** 511-523.

Byrnes, L. J., and H. Sondermann, 2011 Structural basis for the nucleotide-dependent dimerization of the large G protein atlastin-1/SPG3A. Proc Natl Acad Sci U S A 108**:** 2216-2221.
Capelson, M., C. Doucet and M. W. Hetzer, 2010 Nuclear pore complexes: guardians of the nuclear genome. Cold Spring Harb Symp Quant Biol 75**:** 585-597.
Casey, A. K., T. R. Dawson, J. Chen, J. M. Friederichs, S. L. Jaspersen *et al.*, 2012 Integrity and function of the Saccharomyces cerevisiae spindle pole body depends on connections between the membrane proteins Ndc1, Rtn1, and Yop1. Genetics 192**:** 441-455.
Castillo, A. R., J. B. Meehl, G. Morgan, A. Schutz-Geschwender and M. Winey, 2002 The yeast protein kinase Mps1p is required for assembly of the integral spindle pole body component Spc42p. J Cell Biol 156**:** 453-465.
Cau, P., C. Navarro, K. Harhouri, P. Roll, S. Sigaudy *et al.*, 2014 Nuclear matrix, nuclear envelope and premature aging syndromes in a translational research perspective. Semin Cell Dev Biol 29**:** 125-147.
Chadrin, A., B. Hess, M. San Roman, X. Gatti, B. Lombard *et al.*, 2010 Pom33, a novel transmembrane nucleoporin required for proper nuclear pore complex distribution. J Cell Biol 189**:** 795-811.
Chen, S., T. Desai, J. A. McNew, P. Gerard, P. J. Novick *et al.*, 2014 Lunapark stabilizes nascent three-way junctions in the endoplasmic reticulum. Proc Natl Acad Sci U S A 14**:** 707-716.
Chen, S., P. Novick and S. Ferro-Novick, 2012 ER network formation requires a balance of the dynamin-like GTPase Sey1p and the Lunapark family member Lnp1p. Nature Cell Biology 14**:** 707-716.
Chen, S., P. Novick and S. Ferro-Novick, 2013 ER structure and function. Curr Opin Cell Biol 25**:** 428-433.
Chial, H. J., T. H. Giddings, E. A. Siewert, M. A. Hoyt and M. Winey, 1999 Altered dosage of the Saccharomyces cerevisiae spindle pole body duplication gene, NDC1, leads to aneuploidy and polyploidy. Proc Natl Acad Sci U S A 96**:** 10200-10205.
Chial, H. J., M. P. Rout, T. H. Giddings and M. Winey, 1998 Saccharomyces cerevisiae Ndc1p is a shared component of nuclear pore complexes and spindle pole bodies. J Cell Biol 143**:** 1789-1800.
Chowdhury, S., K. W. Smith and M. C. Gustin, 1992 Osmotic stress and the yeast cytoskeleton: phenotype-specific suppression of an actin mutation. J Cell Biol 118**:** 561-571.
Christianson, T. W., R. S. Sikorski, M. Dante, J. H. Shero and P. Hieter, 1992 Multifunctional yeast high-copy-number shuttle vectors. Gene 110**:** 119-122.
Copic, A., C. F. Latham, M. A. Horlbeck, J. G. D'Arcangelo and E. A. Miller, 2012 ER cargo properties specify a requirement for COPII coat rigidity mediated by Sec13p. Science 335**:** 1359-1362.
Corbett, A. H., D. M. Koepp, G. Schlenstedt, M. S. Lee, A. K. Hopper *et al.*, 1995 Rna1p, a Ran/TC4 GTPase activating protein, is required for nuclear import. J Cell Biol 130**:** 1017-1026.
D'Angelo, M. A., D. J. Anderson, E. Richard and M. W. Hetzer, 2006 Nuclear pores form de novo from both sides of the nuclear envelope. Science 312**:** 440-443.

Daigle, N., J. Beaudouin, L. Hartnell, G. Imreh, E. Hallberg *et al.*, 2001 Nuclear pore complexes form immobile networks and have a very low turnover in live mammalian cells. J Cell Biol 154**:** 71-84.

Dawson, T. R., M. D. Lazarus, M. W. Hetzer and S. R. Wente, 2009 ER membrane-bending proteins are necessary for de novo nuclear pore formation. J Cell Biol 184**:** 659-675.

De Craene, J. O., J. Coleman, P. Estrada de Martin, M. Pypaert, S. Anderson *et al.*, 2006a Rtn1p is involved in structuring the cortical endoplasmic reticulum. Mol Biol Cell 17**:** 3009-3020.

De Craene, J. O., J. Coleman, P. Estrada de Martin, M. Pypaert, S. Anderson *et al.*, 2006b Rtn1p is involved in structuring the cortical endoplasmic reticulum. Mol Biol Cell 17**:** 3009-3020.

de Las Heras, J. I., P. Meinke, D. G. Batrakou, V. Srsen, N. Zuleger *et al.*, 2013 Tissue specificity in the nuclear envelope supports its functional complexity. Nucleus 4**:** 460-477.

De Souza, C. P., A. H. Osmani, S. B. Hashmi and S. A. Osmani, 2004 Partial nuclear pore complex disassembly during closed mitosis in Aspergillus nidulans. Curr Biol 14**:** 1973-1984.

Debler, E. W., Y. Ma, H. S. Seo, K. C. Hsia, T. R. Noriega *et al.*, 2008 A fence-like coat for the nuclear pore membrane. Mol Cell 32**:** 815-826.

DeGrasse, J. A., K. N. DuBois, D. Devos, T. N. Siegel, A. Sali *et al.*, 2009 Evidence for a shared nuclear pore complex architecture that is conserved from the last common eukaryotic ancestor. Mol Cell Proteomics 8**:** 2119-2130.

Devos, D., S. Dokudovskaya, F. Alber, R. Williams, B. T. Chait *et al.*, 2004 Components of coated vesicles and nuclear pore complexes share a common molecular architecture. PLoS Biol 2**:** e380.

Devos, D., S. Dokudovskaya, R. Williams, F. Alber, N. Eswar *et al.*, 2006 Simple fold composition and modular architecture of the nuclear pore complex. Proc Natl Acad Sci U S A 103**:** 2172-2177.

Di Sano, F., P. Bernardoni and M. Piacentini, 2012 The reticulons: guardians of the structure and function of the endoplasmic reticulum. Exp Cell Res 318**:** 1201-1207.

Dokudovskaya, S., and M. P. Rout, 2011 A novel coatomer-related SEA complex dynamically associates with the vacuole in yeast and is implicated in the response to nitrogen starvation. Autophagy 7.

Dokudovskaya, S., F. Waharte, A. Schlessinger, U. Pieper, D. P. Devos *et al.*, 2011 A conserved coatomer-related complex containing Sec13 and Seh1 dynamically associates with the vacuole in Saccharomyces cerevisiae. Mol Cell Proteomics 10**:** M110.006478.

Donaldson, A. D., and J. V. Kilmartin, 1996 Spc42p: a phosphorylated component of the S. cerevisiae spindle pole body (SPD) with an essential function during SPB duplication. J Cell Biol 132**:** 887-901.

Doucet, C. M., and M. W. Hetzer, 2010 Nuclear pore biogenesis into an intact nuclear envelope. Chromosoma 119**:** 469-477.

Doucet, C. M., J. A. Talamas and M. W. Hetzer, 2010 Cell cycle-dependent differences in nuclear pore complex assembly in metazoa. Cell 141**:** 1030-1041.

Doye, V., R. Wepf and E. C. Hurt, 1994 A novel nuclear pore protein Nup133p with distinct roles in poly(A)+ RNA transport and nuclear pore distribution. EMBO J 13**:** 6062-6075.
Drin, G., and B. Antonny, 2010 Amphipathic helices and membrane curvature. FEBS Lett 584**:** 1840-1847.
Drin, G., J. F. Casella, R. Gautier, T. Boehmer, T. U. Schwartz *et al.*, 2007 A general amphipathic alpha-helical motif for sensing membrane curvature. Nat Struct Mol Biol 14**:** 138-146.
Dultz, E., and J. Ellenberg, 2010 Live imaging of single nuclear pores reveals unique assembly kinetics and mechanism in interphase. J Cell Biol 191**:** 15-22.
Egecioglu, D., and J. H. Brickner, 2011 Gene positioning and expression. Curr Opin Cell Biol 23**:** 338-345.
Elrod-Erickson, M. J., and C. A. Kaiser, 1996 Genes that control the fidelity of endoplasmic reticulum to Golgi transport identified as suppressors of vesicle budding mutations. Mol Biol Cell 7**:** 1043-1058.
Emtage, J. L., M. Bucci, J. L. Watkins and S. R. Wente, 1997 Defining the essential functional regions of the nucleoporin Nup145p. J Cell Sci 110 (Pt 7)**:** 911-925.
Enenkel, C., 2014 Nuclear transport of yeast proteasomes. Biomolecules 4**:** 940-955.
Enenkel, C., G. Blobel and M. Rexach, 1995 Identification of a yeast karyopherin heterodimer that targets import substrate to mammalian nuclear pore complexes. J Biol Chem 270**:** 16499-16502.
Erkmann, J. A., and U. Kutay, 2004 Nuclear export of mRNA: from the site of transcription to the cytoplasm. Exp Cell Res 296**:** 12-20.
Faust, J. E., T. Desai, A. Verma, I. Ulengin, T. L. Sun *et al.*, 2015 The Atlastin C-terminal Tail is an Amphipathic Helix that Perturbs Bilayer Structure during Endoplasmic Reticulum Homotypic Fusion. J Biol Chem.
Fernandez-Martinez, J., J. Phillips, M. D. Sekedat, R. Diaz-Avalos, J. Velazquez-Muriel *et al.*, 2012 Structure-function mapping of a heptameric module in the nuclear pore complex. J Cell Biol 196**:** 419-434.
Fernandez-Martinez, J., and M. P. Rout, 2009 Nuclear pore complex biogenesis. Curr Opin Cell Biol 21**:** 603-612.
Fichtman, B., and A. Harel, 2014 Stress and aging at the nuclear gateway. Mech Ageing Dev 135**:** 24-32.
Fichtman, B., C. Ramos, B. Rasala, A. Harel and D. J. Forbes, 2010 Inner/Outer nuclear membrane fusion in nuclear pore assembly: biochemical demonstration and molecular analysis. Mol Biol Cell 21**:** 4197-4211.
Field, M. C., A. Sali and M. P. Rout, 2011 Evolution: On a bender--BARs, ESCRTs, COPs, and finally getting your coat. J Cell Biol 193**:** 963-972.
Flemming, D., P. Sarges, P. Stelter, A. Hellwig, B. Bottcher *et al.*, 2009 Two structurally distinct domains of the nucleoporin Nup170 cooperate to tether a subset of nucleoporins to nuclear pores. J Cell Biol 185**:** 387-395.
Folkmann, A. W., S. E. Collier, X. Zhan, Aditi, M. D. Ohi *et al.*, 2013 Gle1 functions during mRNA export in an oligomeric complex that is altered in human disease. Cell 155**:** 582-593.

Folkmann, A. W., T. R. Dawson and S. R. Wente, 2014 Insights into mRNA export-linked molecular mechanisms of human disease through a Gle1 structure-function analysis. Adv Biol Regul 54**:** 74-91.
Folkmann, A. W., K. N. Noble, C. N. Cole and S. R. Wente, 2011 Dbp5, Gle1-IP6 and Nup159: a working model for mRNP export. Nucleus 2**:** 540-548.
Fried, H., and U. Kutay, 2003 Nucleocytoplasmic transport: taking an inventory. Cell Mol Life Sci 60**:** 1659-1688.
Friederichs, J. M., S. Ghosh, C. J. Smoyer, S. McCroskey, B. D. Miller *et al.*, 2011 The SUN protein Mps3 is required for spindle pole body insertion into the nuclear membrane and nuclear envelope homeostasis. PLoS Genet 7**:** e1002365.
Friedman, J. R., and G. K. Voeltz, 2011 The ER in 3D: a multifunctional dynamic membrane network. Trends Cell Biol 21**:** 709-717.
Gerace, L., and G. Blobel, 1980 The nuclear envelope lamina is reversibly depolymerized during mitosis. Cell 19**:** 277-287.
Gerace, L., and B. Burke, 1988 Functional organization of the nuclear envelope. Annu Rev Cell Biol 4**:** 335-374.
Gomez-Cavazos, J. S., and M. W. Hetzer, 2012 Outfits for different occasions: tissue-specific roles of Nuclear Envelope proteins. Curr Opin Cell Biol 24**:** 775-783.
Gorsch, L. C., T. C. Dockendorff and C. N. Cole, 1995 A conditional allele of the novel repeat-containing yeast nucleoporin RAT7/NUP159 causes both rapid cessation of mRNA export and reversible clustering of nuclear pore complexes. J Cell Biol 129**:** 939-955.
Goyal, U., and C. Blackstone, 2013 Untangling the web: mechanisms underlying ER network formation. Biochim Biophys Acta 1833**:** 2492-2498.
Grandi, P., V. Doye and E. C. Hurt, 1993 Purification of NSP1 reveals complex formation with 'GLFG' nucleoporins and a novel nuclear pore protein NIC96. EMBO J 12**:** 3061-3071.
Greenland, K. B., H. Ding, M. Costanzo, C. Boone and T. N. Davis, 2010 Identification of Saccharomyces cerevisiae spindle pole body remodeling factors. PLoS One 5**:** e15426.
Guttinger, S., E. Laurell and U. Kutay, 2009 Orchestrating nuclear envelope disassembly and reassembly during mitosis. Nat Rev Mol Cell Biol 10**:** 178-191.
Hatch, E., and M. Hetzer, 2014 Breaching the nuclear envelope in development and disease. J Cell Biol 205**:** 133-141.
Hayakawa, A., A. Babour, L. Sengmanivong and C. Dargemont, 2012 Ubiquitylation of the nuclear pore complex controls nuclear migration during mitosis in S. cerevisiae. J Cell Biol 196**:** 19-27.
Heath, C. V., C. S. Copeland, D. C. Amberg, V. Del Priore, M. Snyder *et al.*, 1995 Nuclear pore complex clustering and nuclear accumulation of poly(A)+ RNA associated with mutation of the Saccharomyces cerevisiae RAT2/NUP120 gene. J Cell Biol 131**:** 1677-1697.
Heessen, S., and M. Fornerod, 2007 The inner nuclear envelope as a transcription factor resting place. EMBO Rep 8**:** 914-919.
Hetzer, M. W., 2010a The nuclear envelope. Cold Spring Harb Perspect Biol 2**:** a000539.

Hetzer, M. W., 2010b The nuclear envelope. Cold Spring Harb Perspect Biol 21**:** 347-380.
Hetzer, M. W., T. C. Walther and I. W. Mattaj, 2005 Pushing the envelope: structure, function, and dynamics of the nuclear periphery. Annu Rev Cell Dev Biol 21**:** 347-380.
Hetzer, M. W., and S. R. Wente, 2009 Border control at the nucleus: biogenesis and organization of the nuclear membrane and pore complexes. Dev Cell 17**:** 606-616.
Hiraoka, Y., and A. F. Dernburg, 2009 The SUN rises on meiotic chromosome dynamics. Dev Cell 17**:** 598-605.
Hodge, C. A., V. Choudhary, M. J. Wolyniak, J. J. Scarcelli, R. Schneiter *et al.*, 2010 Integral membrane proteins Brr6 and Apq12 link assembly of the nuclear pore complex to lipid homeostasis in the endoplasmic reticulum. J Cell Sci 123**:** 141-151.
Hodge, C. A., E. J. Tran, K. N. Noble, A. R. Alcazar-Roman, R. Ben-Yishay *et al.*, 2011 The Dbp5 cycle at the nuclear pore complex during mRNA export I: dbp5 mutants with defects in RNA binding and ATP hydrolysis define key steps for Nup159 and Gle1. Genes Dev 25**:** 1052-1064.
Hoepfner, D., F. Schaerer, A. Brachat, A. Wach and P. Philippsen, 2002 Reorientation of mispositioned spindles in short astral microtubule mutant spc72Delta is dependent on spindle pole body outer plaque and Kar3 motor protein. Mol Biol Cell 13**:** 1366-1380.
Hopper, A. K., H. M. Traglia and R. W. Dunst, 1990 The yeast RNA1 gene product necessary for RNA processing is located in the cytosol and apparently excluded from the nucleus. J Cell Biol 111**:** 309-321.
Hsia, K. C., P. Stavropoulos, G. Blobel and A. Hoelz, 2007 Architecture of a coat for the nuclear pore membrane. Cell 131**:** 1313-1326.
Hu, J., Y. Shibata, C. Voss, T. Shemesh, Z. Li *et al.*, 2008 Membrane proteins of the endoplasmic reticulum induce high-curvature tubules. Science 319**:** 1247-1250.
Hu, J., Y. Shibata, P. P. Zhu, C. Voss, N. Rismanchi *et al.*, 2009 A class of dynamin-like GTPases involved in the generation of the tubular ER network. Cell 138**:** 549-561.
Huh, W. K., J. V. Falvo, L. C. Gerke, A. S. Carroll, R. W. Howson *et al.*, 2003 Global analysis of protein localization in budding yeast. Nature 425**:** 686-691.
Hulsmann, B. B., A. A. Labokha and D. Gorlich, 2012 The permeability of reconstituted nuclear pores provides direct evidence for the selective phase model. Cell 150**:** 738-751.
Iovine, M. K., J. L. Watkins and S. R. Wente, 1995 The GLFG repetitive region of the nucleoporin Nup116p interacts with Kap95p, an essential yeast nuclear import factor. J Cell Biol 131**:** 1699-1713.
Ito, H., Y. Fukuda, K. Murata and A. Kimura, 1983 Transformation of intact yeast cells treated with alkali cations. J Bacteriol 153**:** 163-168.
Jacobs, C. W., A. E. Adams, P. J. Szaniszlo and J. R. Pringle, 1988 Functions of microtubules in the Saccharomyces cerevisiae cell cycle. J Cell Biol 107**:** 1409-1426.

Jaspersen, S. L., T. H. Giddings and M. Winey, 2002 Mps3p is a novel component of the yeast spindle pole body that interacts with the yeast centrin homologue Cdc31p. J Cell Biol 159**:** 945-956.
Jaspersen, S. L., A. E. Martin, G. Glazko, T. H. Giddings, G. Morgan *et al.*, 2006 The Sad1-UNC-84 homology domain in Mps3 interacts with Mps2 to connect the spindle pole body with the nuclear envelope. J Cell Biol 174**:** 665-675.
Jaspersen, S. L., and M. Winey, 2004 The budding yeast spindle pole body: structure, duplication, and function. Annu Rev Cell Dev Biol 20**:** 1-28.
Jeyasekharan, A. D., Y. Liu, H. Hattori, V. Pisupati, A. B. Jonsdottir *et al.*, 2013 A cancer-associated BRCA2 mutation reveals masked nuclear export signals controlling localization. Nat Struct Mol Biol 20**:** 1191-1198.
Jovanovic-Talisman, T., B. T. Chait and M. P. Rout, 2014 NPC mimics: probing the mechanism of nucleocytoplasmic transport. Methods Cell Biol 122**:** 379-393.
Kaneb, H. M., A. W. Folkmann, V. V. Belzil, L. E. Jao, C. S. Leblond *et al.*, 2014 Deleterious mutations in the essential mRNA metabolism factor, hGle1, in amyotrophic lateral sclerosis. Hum Mol Genet.
Kim, S. J., J. Fernandez-Martinez, P. Sampathkumar, A. Martel, T. Matsui *et al.*, 2014 Integrative structure-function mapping of the nucleoporin Nup133 suggests a conserved mechanism for membrane anchoring of the nuclear pore complex. Mol Cell Proteomics 13**:** 2911-2926.
Kind, B., K. Koehler, M. Lorenz and A. Huebner, 2009 The nuclear pore complex protein ALADIN is anchored via NDC1 but not via POM121 and GP210 in the nuclear envelope. Biochem Biophys Res Commun 390**:** 205-210.
Kupke, T., L. Di Cecco, H. M. Müller, A. Neuner, F. Adolf *et al.*, 2011 Targeting of Nbp1 to the inner nuclear membrane is essential for spindle pole body duplication. EMBO J 30**:** 3337-3352.
Kuss, S. K., M. A. Mata, L. Zhang and B. M. Fontoura, 2013 Nuclear imprisonment: viral strategies to arrest host mRNA nuclear export. Viruses 5**:** 1824-1849.
Laba, J. K., A. Steen and L. M. Veenhoff, 2014 Traffic to the inner membrane of the nuclear envelope. Curr Opin Cell Biol 28**:** 36-45.
Lau, C. K., T. H. Giddings and M. Winey, 2004 A novel allele of Saccharomyces cerevisiae NDC1 reveals a potential role for the spindle pole body component Ndc1p in nuclear pore assembly. Eukaryot Cell 3**:** 447-458.
Le Sage, V., and A. J. Mouland, 2013 Viral subversion of the nuclear pore complex. Viruses 5**:** 2019-2042.
Leksa, N. C., S. G. Brohawn and T. U. Schwartz, 2009 The structure of the scaffold nucleoporin Nup120 reveals a new and unexpected domain architecture. Structure 17**:** 1082-1091.
Leksa, N. C., and T. U. Schwartz, 2010 Membrane-coating lattice scaffolds in the nuclear pore and vesicle coats: Commonalities, differences, challenges. Nucleus 1**:** 314-318.
Lim, R. Y., and B. Fahrenkrog, 2006 The nuclear pore complex up close. Curr Opin Cell Biol 18**:** 342-347.
Liu, J., A. J. Prunuske, A. M. Fager and K. S. Ullman, 2003 The COPI complex functions in nuclear envelope breakdown and is recruited by the nucleoporin Nup153. Dev Cell 5**:** 487-498.

Liu, J., T. Rolef Ben-Shahar, D. Riemer, M. Treinin, P. Spann *et al.*, 2000 Essential roles for Caenorhabditis elegans lamin gene in nuclear organization, cell cycle progression, and spatial organization of nuclear pore complexes. Mol Biol Cell 11**:** 3937-3947.

Lord, C., S. Ferro-Novick and E. A. Miller, 2013 The highly conserved COPII coat complex sorts cargo from the endoplasmic reticulum and targets it to the golgi. Cold Spring Harb Perspect Biol 5.

Lusk, C. P., G. Blobel and M. C. King, 2007 Highway to the inner nuclear membrane: rules for the road. Nat Rev Mol Cell Biol 8**:** 414-420.

Lutzmann, M., R. Kunze, A. Buerer, U. Aebi and E. Hurt, 2002 Modular self-assembly of a Y-shaped multiprotein complex from seven nucleoporins. EMBO J 21**:** 387-397.

Madrid, A. S., J. Mancuso, W. Z. Cande and K. Weis, 2006 The role of the integral membrane nucleoporins Ndc1p and Pom152p in nuclear pore complex assembly and function. J Cell Biol 173**:** 361-371.

Maeshima, K., H. Iino, S. Hihara and N. Imamoto, 2011 Nuclear size, nuclear pore number and cell cycle. Nucleus 2**:** 113-118.

Maggio, R., P. Siekevitz and G. E. Palade, 1963 STUDIES ON ISOLATED NUCLEI. I. ISOLATION AND CHEMICAL CHARACTERIZATION OF A NUCLEAR FRACTION FROM GUINEA PIG LIVER. J Cell Biol 18**:** 267-291.

Maimon, T., N. Elad, I. Dahan and O. Medalia, 2012 The human nuclear pore complex as revealed by cryo-electron tomography. Structure 20**:** 998-1006.

Makio, T., L. H. Stanton, C. C. Lin, D. S. Goldfarb, K. Weis *et al.*, 2009 The nucleoporins Nup170p and Nup157p are essential for nuclear pore complex assembly. J Cell Biol 185**:** 459-473.

Malhas, A., C. F. Lee, R. Sanders, N. J. Saunders and D. J. Vaux, 2007 Defects in lamin B1 expression or processing affect interphase chromosome position and gene expression. J Cell Biol 176**:** 593-603.

Mans, B. J., V. Anantharaman, L. Aravind and E. V. Koonin, 2004 Comparative genomics, evolution and origins of the nuclear envelope and nuclear pore complex. Cell Cycle 3**:** 1612-1637.

Mansfeld, J., S. Güttinger, L. A. Hawryluk-Gara, N. Panté, M. Mall *et al.*, 2006 The conserved transmembrane nucleoporin NDC1 is required for nuclear pore complex assembly in vertebrate cells. Mol Cell 22**:** 93-103.

Marelli, M., C. P. Lusk, H. Chan, J. D. Aitchison and R. W. Wozniak, 2001 A link between the synthesis of nucleoporins and the biogenesis of the nuclear envelope. J Cell Biol 153**:** 709-724.

Maul, G. G., J. W. Price and M. W. Lieberman, 1971 Formation and distribution of nuclear pore complexes in interphase. J Cell Biol 51**:** 405-418.

McDonald, K., 1999 High-pressure freezing for preservation of high resolution fine structure and antigenicity for immunolabeling. Methods Mol Biol 117**:** 77-97.

Meinema, A. C., J. K. Laba, R. A. Hapsari, R. Otten, F. A. Mulder *et al.*, 2011 Long unfolded linkers facilitate membrane protein import through the nuclear pore complex. Science 333**:** 90-93.

Meinema, A. C., B. Poolman and L. M. Veenhoff, 2013 Quantitative analysis of membrane protein transport across the nuclear pore complex. Traffic 14**:** 487-501.
Melchior, F., B. Paschal, J. Evans and L. Gerace, 1993 Inhibition of nuclear protein import by nonhydrolyzable analogues of GTP and identification of the small GTPase Ran/TC4 as an essential transport factor. J Cell Biol 123**:** 1649-1659.
Miao, M., K. J. Ryan and S. R. Wente, 2006 The integral membrane protein Pom34p functionally links nucleoporin subcomplexes. Genetics 172**:** 1441-1457.
Miller, J. P., R. S. Lo, A. Ben-Hur, C. Desmarais, I. Stagljar *et al.*, 2005 Large-scale identification of yeast integral membrane protein interactions. Proc Natl Acad Sci U S A 102**:** 12123-12128.
Miller, R. K., and M. D. Rose, 1998 Kar9p is a novel cortical protein required for cytoplasmic microtubule orientation in yeast. J Cell Biol 140**:** 377-390.
Moore, J. K., M. D. Stuchell-Brereton and J. A. Cooper, 2009 Function of dynein in budding yeast: mitotic spindle positioning in a polarized cell. Cell Motil Cytoskeleton 66**:** 546-555.
Moore, M. S., and G. Blobel, 1993 The GTP-binding protein Ran/TC4 is required for protein import into the nucleus. Nature 365**:** 661-663.
Moriya, K., K. Nagatoshi, Y. Noriyasu, T. Okamura, E. Takamitsu *et al.*, 2013 Protein N-myristoylation pays a critical role in the endoplasmic reticulum morphological change induced by overexpression of protein lunapark, an integral membrane protein of the endoplasmic eeticulum. PLoS One 8.
Mortimer, R. K., and J. R. Johnston, 1986 Genealogy of principal strains of the yeast genetic stock center. Genetics 113**:** 35-43.
Muñoz-Centeno, M. C., S. McBratney, A. Monterrosa, B. Byers, C. Mann *et al.*, 1999 Saccharomyces cerevisiae MPS2 encodes a membrane protein localized at the spindle pole body and the nuclear envelope. Mol Biol Cell 10**:** 2393-2406.
Nehrbass, U., M. P. Rout, S. Maguire, G. Blobel and R. W. Wozniak, 1996 The yeast nucleoporin Nup188p interacts genetically and physically with the core structures of the nuclear pore complex. J Cell Biol 133**:** 1153-1162.
Neumann, N., D. Lundin and A. M. Poole, 2010 Comparative genomic evidence for a complete nuclear pore complex in the last eukaryotic common ancestor. PLoS One 5**:** e13241.
Newport, J. W., and D. J. Forbes, 1987 The nucleus: structure, function, and dynamics. Annu Rev Biochem 56**:** 535-565.
Niepel, M., K. R. Molloy, R. Williams, J. C. Farr, A. C. Meinema *et al.*, 2013 The nuclear basket proteins Mlp1p and Mlp2p are part of a dynamic interactome including Esc1p and the proteasome. Mol Biol Cell 24**:** 3920-3938.
Niepel, M., C. Strambio-de-Castillia, J. Fasolo, B. T. Chait and M. P. Rout, 2005 The nuclear pore complex-associated protein, Mlp2p, binds to the yeast spindle pole body and promotes its efficient assembly. J Cell Biol 170**:** 225-235.
Noble, K. N., E. J. Tran, A. R. Alcazar-Roman, C. A. Hodge, C. N. Cole *et al.*, 2011 The Dbp5 cycle at the nuclear pore complex during mRNA export II: nucleotide cycling and mRNP remodeling by Dbp5 are controlled by Nup159 and Gle1. Genes Dev 25**:** 1065-1077.

Onischenko, E., L. H. Stanton, A. S. Madrid, T. Kieselbach and K. Weis, 2009 Role of the Ndc1 interaction network in yeast nuclear pore complex assembly and maintenance. J Cell Biol 185**:** 475-491.
Orso, G., D. Pendin, S. Liu, J. Tosetto, T. J. Moss *et al.*, 2009 Homotypic fusion of ER membranes requires the dynamin-like GTPase atlastin. Nature 460**:** 978-983.
Park, S. H., and C. Blackstone, 2010 Further assembly required: construction and dynamics of the endoplasmic reticulum network. EMBO Rep 11**:** 515-521.
Patel, S. S., B. J. Belmont, J. M. Sante and M. F. Rexach, 2007 Natively unfolded nucleoporins gate protein diffusion across the nuclear pore complex. Cell 129**:** 83-96.
Pemberton, L. F., M. P. Rout and G. Blobel, 1995 Disruption of the nucleoporin gene NUP133 results in clustering of nuclear pore complexes. Proc Natl Acad Sci U S A 92**:** 1187-1191.
Plotnikov, A., E. Zehorai, S. Procaccia and R. Seger, 2011 The MAPK cascades: signaling components, nuclear roles and mechanisms of nuclear translocation. Biochim Biophys Acta 1813**:** 1619-1633.
Radu, A., G. Blobel and M. S. Moore, 1995 Identification of a protein complex that is required for nuclear protein import and mediates docking of import substrate to distinct nucleoporins. Proc Natl Acad Sci U S A 92**:** 1769-1773.
Razafsky, D., and D. Hodzic, 2009 Bringing KASH under the SUN: the many faces of nucleo-cytoskeletal connections. J Cell Biol 186**:** 461-472.
Ries, J., C. Kaplan, E. Platonova, H. Eghlidi and H. Ewers, 2012 A simple, versatile method for GFP-based super-resolution microscopy via nanobodies. Nat Methods 9**:** 582-584.
Rismanchi, N., C. Soderblom, J. Stadler, P. P. Zhu and C. Blackstone, 2008 Atlastin GTPases are required for Golgi apparatus and ER morphogenesis. Hum Mol Genet 17**:** 1591-1604.
Rogers, J. V., T. Arlow, E. R. Inkellis, T. S. Koo and M. D. Rose, 2013 ER-associated SNAREs and Sey1p mediate nuclear fusion at two distinct steps during yeast mating. Mol Biol Cell 24**:** 3896-3908.
Rogers, J. V., C. McMahon, A. Baryshnikova, F. M. Hughson and M. D. Rose, 2014 ER-associated retrograde SNAREs and the Dsl1 complex mediate an alternative, Sey1p-independent homotypic ER fusion pathway. Mol Biol Cell 25**:** 3401-3412.
Romero-Santacreu, L., J. Moreno, J. E. Pérez-Ortín and P. Alepuz, 2009 Specific and global regulation of mRNA stability during osmotic stress in Saccharomyces cerevisiae. RNA 15**:** 1110-1120.
Rout, M. P., J. D. Aitchison, A. Suprapto, K. Hjertaas, Y. Zhao *et al.*, 2000 The yeast nuclear pore complex: composition, architecture, and transport mechanism. J Cell Biol 148**:** 635-651.
Salina, D., K. Bodoor, D. M. Eckley, T. A. Schroer, J. B. Rattner *et al.*, 2002 Cytoplasmic dynein as a facilitator of nuclear envelope breakdown. Cell 108**:** 97-107.
Scarcelli, J. J., C. A. Hodge and C. N. Cole, 2007 The yeast integral membrane protein Apq12 potentially links membrane dynamics to assembly of nuclear pore complexes. J Cell Biol 178**:** 799-812.

Schirmer, E. C., L. Florens, T. Guan, J. R. Yates and L. Gerace, 2003 Nuclear membrane proteins with potential disease links found by subtractive proteomics. Science 301**:** 1380-1382.
Schirmer, E. C., and L. Gerace, 2005 The nuclear membrane proteome: extending the envelope. Trends Biochem Sci 30**:** 551-558.
Schneiter, R., and C. N. Cole, 2010 Integrating complex functions: coordination of nuclear pore complex assembly and membrane expansion of the nuclear envelope requires a family of integral membrane proteins. Nucleus 1**:** 387-392.
Schramm, C., S. Elliott, A. Shevchenko and E. Schiebel, 2000 The Bbp1p-Mps2p complex connects the SPB to the nuclear envelope and is essential for SPB duplication. EMBO J 19**:** 421-433.
Sezen, B., M. Seedorf and E. Schiebel, 2009 The SESA network links duplication of the yeast centrosome with the protein translation machinery. Genes Dev 23**:** 1559-1570.
Shaner, N. C., R. E. Campbell, P. A. Steinbach, B. N. Giepmans, A. E. Palmer *et al.*, 2004 Improved monomeric red, orange and yellow fluorescent proteins derived from Discosoma sp. red fluorescent protein. Nat Biotechnol 22**:** 1567-1572.
Sherman, F., F. G. R. and H. J. B., 1986 *Methods in Yeast Genetics: Laboratory Course Manual for Methods in Genetics.*, pp. 186 pp. *Cold Spring Harbor Laboratory*, *Cold Spring Harbo, NY*.
Shi, Y., J. Fernandez-Martinez, E. Tjioe, R. Pellarin, S. J. Kim *et al.*, 2014 Structural characterization by cross-linking reveals the detailed architecture of a coatomer-related heptameric module from the nuclear pore complex. Mol Cell Proteomics 13**:** 2927-2943.
Shibata, Y., T. Shemesh, W. A. Prinz, A. F. Palazzo, M. M. Kozlov *et al.*, 2010 Mechanisms determining the morphology of the peripheral ER. Cell 143**:** 774-788.
Shibata, Y., C. Voss, J. M. Rist, J. Hu, T. A. Rapoport *et al.*, 2008 The reticulon and DP1/Yop1p proteins form immobile oligomers in the tubular endoplasmic reticulum. J Biol Chem 283**:** 18892-18904.
Sikorski, R. S., and P. Hieter, 1989 A system of shuttle vectors and yeast host strains designed for efficient manipulation of DNA in Saccharomyces cerevisiae. Genetics 122**:** 19-27.
Siniossoglou, S., M. Lutzmann, H. Santos-Rosa, K. Leonard, S. Mueller *et al.*, 2000 Structure and assembly of the Nup84p complex. J Cell Biol 149**:** 41-54.
Snider, J., S. Kittanakom, D. Damjanovic, J. Curak, V. Wong *et al.*, 2010 Detecting interactions with membrane proteins using a membrane two-hybrid assay in yeast. Nat Protoc 5**:** 1281-1293.
Solmaz, S. R., G. Blobel and I. Melcak, 2013 Ring cycle for dilating and constricting the nuclear pore. Proc Natl Acad Sci U S A 110**:** 5858-5863.
Stage-Zimmermann, T., U. Schmidt and P. A. Silver, 2000 Factors affecting nuclear export of the 60S ribosomal subunit in vivo. Mol Biol Cell 11**:** 3777-3789.
Starr, D. A., 2007 Communication between the cytoskeleton and the nuclear envelope to position the nucleus. Mol Biosyst 3**:** 583-589.

Stavru, F., B. B. Hülsmann, A. Spang, E. Hartmann, V. C. Cordes *et al.*, 2006 NDC1: a crucial membrane-integral nucleoporin of metazoan nuclear pore complexes. J Cell Biol 173**:** 509-519.

Steinberg, G., M. Schuster, U. Theisen, S. Kilaru, A. Forge *et al.*, 2012 Motor-driven motility of fungal nuclear pores organizes chromosomes and fosters nucleocytoplasmic transport. J Cell Biol 198**:** 343-355.

Strambio-De-Castillia, C., M. Niepel and M. P. Rout, 2010 The nuclear pore complex: bridging nuclear transport and gene regulation. Nat Rev Mol Cell Biol 11**:** 490-501.

Strawn, L. A., T. Shen, N. Shulga, D. S. Goldfarb and S. R. Wente, 2004 Minimal nuclear pore complexes define FG repeat domains essential for transport. Nat Cell Biol 6**:** 197-206.

Suntharalingam, M., and S. R. Wente, 2003 Peering through the pore: nuclear pore complex structure, assembly, and function. Dev Cell 4**:** 775-789.

Szymborska, A., A. de Marco, N. Daigle, V. C. Cordes, J. A. Briggs *et al.*, 2013 Nuclear pore scaffold structure analyzed by super-resolution microscopy and particle averaging. Science 341**:** 655-658.

Talamas, J. A., and M. W. Hetzer, 2011 POM121 and Sun1 play a role in early steps of interphase NPC assembly. J Cell Biol 194**:** 27-37.

Tamm, T., A. Grallert, E. P. Grossman, I. Alvarez-Tabares, F. E. Stevens *et al.*, 2011 Brr6 drives the Schizosaccharomyces pombe spindle pole body nuclear envelope insertion/extrusion cycle. J Cell Biol 195**:** 467-484.

Tcheperegine, S. E., M. Marelli and R. W. Wozniak, 1999 Topology and functional domains of the yeast pore membrane protein Pom152p. J Biol Chem 274**:** 5252-5258.

Terry, L. J., and S. R. Wente, 2007 Nuclear mRNA export requires specific FG nucleoporins for translocation through the nuclear pore complex. J Cell Biol 178**:** 1121-1132.

Tetenbaum-Novatt, J., and M. P. Rout, 2010 The mechanism of nucleocytoplasmic transport through the nuclear pore complex. Cold Spring Harb Symp Quant Biol 75**:** 567-584.

Thierbach, K., A. von Appen, M. Thoms, M. Beck, D. Flemming *et al.*, 2013 Protein interfaces of the conserved Nup84 complex from Chaetomium thermophilum shown by crosslinking mass spectrometry and electron microscopy. Structure 21**:** 1672-1682.

Tran, E. J., Y. Zhou, A. H. Corbett and S. R. Wente, 2007 The DEAD-box protein Dbp5 controls mRNA export by triggering specific RNA:protein remodeling events. Mol Cell 28**:** 850-859.

Urade, T., Y. Yamamoto, X. Zhang, Y. Ku and T. Sakisaka, 2014 Identification and Characterization of TMEM33 as a Reticulon-binding Protein. Kobe J Med Sci 60**:** E57-65.

Voeltz, G. K., W. A. Prinz, Y. Shibata, J. M. Rist and T. A. Rapoport, 2006 A class of membrane proteins shaping the tubular endoplasmic reticulum. Cell 124**:** 573-586.

Vollmer, B., A. Schooley, R. Sachdev, N. Eisenhardt, A. M. Schneider *et al.*, 2012 Dimerization and direct membrane interaction of Nup53 contribute to nuclear pore complex assembly. Embo j 31**:** 4072-4084.
Waterman-Storer, C. M., and E. D. Salmon, 1998 Endoplasmic reticulum membrane tubules are distributed by microtubules in living cells using three distinct mechanisms. Curr Biol 8**:** 798-806.
Wente, S. R., and G. Blobel, 1994 NUP145 encodes a novel yeast glycine-leucine-phenylalanine-glycine (GLFG) nucleoporin required for nuclear envelope structure. J Cell Biol 125**:** 955-969.
Wente, S. R., and M. P. Rout, 2010 The nuclear pore complex and nuclear transport. Cold Spring Harb Perspect Biol 2**:** a000562.
West, M., N. Zurek, A. Hoenger and G. K. Voeltz, 2011 A 3D analysis of yeast ER structure reveals how ER domains are organized by membrane curvature. J Cell Biol 193**:** 333-346.
Wilson, K. L., and S. C. Dawson, 2011 Evolution: functional evolution of nuclear structure. J Cell Biol 195**:** 171-181.
Winey, M., and K. Bloom, 2012 Mitotic spindle form and function. Genetics 190**:** 1197-1224.
Winey, M., L. Goetsch, P. Baum and B. Byers, 1991 MPS1 and MPS2: novel yeast genes defining distinct steps of spindle pole body duplication. J Cell Biol 114**:** 745-754.
Winey, M., M. A. Hoyt, C. Chan, L. Goetsch, D. Botstein *et al.*, 1993 NDC1: a nuclear periphery component required for yeast spindle pole body duplication. J Cell Biol 122**:** 743-751.
Winey, M., D. Yarar, T. H. Giddings and D. N. Mastronarde, 1997 Nuclear pore complex number and distribution throughout the Saccharomyces cerevisiae cell cycle by three-dimensional reconstruction from electron micrographs of nuclear envelopes. Mol Biol Cell 8**:** 2119-2132.
Winzeler, E. A., D. D. Shoemaker, A. Astromoff, H. Liang, K. Anderson *et al.*, 1999 Functional characterization of the S. cerevisiae genome by gene deletion and parallel analysis. Science 285**:** 901-906.
Witkin, K. L., J. M. Friederichs, O. Cohen-Fix and S. L. Jaspersen, 2010 Changes in the nuclear envelope environment affect spindle pole body duplication in Saccharomyces cerevisiae. Genetics 186**:** 867-883.
Wozniak, R. W., G. Blobel and M. P. Rout, 1994 POM152 is an integral protein of the pore membrane domain of the yeast nuclear envelope. J Cell Biol 125**:** 31-42.
Xiang, X., and R. Fischer, 2004 Nuclear migration and positioning in filamentous fungi. Fungal Genet Biol 41**:** 411-419.
Yarbrough, M. L., M. A. Mata, R. Sakthivel and B. M. Fontoura, 2014 Viral subversion of nucleocytoplasmic trafficking. Traffic 15**:** 127-140.
Yewdell, W. T., P. Colombi, T. Makhnevych and C. P. Lusk, 2011 Lumenal interactions in nuclear pore complex assembly and stability. Mol Biol Cell 22**:** 1375-1388.
Yoder, T. J., C. G. Pearson, K. Bloom and T. N. Davis, 2003 The Saccharomyces cerevisiae spindle pole body is a dynamic structure. Mol Biol Cell 14**:** 3494-3505.

Zhang, D., and S. Oliferenko, 2014 Tts1, the fission yeast homolog of TMEM33 family, functions in NE remodeling during mitosis. Mol Biol Cell 25**:** 2970-2983.